MOTOR NEURON-SPECIFIC RESTORATION OF SMN IN TWO SMA MOUSE MODELS: INSIGHTS INTO THE ROLE OF MOTOR NEURONS IN SPINAL MUSCULAR ATROPHY

A Dissertation

by

XIMENA PAEZ

Submitted to the Office of Graduate and Professional Studies of
Texas A&M University
in partial fulfillment of the requirements for the degree of

DOCTOR OF PHILOSOPHY

Chair of Committee,	Mendell Rimer
Committee Members,	Farida Sohrabji
	Rajesh Miranda
	Mark Harlow
Head of Department,	William Griffith

August 2014

Major Subject: Neuroscience

ABSTRACT

Spinal muscular atrophy (SMA) results from α-motor neuron loss in the spinal cord due to low levels of the survival of motor neuron (SMN) protein, required for proper spliceosome assembly. The reduced levels of SMN cause muscle atrophy and ultimately death in the most severe cases. Although mouse models of SMA recapitulate many features of the human disease, it is still unclear whether their phenotypes are primarily due to motor neuron deficits. If so, motor neuron-selective restoration of normal SMN levels should have a great positive impact on SMA mice. To test this, we first exogenously raised normal human SMN in severe SMA mice that die perinatally, by driving its expression selectively in motor neurons with an *Hb9* promoter. We found no extension of survival. We detected motor neuronal-SMN protein expression in *Hb9-SMN* transgenic mice from mid embryogenesis to postnatal day 6. However, *mRNA* for transgenic *SMN* was undetected by late embryogenesis. These results suggest that expression of *Hb9-SMN* declines before SMN levels are most needed perinatally. Second, we increased endogenous motor neuronal-SMN expression following embryonic *Hb9*-dependent Cre recombination of a conditional hybrid mutant allele (Smn^{res}) in another severe SMA mouse model (SMAΔ7-like). Cre recombination irreversibly transforms the Smn^{res} allele to WT. We confirmed that recombination of Smn^{res} occured exclusively in the spinal cord. Yet, unlike a previous study that used choline acetyltransferase (*ChAT*) as a driver on the same mice, we found no improvement in survival, weight, motor behavior or presynaptic neurofilament

accumulation. However, like in *ChAT*$^{Cre+}$ SMA mice, we detected rescue of endplate size and mitigation of neuromuscular junction (NMJ) denervation status. Real time-PCR showed that the expression of spinal cord SMN transcript was sharply reduced in *Hb9*$^{Cre+}$ SMA mice relative to *ChAT*$^{Cre+}$ SMA mice. This suggests that our lack of overall phenotypic improvement was most likely due to an unexpectedly poor recombination efficiency driven by *Hb9*^{Cre}. Nonetheless, the low levels of SMN were sufficient to rescue two NMJ structural parameters indicating that these motor neuron cell-autonomous phenotypes are very sensitive to changes in motor neuronal-SMN levels.

DEDICATION

This dissertation is dedicated, first of all, to the Families of SMA Organization (fSMA) for their perseverance, devotion, commitment, hard work and, support to all of those afflicted by Spinal Muscular Atrophy and their families; for promoting and supporting basic and translational research to find treatments and ultimately a cure for this devastating disease. I hope I am contributing a small grain of sand to this field.

My work is also dedicated to my family. To my mother and father that have motivated and pushed me towards success everyday; for their unconditional love and support that have always kept me going. I would not be where I am today without them. Rodolfo, you are a role model to follow. I truly admire your hard work, discipline, personal motivation, and humongous brain. Mediocrity does not exist in your vocabulary. I only wish I could be more like you. This would have been done a lot sooner and a lot better if I were! Thank you for all of your love and for being my pillar of support (P.F.s). Lastly, I would like to dedicate this to my aunt and godmother Ximena for being an example to follow in her passion for work, science, research, and ethical conduct.

ACKNOWLEDGEMENTS

I would like to thank my committee chair, Dr. Mendell Rimer, and my committee members, Dr. Sohrabji, Dr. Miranda, and Dr. Harlow, for their guidance and support throughout the course of this research. Thank you Dr. Rimer for the opportunity to be a part of your projects, for your mentoring and, patience. I thank the Texas Brain and Spine Institute and it's directors for believing in me, their motivation, and for my financial support during 2013.

Bonnie, working with you has been a unique experience for sure. Thank you so much for your advice, professional and personal, for being a shoulder to cry and vent on, for your solidarity, and all your assistance with this project. Thanks to Dr. William Griffith for always supporting me and standing by my side, along with Drs. Van Wilson and Emily Wilson in the graduate office for their efforts in making the graduate program a successful one; for their kindness and for always having their doors wide open to any student in need. Also, a big thanks to Rachel Levins and Amanda Watkins-Borths for never abandoning me in time of need and always helping me solve all of the logistical and administrative issues I've encountered.

Thank you: to Sridevi Balaraman for extensive help with qRT-PCR experiments, Dr. Rajesh Miranda for access to the real-time PCR machine, Melissa Osborne and Cathy Lutz for advice on breeding and genotyping and for positive control tissue used in recombined allele genomic PCR, the Sumner lab for providing tissue and advice which has been crucial to our Aim 2, Sandra Garraway for initial help with spinal cord

dissections, as well as Young il (Matt) Lee and Wes Thompson for critically reading our published manuscript. A big thanks also goes out to all my HSC friends, GSO buddies, colleagues, faculty members, and NExT staff for making my time here a memorable and successful experience.

I am most thankful for the wonderful support from my amazing parents, loving husband, and incredible friends. Last but definitely not least, I thank all of my mice that very generously "donated" their lives in the name of *Science*.

NOMENCLATURE

AchR	Acetyl choline receptor
ANS	Autonomic Nervous System
CNS	Central Nervous System
ChAT	Choline acetyltransferase
E	Embryonic (days)
GFP	Green Fluorescent Protein
MN	Motor Neuron
NF	Neurofilament
NMJ	Neuromuscular Junction
P	Postnatal (days)
PCR	Polymerase Chain Reaction
PNS	Peripheral Nervous System
qRT-PCR	Quantitative-Real Time-Polymerase Chain Reaction
RT-PCR	Reverse Transcriptase Polymerase Chain Reaction
SMA	Spinal Muscular Atrophy
Smn	Survival Of Motoneuron Gene (Mouse)
SMN	Survival Of Motoneuron Gene (Human)
SMN	Survival of Motoneuron Protein
TA	Tibialis Anterior
U snRNP	Uridine-Rich Small Nuclear Ribonucleoprotein Particle

TABLE OF CONTENTS

LIST OF FIGURES

LIST OF TABLES

CHAPTER I

INTRODUCTION:

BACKGROUND AND SIGNIFICANCE

1.1 OVERVIEW

Spinal Muscular Atrophy (SMA) is an autosomal recessive neuromuscular disorder affecting approximately 1:10,000 [1] to 1:6,400 children [2, 3] with a frequency of carriers of 1:35 to 1:50 [2]. Second to cystic fibrosis, SMA is the most common genetic infantile disorder and it is included in a group with other neurological disorders caused by alterations in genes with important roles in RNA metabolism [4, 5]. Currently, there is no cure for this disease. SMA is characterized by lower α-motor neuron loss in the ventral horn of the spinal cord [6, 7] giving rise to symmetrical muscle weakness and atrophy of voluntary muscles followed by atrophy of trunk muscles and commonly concluding in death by respiratory failure in the most severe cases [7-10]. This phenotype is caused by the paucity in production of the Survival of Motor Neuron protein (SMN) varying from embryonic lethality to impairment of the motor system. SMA patients have low levels of this protein, particularly in spinal motor neurons [11].

The phenotype and symptoms of SMA vary widely, *i.e.* it is a very heterogeneous disease [12] that makes precise classification a challenging task; the prognosis can range from early infant death to normal adult life with only mild weakness. The different forms of SMA have been grouped into three types depending on the age of onset and symptoms [4, 13], although many patients do not classify cleanly

into a single type. Type I, Werdnig-Hoffmann disease, (Werdnig, 1894; Hoffmann, 1900) is the most severe form of SMA characterized by muscle atrophy and hypotonia with death occurring usually in the first two years of life due to heart and respiratory failure. Type II, is the intermediate form of the disease in which children may survive beyond four years and can develop some muscular functions, such as sitting up, but are unable to walk or stand without assistance. The symptoms usually appear around 18 months of age; these patients have serious respiratory problems and a short life expectancy. Type III SMA (Kugelberg–Welander or juvenile SMA) is a mild form of the disease in which patients could potentially survive to late adulthood but with some muscle weakness observed by the second year of age [4, 8, 14]. There is also a very mild type of SMA that develops in adults over 30 years old often called type IV SMA [8].

1.2 THE SMN PROTEIN

The evolutionarily conserved (294-amino acid long) 38kDa SMN protein is expressed ubiquitously, although not in the same levels (high in brain, spine, kidney, liver; moderate in cardiac and skeletal muscle; low in fibroblasts and lymphocytes) [1, 8, 15]. It is unclear, despite the ample knowledge of SMN biochemistry, why the loss of this protein gives rise to a neuronal phenotype characterized by a degenerative process while other tissues, where it is also expressed, remain unhindered [16, 17]. Spinal cord levels of SMN are much lower in SMA than in healthy patients [17].

Experiments of SMN depletion in yeast have lead to the conclusion that this protein has a conserved essential function in eukaryotes [17, 18]. This is not surprising

since it has been widely accepted that SMN is required for proper spliceosome assembly having a crucial role in the biogenesis of uridine-rich small nuclear ribonucleoprotein particles (U snRNPs) [8, 19]. Small nuclear ribonucleoproteins (snRNPs) are key in the processing of pre-mRNA to mRNAs [5, 8]; certain snRNPs are critical for the recognition of splice sites and the catalytic removal of introns from pre-mRNA. Each snRNP contains a small nuclear RNA (snRNA) and an extremely stable core of seven Sm proteins. The snRNP biogenesis pathway for snRNAs involves nuclear export of snRNA, Sm-core assembly in the cytoplasm, and re-import of the mature snRNP. The assembly of the snRNA:Sm core is carried out by the SMN macromolecular complex, which rigorously identifies RNAs as snRNAs and binds the RNA-binding Sm proteins (See Fig. 1.1 for detailed pathway) [5, 8, 20]. The cytoplasmic SMN complex contains the SMN-interacting protein 1 (SIPI) as well as the Sm proteins. The N-terminal part of the SMN protein is involved in SIPI biding and association with RNA, the middle region constitutes a Tudor domain, which is necessary and sufficient for the binding of Sm proteins, and the C-terminal of SMN is also important for Sm binding and its oligomerization [21]. Other functions of SMN include transcription, pre-mRNA splicing catalysis, metabolism of snoRNPs, axonal RNA transport, stress responses, and suppression of apoptosis [8, 22-24].

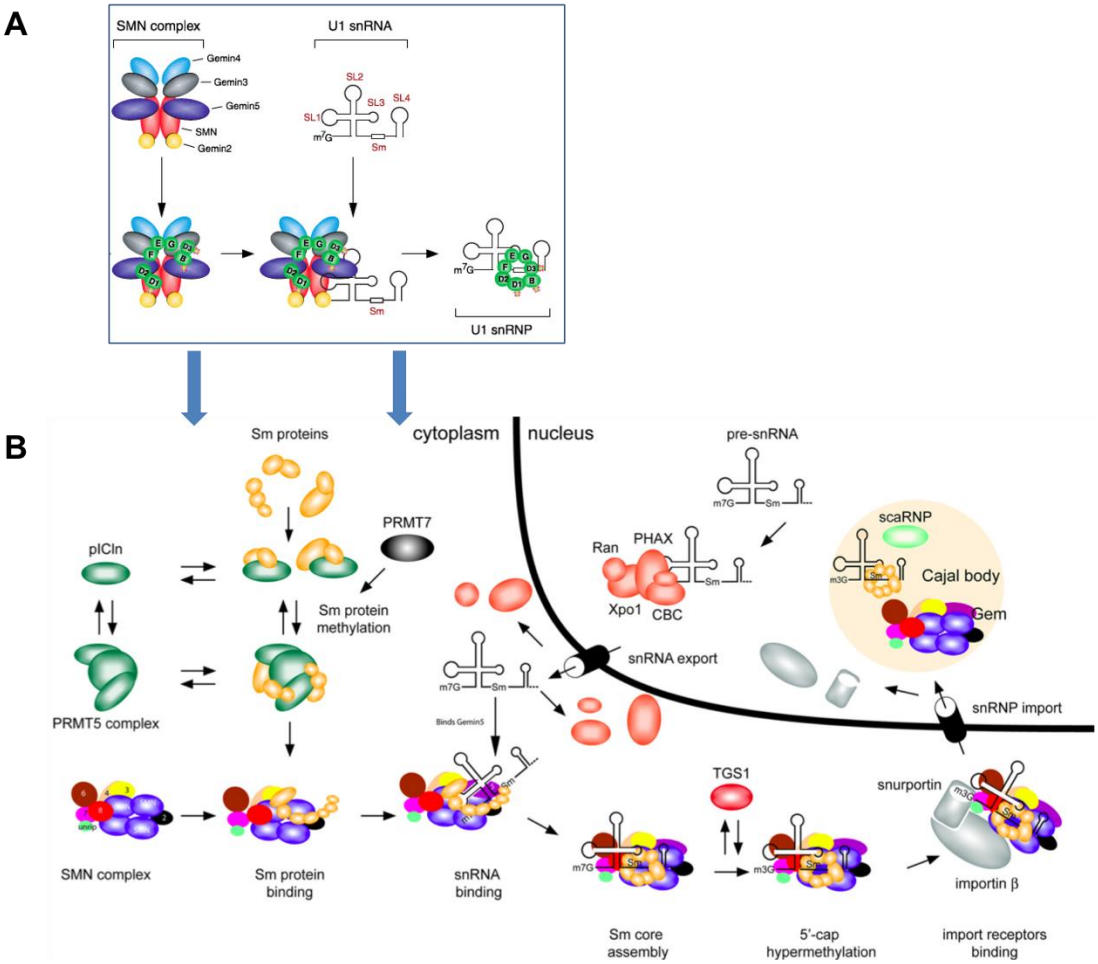

Fig. 1.1. Schematic model of snRNP assembly by the SMN complex. Small nuclear ribonucleoproteins (snRNPs) are active in recognizing and removing introns from pre-mRNA in the nucleus. Each snRNP particle is composed of small nuclear RNA (snRNA), several Sm proteins and a number of specific proteins unique to each snRNP. **A) The SMN complex**: SMN functions in the cytoplasm to assemble Sm proteins onto the snRNAs to produce an active snRNP particle. The SMN complex is composed of SMN, Gemins2-8 and unrip. SMN is an oligomer that self-associates, a critical process for SMN function. **B) Detailed overview of the ordered cellular pathway of SMN in the formation of snRNPs:** in the cytoplasm, the chloride conductance regulatory protein (pICln) and the 20S methylosome capture the 7 Sm proteins. The protein arginine methyltrasferase (PRMT5 complex) and PRMT7 methylate the Sm proteins. This process transforms the Sm proteins into high affinity substrates of the SMN complex. Then, Sm proteins are released from pICln-PRMT5 complex and bind the SMN complex. snRNA is transcribed in the nucleus and then binds the export proteins to be translocated to the cytoplasm. The SMN complex places the Sm proteins onto the snRNA. The stem and loop of the UsnRNA are necessary and sufficient for the association with the SMN complex. The snRNA is hypermethylated, allowing the SnRNA/SMN complex to bind snurportin and importin, which mediates transport of the SMN complex with an assembled snRNP into the nucleus. In the nucleus the SMN complex and snRNPs localize to the Cajal body/gem and snRNPs undergo further maturation. Adapted from Burghes and Beattie (2009) [5] and Pellizzoni et al. (2002) [25].

Liu and Dreyfuss first described an interesting localization pattern for SMN. They determined that SMN is localized in discrete "dot-like" structures named gems (for Gemini coiled bodies) near to coiled (Cajal) bodies in the nucleus (Fig. 1.2) [26]. Gems and Cajal bodies, although they are two distinct structures, have similar functions and achieve a dynamic relationship in which they interact with each other [15, 26, 27].

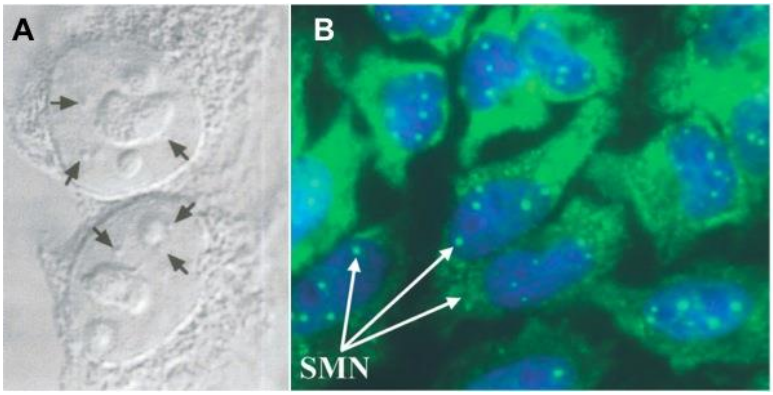

Fig. 1.2. The SMN protein is localized in discrete structures called gems. A) DIC image of gems (pointed out by arrowheads) in *HeLa* cells [26]. B) An anti-SMN monoclonal antibody localizes SMN within gems in *HeLa* cells [8]. Adapted from Liu and Dreyfuss (1996) [26] & Coady and Lorson (2011) [8].

SMN can also be found in the cytoplasm [6, 8, 16, 24, 26] and in axons (*in vivo*), branch points, dendrites and growth cones (*in vitro*) (Fig. 1.3) [9, 16, 17, 28]. The C-terminal of Exon 7 is critical for SMN localization in the cytoplasm [16].

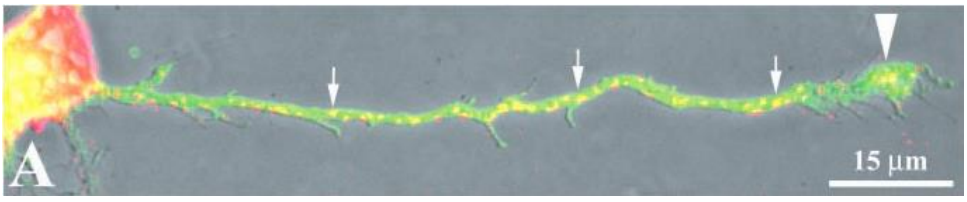

Fig. 1.3. Neuronal localization of SMN. SMN granules localized to the axonal process (arrows) and its growth cone (arrowhead). From Zhang *et al.* (2003) [16].

SMN is known to form a complex with Gemins 2–8 and unrip to allow the assembly of Sm proteins onto snRNAs [28]; SMN also interacts with itself and Gemins 2-6 forming an oligomerized complex [26, 27]. When SMN is found in granules inside axons it is transported bi-directionally with Gemins 2 and 3 [9]. SMN also interacts with arginine and glycine rich-substrate proteins that are high-affinity binders of the SMN complex and regulate the ribonucleoprotein assembly processes [27]; it also associates with fibrillarin and the RGG box region of hnRNP U [26].

The degree of snRNP assembly activity inversely correlates with severity of SMA mice, the decrease in assembly results in decreased levels of UsnRNA (U11 and U12), which are important in splicing minor introns found in a subset of genes [28]. Also, SMN deficiency impairs U7 snRNP assembly; this SMN-dependent U7 reduction affects endonucleolytic cleavage of histone mRNAs and even changes in histone gene expression. This was very recently found both in humans and mouse models in a study by Tisdale and collaborators (2013) [29]. The lack of normal quantities of SMN causes synaptic pathology in the SMA mouse models assayed up to date. One example is that synaptic vesicles have been observed to more likely be located in the periphery of the presynaptic terminal [30]. This indicates that at least one of the compartments of the neuromuscular synapse, the presynaptic compartment, is highly affected during the SMA pathology.

According to Torres-Benito *et al.* (2011), there are two hypotheses attempting to explain why the reduction in SMN expression causes mainly a motor neuron disease. The first hypothesis is based on the assumption that the disruption in RNA processing

has a more detrimental effect on motor neurons, while the other hypothesis under investigation suggests that SMN plays crucial roles in the axons and synapses of these cells, besides the formation of U snRNPs, causing their death upon its depletion [9]. This second hypothesis is not without merit considering that numerous studies have reported SMN in axonal transport granules, and its interaction with numerous mRNA-binding proteins not involved in splicing regulation suggest a role for SMN in axonal RNA metabolism [10, 31].

SMN can be found within axons that contain non Sm-related proteins (hnRNPs Q and R). These proteins are involved in the active transport of some mRNAs, such as β-actin, to the axon growth cone [16, 28]. Some of these mRNAs have been found significantly reduced in the growth cone in SMA mouse models. Thus, axon transport seems to be a critical pathway disrupted in SMA. Fallini *et al.* presented novel findings in 2010 on the fast active transport of SMN-containing granules which move along live primary motor neuron axons anterogradely and retrogradely indicating that SMN does have an axon specific role [31]. Furthermore, the axons of motor neuron cultures from severe SMA mice and zebrafish SMN knock out model are shorter [28]. Zhang *et al.* (2003) determined that SMN is actively transported to neuronal processes and that because exon-7 is involved in cytoplasmic localization, SMN-associated RNPs may show inefficient delivery into axons contributing to the SMA pathology [16]. Although unlikely to contribute to the SMA pathology, an isoform of SMN, including only the amino terminus, has been found solely in axons [5].

In vivo studies disrupting the function of *SMN* have provided clues into the role of the SMN protein on aiding in cell survival [24]. Vyas *et al.* (2002) assessed the role of SMN in apoptosis by expressing human SMN protein in undifferentiated and differentiated PC12 cells or in Rat-l cells, on which apoptosis was induced by withdrawal of trophic support or c-Myc. They determined that SMN delays the onset of apoptosis by acting on mechanisms that mediate cell death through the mitochondrial release of cytochrome c. SMN inhibits the release of cytochrome c and cleavage of caspase-3. The C terminal domain of the protein, in particular exons 6 and 7, plays a key role in fulfilling this function [24].

1.3 THE *SMN* GENE

Lefebvre et al. (1995) identified, cloned and characterized a gene which they coined *SMN* and suggested it was involved in the SMA phenotype. This gene was found duplicated in the SMA locus (a region with low copy repeat elements) mapping to chromosome 5q13 [4]. *SMN* is ~20kb in length and has nine exons termed 1, 2a, 2b, and 3-8 [32]. Although there are two, nearly identical, human genes that produce the SMN protein, *SMN1* (telomeric) and *SMN2* (centromeric) [15], only *SMN1* is the source for full-length SMN (FL-SMN) [11]. *SMN2* differs from *SMN1* in single nucleotide differences in exons 7 and 8 out of the nine exonic regions of the SMN gene. The important single nucleotide difference is a cytosine (C) to thymine (T) transition in exon 7 [1, 11, 19, 33]; this nonpolymorphic nucleotide difference is responsible for exon 7 inclusion in the transcript from *SMN1*. The change causes alternate mRNA splicing, due

to disruption in overlapping regulatory elements, eliminating exon 7 that leads to an approximate 90% reduction in FL-SMN both in healthy and SMA children (Fig. 1.4) [2, 11, 19, 23, 33]. Exon 7 is comprised by 54 nucleotides, is part of an exon splice enhancer (ESE), and contains the translation termination signal for all full-length products [11, 34]. Exon 7 inclusion is tightly regulated by positive and negative regulatory elements [34].

The protein derived from the truncated transcript produced from *SMN2*, designated SMNΔ7, does not associate with other proteins necessary for the formation of the spliceosome complex *i.e.*, it cannot fulfill its canonical function, and ultimately becomes degraded due to instability [8, 11, 35, 36]. It is important to mention that in both *SMN1* and *SMN2* the first 4.6kb of their promoters are identical, thus possible promoter differences do not account for the varying levels of SMN produced by each [11, 17].

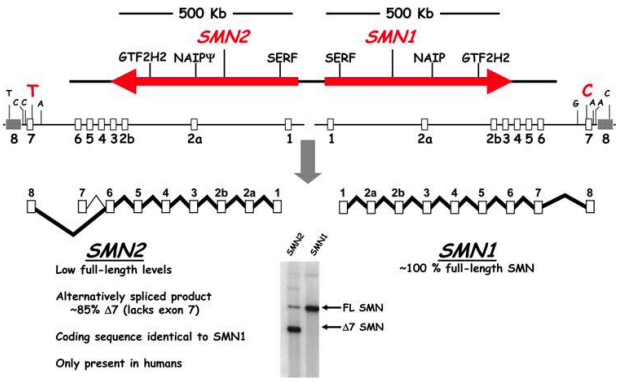

Fig. 1.4. Representation of the human *SMN* locus. Telomeric *SMN1* and centromeric *SMN2*, map on chromosome 5. They both have nine exons and eight introns but encode varying levels of the SMN protein. A C–T transition in exon 7 explains the difference between the two almost identical genes. In *SMN2* this alters a critical exonic splice enhancer preventing exon 7 inclusion during splicing causing over 85% reduction in full-length SMN. *SMN2* produces mostly a minimally functional truncated product (SMNΔ7). Bands for the full-length and truncated products are seen in the lower middle panel. From Lorson *et al.* (2010) [34].

Mutations in *SMN1* cause the SMA phenotype [2, 8, 37, 38]. Approximately 96% of SMA patients have a deletion in *SMN1* (Fig. 1.5). In the cases where the gene is retained, patients can suffer the disease due to intragenic mutations [7]. According to Coovert *et al.* (1997), some of the *SMN1* mutations observed in patients are deletions that disrupt exon 7 splicing, deletion of 4-5 base pairs in exon 3, a duplication of 11 base pairs in exon 6 or other possible missense mutations in exons 6 and 7. Most of the small mutations are compound heterozygotes and about 75% are non-deletion/conversion mutations. Because mutations in the telomeric *SMN1* gene were consistently found in patients with the SMA phenotype, it was coined as the gene responsible for this neurodegenerative disorder.. The coding region between exons 6 and 7 became the focus of many studies because its transcript appeared to be essential for the normal functioning of both motor neurons and their targets [15].

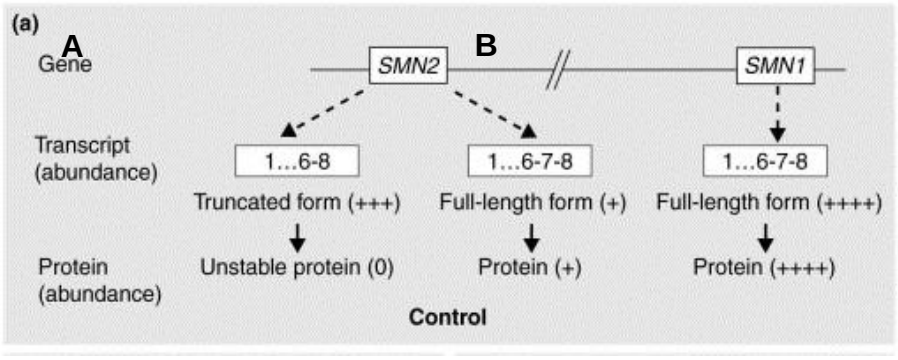

Fig. 1.5. Genomic organization of the *SMN* locus in type I and III SMA patients. A) SMA occurs due to a deletion of the *SMN1* gene causing significant decrease in full-length SMN. SMN2 gene remains present and compensates for the loss when present in several copies. **B)** SMA type III occurs because *SMN1* is converted into *SMN2*. Despite the absence of *SMN1*, type III SMA is less severe because there are an increased number of *SMN2* genes on each chromosome; this would lead to a higher amount of SMN protein. Modified from Frugier *et al.* (2002) [39].

Homozygous absence of *Smn* in mice and all the other SMA animal models is embryonic lethal [5, 40, 41]. In mice, there is massive cell death before embryo implantation [10]. In other animals, the timing of lethality is dependent upon the levels of SMN provided by the mother's SMN gene [5].The absolute lack of SMN in humans is unknown. Thus, it can be assumed that it is also embryonic lethal [8, 23]. Only one copy of *SMN1* or *Smn* (in animal models) is enough to be asymptomatic. Carriers show no obvious signs of pathology. This is evident in animal models heterozygous for a mutation in *Smn* as well as humans with just one copy of *SMN1* and no copies of *SMN2* to compensate [42]. Only humans possess the two genes *SMN1* and *SMN2*. According to Rochette *et al.* (2001), their genetic analysis of allelic variants in chimpanzee's prove that even though the *SMN* gene duplication occurred more than 5 million years ago, before humans and chimpanzee diverged evolutionarily, *SMN2* appears only in the lineage of *Homo sapiens* [43]; thus compensatory mechanisms provided by the existence of more than one allele expressing the SMN protein are unique to humans. This functional advantage in humans may be due to quantitative differences between humans and other animals in terms of their motoneuron-muscle physiology [17].

In spite this gene duplication providing a counterbalance, the centromeric gene *SMN2* can only compensate for the lack of *SMN1,* lessening the severity of the disease, when it is present in multiple copies producing larger quantities of FL-SMN and the truncated SMNΔ7 protein [40, 44-46]. Swoboda *et al.* (2005) have demonstrated that when *SMN2* is found in a low copy number (< 3) the phenotype of the disease is more severe in terms of motor unit number estimation [14]. A study that performed a

quantitative analysis on the copy number of *SMN2* in 375 SMA patients found that about 80% of the type I SMA patients assayed carry one or two copies of *SMN2*, 82% of patients with type II SMA carry three copies of *SMN2*, and 96% of patients with type III SMA carry three or four copies of *SMN2* [47].

Even though *SMN1* is the gene widely accepted as the responsible for causing the SMA pathology, a study by Srivastava and co-authors (2001) stated that homozygous absence of *SMN2* could cause childhood onset of the disease without any disruption of the *SMN1* gene. Their data came from one 5 year-old patient with childhood SMA presenting symptoms such as distal muscle weakness and wasting, delayed motor development and hypotonia. They concluded that *SMN2* might add more susceptibility in some populations of SMA patients [12]. Additionally, it is worthy to note that there seems to be a correlation between homozygous deletions of *SMN2* and patients with sporadic adult-onset lower motor neuron disease (LMND) since 36% of patients assayed by Moulard *et al.* (1998) presented this genetic alteration [48].

1.4 SMA PATHOLOGICAL HALLMARKS

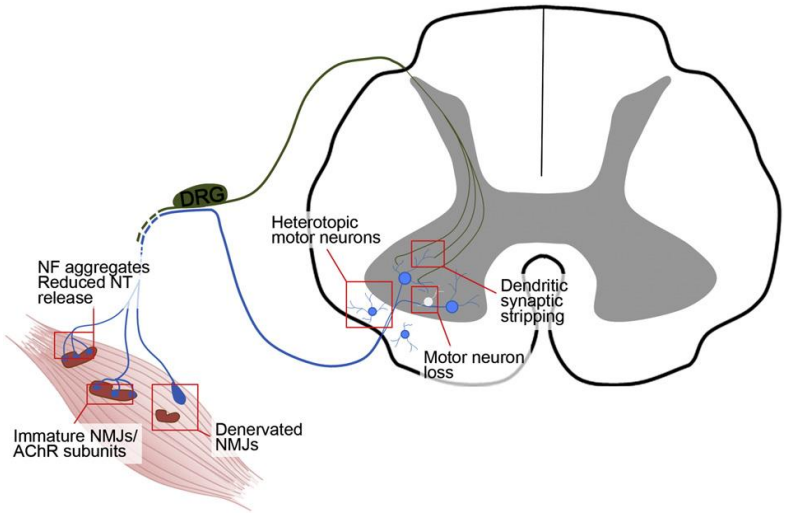

Fig. 1.6. Schematic representation of some neuropathological hallmarks of SMA patients and SMA animal models. Cell death characterizes spinal motor neurons; there are signs of denervation, reduction in the number of afferent synapses with proprioceptive neurons, neurofilament (NF) aggregates at the endplates, reduced neurotransmitter (NT) release, and immature acetylcholine receptor (AChR) subunits. In the case of humans, heterotopic (mispositioning) motor neurons located around the gray matter of the anterior horn can be seen. From Fallini *et al.* (2012) [10].

When SMN is reduced below normal levels an aberrant neuromuscular phenotype is observed in SMA patients and animal models. The pathological hallmark is the loss of α-motor neurons of the ventral spinal cord (Fig. 1.6 and 1.7B) and lower brainstem with some heterotopy of these cells in the ventral white matter (Fig. 1.6) [10, 49]. Remaining motor neurons may appear swollen or chromatolytic, and intramuscular nerves show abnormal beading and Wallerian degeneration [49]. There is a reduction in the number of afferent synapses with proprioceptive neurons (Fig. 1.6) [10, 50] with

sensory axons degenerating in type I patients [51]. Additionally, osteoporosis and scoliosis may accompany neuromuscular symptoms [52].

Muscles are affected in both anatomy and function. Moderate to severe weakness, neurogenic atrophy, and acute or chronic denervation of specific muscle groups characterizes SMA. Mainly, patients experience profound hypotonia (floppy infant syndrome) [49]. Severe SMA skeletal muscles consist of numerous rounded, atrophic fibers interspersed with one or more hypertrophic myofibers (Fig 1.7C); fibers also appear immature, resembling myotubes with central nuclei and persistence of the checkerboard pattern of type I and type II fibers, while muscle from patients with milder forms of SMA show signs of numerous cycles of denervation and re-innervation and may sometimes exhibit myopathic features such as fiber splitting, central nuclei, basophilia and an increase in endomysial connective tissue [53].

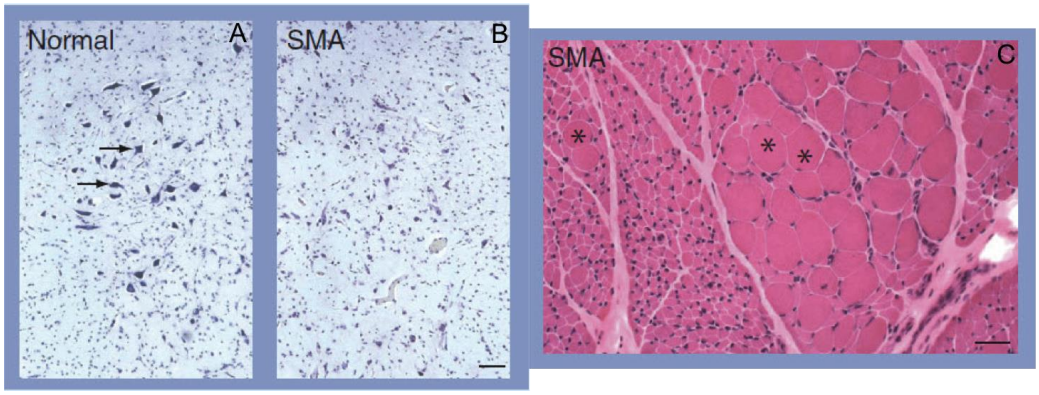

Fig. 1.7. Main neuronal and muscular pathological phenotype in Spinal Muscular Atrophy. Cresyl echt violet staining from a control hypoglossal nucleus section reveals clear presence of α-motor neurons (arrowheads) in A) while the post-mortem tissue from an SMA patient B) lacks this staining indicating motor neuron loss. C) Hematoxylin-eosin (H&E) staining of skeletal muscle fibers shows atrophic muscle fibers interspersed with hypertrophic fibers (asterisks). Scale bar: A) and B): 30 μM; C): 20μM. Adapted from Monani and De Vivo (2013) [49].

The *Smn* defect can destabilize the sarcolemma as determined by a clear reduction of dystrophin expression and upregulation of utrophin, which are components of skeletal muscle fibers linking the F-actin cytoskeleton to the extracellular matrix, at least from observations in mice [54].

Mice show signs of denervation in a subset of muscles [51], indicating that there are differing levels of vulnerability between distinct pools of motor neurons; meanwhile, generalized muscle denervation is not as widely observed in humans [10], even though this would be the assumption considering that weakness and paralysis of skeletal muscles are hallmarks of SMA. Motor neuronal synaptic defects could better explain this phenomenon.

Spinal circuitry dysfunction, both in humans and mouse models, is an important characteristic in the disease that appears very early. In mouse models, primary afferent boutons onto motor neuron somata and proximal dendrites are lost, thus greatly and progressively weakening the synapses between these two cell types. This phenomenon precedes motor neuron death and follows a pattern that emulates the pattern of progressive muscle weakness that occurs initially in projections towards proximal muscle targets [55].

Pathology also includes defects of the pre- and post-neuromuscular synapse. These are probably the earliest pathological hallmarks of the disease and there is evidence that abnormalities of the distal end of the motor unit likely precede those of the motor neuron cell body [30]. These defects were initially observed in model mice but have been confirmed in patient tissue as well [49].

Normal postsynaptic clusters of acetylcholine receptors (AChRs) at the neuromuscular junction (NMJ) appear at first shaped as simple plaques and then become successively more complex as perforated plaques, "C"-shaped, branched configurations, and eventually the mature "pretzels" [40]. AChR clusters in mutant mice do not differentiate at the same rate and when compared to control mice have a higher percentage of plaque-shaped receptors [40], which should have developed into more complex forms at that stage; thus a hallmark of the SMA-NMJ is immature AChR clusters (Fig. 1.5) [10].

An important early sign of pathology at the NMJ is the accumulation of phosphorylated neuronal intermediate filaments, neurofilament (NF), at perykarions and axon terminals [10, 56-58]. This may be seen in conjunction with a reduction of the postsynaptic region and defect of axonal sprouting [10, 58]. This abnormal accumulation seems to be the result of changes in cellular NF distribution and not expression [58]. In Cifuente-Diaz's (2002) experiments using an SMA mouse model, accumulation of phosphorylated NF is neither associated with hyperphosphorylated tau nor caused by deregulation of Cdk5/p35 activity or distribution even though NF is a substrate of protein kinases [58]. Atypical neurofilament accumulation has been linked to several other neurodegenerative diseases, such as amyotrophic lateral sclerosis, Parkinson's disease, and Alzheimer's disease [59]. Mutant motor neurons may also have eccentrically positioned nuclei associated with indentations of the nuclear membrane [58].

Pathology in non-neuronal tissue can also greatly contribute to the overall decline in SMA patients and animal models. For example, patients (usually the ones with only one copy of *SMN2*) can present severe symptomatic bradycardia, heart defects such as atrial and ventricular septal defects, arrhythmias, dilated right ventricle, hypoplastic left heart syndrome, respiratory failure and sudden death [52, 60]. Even patients with milder types of SMA present cardiac problems such as heart block progressing to complete atrioventricular block. Some other cardiac symptoms in severe to intermediate mild patients include arrhythmias co-occuring with cardiomyopathies, hyperhidrosis, poor circulation, tachyarrhythmia, altered RR interval variation, decreased sympathetic skin response, and affected vasodilation [61]. SMA mice also suffer from cardiac problems such as cardiomyopathy and autonomic nervous system (ANS) defects leading to congenital bradyarrhythmia and heart block. If these symptoms progress the mice will eventually die from heart failure. SMA mouse hearts are smaller in size and flaccid [61-63]. Liver alterations such as the reduction of circulating insulin-like growth factor (IGF1) seen in severe SMA mice indicate the importance of other tissues in the diseased states [64].

Also, additional to the main cellular pathology observed, other cellular impairments are present and contribute to the overall deterioration. For example, some cytoskeletal elements are altered with SMN-deficient cells having impairments in microtubules [10].

1.5 THERAPEUTIC STRATEGIES

Outside of supportive care there is no cure for SMA at present. Several drugs have been tested in clinical trials but so far none have proven both efficacious and safe. Nonetheless, therapeutic efforts aiming at increasing availability of the SMN protein, either by direct viral delivery or by enhancing full-length SMN protein expression from *SMN2* [37], are approaching the translational stage of development. Past and present efforts have focused on using small RNA molecules to modulate the endogenous *SMN2* gene by activating the *SMN2* promoter or to reprogram the splicing of *SMN2* pre-mRNA to restore expression of the normal SMN protein (antisense oligonucleotides), gene therapy for *SMN* replacement, stem cells that can differentiate into motor neurons, neuroprotective molecules and pathways, and targets downstream of SMN deficiency [36, 65]. A summary of therapeutic approaches can be found in Table 1.1.

1.5.1 Antisense Oligonucleotides

All humans have at least one functional copy of *SMN2*, even in SMA, thus correcting *SMN2* exon 7 splicing is a compelling potential treatment. Postnatal increase of SMN levels using small compounds and antisense oligonucleotides (ASOs) has yielded benefits in animal models of SMA. ASO based therapy is a great approach since there can be a limitless number of compounds that could be tested for the same target [66]. Several antisense approaches exist including blocking exonic splicing silencers (EESs), intronic splicing silencers (ISSs) or the intron 7–exon 8 junction.

To restore *SMN2* exon 7 inclusion in SMA, it is essential that splice-switching

ASOs target an inhibitory cis-element located within an intronic sequence. The intronic splicing silencer (N1 ISS-N1, discovered by Singh et al. 2006) is the main checkpoint of *SMN2* exon 7 splicing regulation. Once ISS-N1 is deleted exon 7 is included. Anti-N1 treatment was capable of elevating SMN levels in type I SMA patient cells [67].

ISIS Pharmaceuticals has a proprietary product called MOE (ASOs with phosphorothioate backbone and 2′-O-methoxyethyl modification) that confers increased nuclease resistance and decrease non-specific protein interactions. MOE gives reduced efficacy with a single cerebrospinal fluid delivery but an enhanced efficacy when delivered at multiple time points and at high doses peripherally, with an increase in survival in mice [68]. Dr. Adrian Krainer's group and ISIS performed independent studies and found that ISS-N1-targeting ASOs stimulate exon 7 inclusion by displacing inhibitory factors in *SMN2,* thus reconstructing a version of the *SMN* gene capable of expressing functional FL-SMN protein [66, 69]. The first *in vivo* study of an ISS-N1 targeting ASO was done in severe SMA mice, the SMAΔ7 model (described in detail, along with others in the section to follow on SMA animal models). With SMA ASO which increased SMN levels in brain and spinal cord, improved body weight and motor behavior [70]. Later on, Krainer *et al.* along with ISIS performed other *in vivo* experiments on a mild SMA model with ISS-N1 targeting MOE ASOs. They used an 18-mer MOE ASO (ASO-10-27) that base pairs with ISS-N1; this frees up exon 7 so that it can be incorporated into *SMN2* mRNA upon splicing. Single intracerebroventricular embryonic or neonatal ICV injection completely rescued the phenotype [65].

The efficacy of the ASO-10-27 was tested in 2011 (Passini group) when

introduced into the cerebral lateral ventricles of SMAΔ7 mice. They found an increase in both the number of motor neurons and SMN, improvements in muscle physiology, motor behavior and most importantly survival (from two to three/four weeks). They performed preliminary testing of this treatment in cynomolgus monkeys. They administered intrathecal infusions of ASO-10-27 to all regions of the spinal cord and observed that nervous system–directed ASO therapy is tolerable in non-human primates and efficacious achieving therapeutically relevant levels of ASO 10-27 [71]. However, there is toxicity with this MOE at doses >1.16 mM [72]. Porensky *et al.* (2012), from the Dr. Arthur Burghes group, also demonstrated the efficacy of using small compounds against ISS-N1. Using an ICV-delivered phosphorodiamidate morpholino oligomer (MO) they found a significant increase in the lifespan of SMA mice (from 15 to >100 days), specifically when treatment was administered early on (P0). MOs have a low toxicity and a wide distribution of uptake. This MO [HSMN2Ex7D(-10,-29)] is similar in sequence to the ASO 10-27 of the Krainer group but with slightly different chemistry [72]. More recently, the same group has optimized a type of ASO, the phosphorodiamidate morpholino oligonucleotides (PMO). PMOs also promote exon 7 retention to levels that were high enough to rescue the phenotype in a severe mouse model of SMA after a single intracerebroventricular injection. Fourteen PMOs of varying lengths were designed to anneal downstream of *SMN2* exon 7. Efficiency was first studied *in vitro* in cultured fibroblasts from a type I SMA patient and later on it was confirmed *in vivo* after the lead compound rescued a severely affected mouse model actually with a single dose. Out of the fourteen assayed, PMO(-10-34) was identified as

the most effective compound for induction of SMN protein after two different *in vitro* delivery systems and this oligonucleotide was the one used for *in vivo* evaluation. They found that PMO(-10-34) gives the longest survival reported to date for this SMA mouse model [73].

Even though CNS treatment has been efficacious, a study by Hua *et al.* (2011) indicates that peripheral targets are also required to rescue the SMA phenotype using MOEs [64].

ISIS Pharmaceuticals has lead the first clinical trial for an ASO-mediated restoration of exon inclusion in a human disease (ISIS-SMN_{Rx}). Phase I has concluded. Intrathecal infusion of ISIS-SMNRx was well tolerated in SMA patients and experiments for future stages of the trial are ongoing [66].

Using ASOs can be advantageous for SMA therapy since their efficacy has been proven, they are very specific, cost-efficient, and minimally toxic. However, a down side of ASO-mediated approaches is that they require sequestration of a splicing cis-element. Because the majority of the human genome is transcribed, there is always a risk that an ASO could have off-target effects as well as unwanted interactions with proteins, both of which contribute to reduced antisense efficacy. Furthermore, there is a lack of clear knowledge with the optimal chemistry and the difficulty of repeat dosing [66, 68].

Another approach to using ASOs has been to redirect splicing by blocking the 3′ splice site of exon 8 and to inhibit the function of a negative splicing regulator within intron 6. The ASO targeting the 3′ splice site of exon 8 incorporated into U7 snRNA for

stable expression and increased exon 7 inclusion and SMN protein levels following delivery into SMA type-I patient fibroblasts using adeno-associated virus (AAV-5) [34].

1.5.2 Transplicing RNAs

The Lorson lab from the University of Missouri has proposed an alternative RNA therapy encompassing SMN trans-splicing. Trans-splicing requires a synthetic RNA (tsRNA) having three domains. The trans-spliced product is a chimeric mRNA that expresses functional FL-SMN. The first SMN tsRNA targeted intron 6 and replaced *SMN2* exon 7 with *SMN1* exon 7. SMN protein was augmented after AAV-2 delivery of this construct into a cell line. Next, the tsRNA vector was co-expressed with a short ASO designed to block the downstream splicing at exon 8 to promote a trans-splicing event. This was very effective in vivo with higher levels of the SMN protein in the brain and spinal cord of injected mice extending the lifespan about 70% [74-76].

There is a unique therapeutic candidate, Tetracycline-like compound, (PTK-SMA1), which is a synthetic small molecule compound that directly stimulates exon 7 splicing and increases SMN protein levels in vitro and in vivo in mice. PTK-SMA1 offers an alternative to antisense oligonucleotide therapies [77].

1.5.3 Gene Therapy

Gene therapy vectors are used to provide a continuous source of exogenous FL-SMN. Several groups have more recently used gene therapy to replace SMN with an adeno-associated virus (AAV)-based vector (scAAV9) delivered systemically intravenously, intrathecally or intracerebroventricular. This has already been tested in larger animals such as pigs and primates with results showing that delivery through the

vasculature, crossing the blood brain barrier, is able to transduce motor neurons at several levels of the spinal cord [31, 68]. Passini *et al.* (2010) treated SMAΔ7 mice with a single administration of a recombinant adeno-associated virus (AAV8) vector encoding hSMN into the CNS (cerebral lateral ventricles and upper lumbar spinal cord) and observed an elevation in expression of SMN in the spinal cord, which induced an improvement of pathology along with an increase in lifespan to 50 days in comparison to the average 14 days for non-treated mice. They also treated the mice with injections of a self-complementary AAV (scAAV) vector (recombinant virus having a double-stranded DNA genome) that results in earlier onset of gene expression leading to an increase survival of 157 days. They concluded that increasing SMN by AAV injections in the CNS is very efficient at improving both neuronal and muscular pathologies in a severe mouse model of SMA [78]. Gene therapy currently shows promising preclinical efficacy without vast toxic effects, it is a one-time treatment and problems with autoimmunity are not predicted. However, large amounts of viral doses are required thus it is not the safest approach [68]; also the delivery issue has long been an obstacle, because the blood brain barrier restricts delivery of therapeutics to the central nervous system (CNS), where an insufficiency of functional SMN has the most severe consequences [73].

1.5.4 Stem Cells

Numerous SMA studies have used fibroblasts from patients or immortalized non-motor neuron cell lines, but the possibility of using human SMA motor neurons generated from induced pluripotent stem cells (iPSCs) open new windows to further understand the pathology as well as to serve for accurate drug screening and therapeutic

efforts [79]. Stem cell therapy for many diseases including SMA is a compelling strategy of cutting edge research. However, more than functioning to replace motor neurons, stem cell research for SMA is promising in aiding the amelioration of the symptoms by providing trophic support to motor neurons [34]. iPSCs from skin fibroblasts of a young SMA patient were successfully differentiated into motor neurons expressing specific transcription factors and markers such as choline acetyltransferase (ChAT). This work by Ebert et al. (2009) opens the possibility that the underlying genetic defect can be repaired in vitro and then non-diseased cells in a state of pre-differentiation can then be transplanted into the SMA patient [79]. A leading group in stem cell research for SMA is that of Dr. S. Corti from the University of Milan (Italy). Corti and collaborators have rescued some of the pathological hallmarks and increased survival of SMAΔ7 mice after spinal cords were engrafted with primary neural stem cells from the spinal cord and embryonic stem (ES) cell-derived neural cell precursors. These cells exhibited mostly astrocytic but modest motor neuron characteristics. Mitigation of cell loss in the ventral horn suggests that the transplanted cells provided a neuroprotective effect. Furthermore, the stem cells secreted neurotrophic factors in culture and transplanted spinal cords had increased levels as well, thus the engrafted stem cells may be important to provide trophic support to motor neurons [38].

In a joint effort, a group led by H.S. Keirstead at the University of California (Irvin, CA) and the California Stem Cell Inc. (Irvine, CA), have also made use of stem cells as a therapeutic approach to treat SMA type I. They found that transplantation of human motor neuron progenitors (hMNP) from human ES cells into SMAΔ7 mice

improves muscle atrophy and significantly enhances the number of spared endogenous neurons following transplantation by counteracting the disease process through secretion of neurotrophic factors to delay the loss of motor neurons; thus corroborating the findings by the Corti lab. This group had previously determined an efficient method to differentiate human ES cells into high purity populations of human embryonic stem cell-derived hMNPs reported in Rossi *et al.* (2010) [80]. *In vitro* studies were initially performed to fully characterize the histopathology of the cell line. The hMNP line expressed high levels of Isl1, Hb9, NeuN and Tuj1, all of which are young motor neuron markers, as well as secrete and express the growth factors: NGF, VEGF, and NT-3 and 4. Their *in vivo* studies served to assess the efficacy of the hMNP therapy. The cells did survive and differentiate as expected. A third party GLP facility tested the safety of the hMNPs and delivery methods; the toxicology studies validated the safety of this approach [81, 82]. An option for improved *in vitro* modeling is the use of human ES cells, which permit genetic manipulation and expand indefinitely *in vitro*. ES cells can differentiate into any cell type, are amenable to genetic manipulation, and readily self-renew *in vitro*. Directed differentiation of ES cells into high purity populations of a defined cell type can be used to design effective treatments that are both cell and site specific; also they mimic early human development and processes leading to embryonic death. However, they can usually only model single gene diseases and are accompanied by serious social and political ethical debates for their use, thus limiting their potential for therapy, drug screening and disease modeling [81, 83].

More recently, Corti's group has genetically engineered iPSCs from SMA tissues to generate healthy motor neurons free from exogenous vectors and transgenic sequences. They achieved this by using nonviral, nonintegrating episomal vectors and then they used oligonucleotides to genetically correct *SMN2* to produce a functional *SMN1*-like protein. Motor neurons derived from genetically corrected SMA-iPSCs showed rescue of the disease phenotype. After transplantation into a severe SMA mouse model, corrected SMA-iPSC- derived motor neurons improved the disease phenotype. These results are very important for potential therapy by generating patient-specific iPSCs avoiding problems with immunity, toxicity and ethical issues that come with using embryonic stem cells [84].

1.5.5 SMA Drugs

Quinazolines have been proven to increase *SMN2* promoter activity, and its derivatives that cross the blood brain barrier, can increase SMN *in vitro* as well as extend lifespan and improve the phenotype of several SMA mouse models including SMNΔ7. Quinazolines are currently moving to phase I clinical trials. Oral bioavailability and positive safety results make quinazolines candidates for clinical trials [34, 68]. There are currently several C5-substituted 2,4-diaminoquinazoline derivatives under study. These compounds can increase SMN mRNA and protein levels and elevate gem number in treated SMA patient-derived fibroblast cell lines, and modestly increased survival in severe SMA mice. The molecular target of these compounds is DcpS, a scavenger RNA decapping enzyme. C5-substituted quinazolines robustly inhibit DcpS decapping activity. When C5-substituted quinazolines bind to DcpS, they force the enzyme into an

open conformation rendering it non-functional. The potency of *SMN2* promoter activation strongly correlates with DcpS enzyme inhibition [85]. One quinazoline assayed by several groups is RG3039 [86, 87]. Meerbeke *et al.* (2013) have investigated the effects of RG3039 in SMAΔ7 mice. Animals treated with RG3039 at 10 mg/kg/day showed increased weights, motor function, motor unit function and survival. This group found that RG3039 has an excellent CNS bioavailability *in vivo* and inhibits DcpS enzyme activity both *in vitro* and *in vivo*. However, the phenotypic benefit of RG3039 in SMAΔ7 mice does not appear to correlate with proportional increases of SMN protein expression or snRNP assembly despite some modest changes detected in FL-SMN transcript. Treatment with RG3039 produced even better results when given to $ChAT^{Cre}$ Smn^{Res} conditional SMA mice (described in more detail below in the section on SMA animal models), in which SMN expression had already been restored to motor neurons, thus this compound can have beneficial effects to improve motor neuron function. Recently, a phase I clinical trial was completed with preliminary data indicating good safety results in healthy volunteers [86].

Another group, led by Dr. Christine DiDonato, has pharmacologically characterized the effects of RG3039 on SMA neuromuscular pathologies using the Taiwanese and 2B/- SMA mouse models (described in more detail below in the section on SMA animal models). They determined that RG3039 increased lifespan and improved function in both mouse models, especially upon early treatment. To note, the increase in survival in the 2B/- mice was a very impressive ~600% over vehicle treated littermates. RG3039 treatment doubled the number of motor neurons containing gems

and increased the average number of gems/motor neurons. With their experiments, this group concluded that even though RG3039 modestly increased SMN levels in many tissues, it did nonetheless in motor neurons and redistributed the protein to the nuclear compartment [87].

Another group of compounds, histone deacetylase (HDAC) inhibitors, has shown promise in several models of neurodegeneration. Several different HDAC inhibitors are Food and Drug Administration (FDA) approved and they have been tested in SMA mouse models and in patients [32]. HDAC inhibitors can increase expression of genes by modifying chromatin structure. After cell-based drug screens several of these compounds were found to increase SMN in lymphoblastoid cell lines from SMA patients. HDAC inhibitors can activate the *SMN2* promoter and stimulate the inclusion of exon 7 thus increasing FL-SMN messenger RNA [41]. Trichostatin A (TSA) is an HDAC inhibitor that can augment both *SMN2*-derived transcript and SMN levels in neural tissues and muscle resulting in an increase in lifespan and improvement of symptoms in SMAΔ7 mice, especially when combined with nutritional support. Positive results were also obtained with sodium butyrate and valproic acid [34, 41]. Another HDAC inhibitor, suberoylanilide hydroxamic acid (SAHA), elevated SMN levels in two severe SMA mouse models resulting in an increase in their lifespan and amelioration of pathological symptoms [88].

TSA, sodium valproate and aclarubin are activators of the STAT5 (signal transducers and activator of transcription proteins) pathway, at least in SMA-like mice embryonic fibroblasts. The STAT5 pathway can increase SMN. Prolactin, a protein that

enables the production of milk and crosses the blood brain barrier, is also a potent activator of this pathway and serves as a potential treatment strategy [1]. Farooq *et al.* (2011) have shown that treatment with prolactin increases SMN levels, both *in vitro* and *in vivo* (wild-type (WT) and SMAΔ7 mice), via the transcriptional activation of SMN through the STAT5 pathway [1].

Sodium vanadate is capable of producing improvements in SMA. The problem is that vanadate can be toxic. One group has studied how combining sodium vanadate with L-ascorbic acid, which detoxifies vanadium, can circumvent the issues with toxicity and still yield positive results treating SMA mice. The combined treatment protected cells against vanadate-induced cell death and after a month of treatment, mice with late-onset SMA had a delayed disease progression, improved motor performance in adulthood, enhanced SMN levels and motor neuron numbers, and reduced muscle atrophy while achieving substantially decreased vanadium accumulation in these organs [89].

A downside to the SMA drugs out there is that in most cases these compounds were found by induction of SMN in patient fibroblast lines. Given that these are not motor neurons, it is plausible that these compounds do not induce SMN *in vivo* in the required cell types. This has been true for a number of molecules when tested in mice. Of the compounds reported to induce SMN in cultured cells, including some mentioned above, phenylbutyrate, hydroxyurea, valproic acid and Salbutamol have been taken to clinical trial without evidence of clinical benefit and produced only a modest effect [68].

In some cases, improvements in lifespan and neuromuscular pathology can also be obtained without necessarily incrementing SMN. For example, beneficial results were

seen after treating a mild SMA model with an inhibitor for Rho-kinase [34]. This is something that could also be considered during drug trials.

1.5.6 Others

In one study recombinant follistatin, an inhibitor of myostatin, modestly increased survival and gross motor function of SMAΔ7 mice. Even though rescue was not robust the importance of this is that enhanced muscle conditions may contribute to the maintenance or stabilization of an intact motor unit and that the possibility exists that motor neurons may require additional support for complete rescue. Thus, muscles could also be targets in conjunction to SMN-based approaches [90]. Lastly, the least invasive approach to therapy is exercise. A study by Grondard et al. (2005) demonstrated that physical exercise (running-based training) was successful at increasing lifespan, reducing muscular atrophy, enhancing motor neuron survival via neuroprotective effects, improving motor behavior, and increased exon 7-containing SMN transcripts in the spinal cord of type II SMA mice (mouse model by Hsieh-Li et al. (2000) [46], described further in detail in the section below on SMA animal models). They concluded that exercise employs its beneficial effects in some way by interfering with the splicing regulation of the *SMN2,* but whether or not this is a cause or consequence of neuroprotection was not eluded [91].

Table 1.1. Summary of some therapeutic approaches for SMA. **Adapted from Sumner (2007) [41] and Mercuri *et al.* (2012) [52]**

The problem	Therapeutic targets	Therapeutic approaches	Research and/or clinical trials completed or ongoing
SMN1 mutation	Replacement of SMN	Gene replacement therapy	-
Alternative splicing of *SMN2*	Inclusion of exon 7	Antisense oligonucleotides	New drugs developed by ISIS pharmaceuticals
Decreased FL-SMN transcript	Increased amounts of SMN transcripts	HDAC inhibitors, quinazolines, RG3039, aminoglycerides, albuterol and prolactin	Phenylbutyrate (randomized controlled trial) Valproate (randomized controlled trial) Hydroxyurea (randomized controlled trial) Albuterol (open-label and ongoing randomized controlled trial)
SMN protein deficiency	Stabilization of SMN	Indoprofen, proteasome inhibitors, polyphenols	-
Loss of motor neurons	Neuroprotection	Neurotrophic factors, stem cells	Gabapentin (randomized controlled trial), Riluzole (open-label), Olesoxime (TRO19622)
Clinical symptoms	-	Palliative care	-

1.6 INSIGHTS FROM DIFFERENT GENETIC ANIMAL MODELS

Many animal models have been generated to study the different aspects of SMA. They have all been useful to understand gene function, disease pathology, molecular mechanisms, and to test the possible targets for a cure; however, it is important to note that animal models available have not been able to fully recapitulate the SMA pathology observed in humans.

The complete absence of SMN production in *Caenorhabditis elegans* (in experiments with RNA interference [9]) results in embryonic lethality. When SMN is reduced, though not fully depleted, lethality is prevented but length in lifespan is hindered; there is also a block in the development of late larval stages, infertility, and most importantly a reduction in locomotor function.

In 2009, a genetic model for SMA was generated using zebrafish. Three mutations in *Smn1* were identified, all of which lead the zebrafish to exhibit presynaptic neuromuscular junction defects [7]. During embryogenesis, mutant axons in zebrafish grow abnormally with a reduction in size and numerous branches [9]. It is worthy to mention that SMA zebrafish motor neurons have been rescued from some of their defects when non-SMN-related snRNPs where reintroduced [23].

Drosophila has been used as a model to provide a basis for a better understanding of SMA. One study, by Dr. Brian McCabe's group, found that Drosophila *Smn* mutants have many of the pathological characteristics observed in the human SMA phenotype such as a reduction in muscle size, locomotive impairments, motor rhythm, and deficiencies at the neuromuscular junction and motor circuitry in general [92]. A very important finding for the field has also come from this group. They have attempted to restore SMN in either muscles or motor neurons. The phenotypes were not improved until SMN was restored to proprioceptive neurons and interneurons in the motor circuit to non-autonomously correct defects in motor neurons and muscles and lessen pathology. They have proposed that sensory-motor circuit dysfunction could be the origin of motor system deficits in the Drosophila SMA model [50, 92].

To identify additional potential therapeutic approaches, Artavanis-Tsaconas and collaborators have aimed at identifying genetic and biochemical interactors/modifiers of the Drosophila SMN homolog. This group has identified more than 300 candidate genes that alter an Smn-dependent phenotype *in vivo*. Amongst their important results, they have found that many of the genes are associated with RNA metabolism, however the majority found are not involved with the role of SMN in snRNP biogenesis but with transcription, post-transcriptional modifications, RNA transport, and translation regulation. Also, they identified functional links between *Smn* and the FGF pathway. This has been corroborated in a mouse model [93-95]. Using Drosophila as an animal model has allowed a genome-wide screen detecting specific genes that have a reduced expression in mutants and can be considered novel targets for up-regulation and restoration of expression to counteract the pathology, as well as proteomic studies and bioinformatic analyses to define a unique SMN interactome.

SMA mouse models have been invaluable for understanding the underlying mechanisms of this pathology since the basic elements of the NMJ structure and function are evolutionarily conserved between humans and mice [96]. SMN mutant mice have been widely used to determine the tissue-specific role of the SMN protein by both selective SMN rescue and depletion experiments. Several transgenic mice have been produced to model SMA with varying levels of severity. One of many reasons that mouse models are good subjects for SMA is that in the mouse *Smn,* which produces only the full-length SMN, the sequence at the putative ESE is a perfect match to human *SMN1* over a 15 bp stretch [11, 97]. In several mouse models it seems that most NMJs

develop at a slower rate but quite normally compared to controls, thus this SMN related defect would not be the main developmental defect in SMA [8]. Some of the mouse models are detailed herein.

The mouse model that expresses the most severe form of SMA, surviving to only P5 at best, has the endogenous mouse *Smn* gene completely knocked-out but expresses small amounts of SMN due to an insertion of the human *SMN2* gene to avoid embryonic lethality and test the hypothesis that human *SMN2* acts as a disease modifier (*Smn*$^{-/-}$*; hSMN2[89Ahmb]*$^{+/+}$) [44]. These mice are viable at birth but develop a severe muscle paralysis and die within the first postnatal days when they carry one or two copies of the transgene [10, 44] or can reach adulthood if they carry eight copies of the transgene [44, 96]. The motor neurons of these mice develop normally and do not show defects in motor axon formation or axonal branching but they do have signs of denervation even at embryogenesis [5, 98]. Motor neurons cultured from these animals have decreased axonal length and reduced growth cone size, and reduced levels of β-actin at the growth cone [98]. Reduced levels of SMN in this mouse model yield impaired perinatal brain development. For example, the hippocampus presents decreased cell density, reduced cell proliferation and impaired neurogenesis [99].

Until 2013, no physiological study had been performed on the Tibialis Anterior (TA) muscle of these mice. Boyer *et al.* determined that mutant P2 TA muscle preparations produced 67% lower peak tetanic force than control littermates, indicating that muscle weakness is an early defect, and mutant P5 TA muscle preparations have 47% less twitch force and 39% less maximum peak tetanic force than controls; they also

have an inability to recover from induced muscle fatigue over time [100]. These severe SMA mice have been considered a suitable model since SMA is characterized by a reduction in SMN production rather than a complete absence. However, their short lifespan limits the breath of their pathological assessment. The idea for this model came from a previous study by Monani *et al.* (1999) [11] that proved the unprecedented similarity between *SMN1* and *SMN2*. This is the animal model used for Aim 1 reported in Chapter II of this dissertation. A very similar mouse model also emulating severe SMA was made by Hsieh-Li *et al.* (2000) a group in Taiwan, hence the common name "Taiwanese mouse model". This mouse carries the null allele $Smn^{-/-}$ due to targeted replacement of *Smn* exon 7 ($Smn1^{tm1Hung}$) with the hypoxanthine phosphoribosyl-transferase (HPRT) cassette. It also carries copies of the human *SMN2* allele [*Tg(SMN2)2Hung*]. This was done initially to elucidate the roles of human *SMN1* and *SMN2*. Transgenic mice with a 115-kb genomic DNA fragment including the *hSMN2* region, part of centromeric *NAIP*, and intact centromeric *SERF1* were crossed to the *Smn* mutant mice [46]. These mice survive perinatally but exhibit SMA symptoms ranging from mild to early death even within the same litter, an observation of familial variance not frequently found in SMA patients [46, 96, 101]. Severe SMA pups die within the first week post birth, intermediate pups die by 12-17 postnatal (P) days, and mild SMA mice (carrying four copies of the *SMN2* transgene) have a much longer lifespan but present muscle weakness and a short thick tail that becomes necrotic and falls off by 1 month of age with potential for foot and ear necrosis later on in life [101]. Although there are some differences between the studies reported by Monani *et al.* (2000) and

Hsieh-Li *et al.* (2000), the most important finding through these two similar models is that *SMN2* serves to compensate the absence of *Smn*, avoiding embryonic lethality, and that copy number is inversely proportional to disease severity [13].

Le *et al.* generated a set of mice in 2005 that model severe SMA termed the SMAΔ7 mice (*Smn*$^{-/-}$; *SMN2*$^{+/+}$; SMNΔ7$^{+/+}$). These mice are able to survive longer with an average lifespan of about 2 weeks. They have the same characteristics of the severe ones described above and in addition possess cDNA from the *SMN* locus lacking exon 7 (SMNΔ7) to resemble the functional protein contribution that can be obtained from a copy of the *SMN2* gene. The SMNΔ7 cDNA was initially introduced to assess its potential toxicity since there was evidence stating that over-expression of SMNΔ7 in neurons was pro-apoptotic [6]. These mice have a milder phenotype due to the formation of heterologous complexes between FL-SMN and SMNΔ7 that stabilize SMN by increasing the amount of oligomeric SMN [6, 96]. However, even in SMA mice transgenically expressing extremely high levels of SMNΔ7 transcript, the protein is measurable at only low levels [35]; therefore the truncated protein does not rescue from a severe phenotype. These SMAΔ7 mice were generated by taking cDNA lacking exon 7 and placing it under control of a 3.4kb SMN promoter fragment and this was then inserted into fertilized oocytes of FVB/NJ mice. These mice were later crossed with mice having human *SMN2* and a mouse-*Smn* knockout allele [6]. This engineered mouse exhibits a progressive loss of motor function and behavior, resembling severe SMA in humans [102], and has been found to recapitulate, to some extent, the SMA pathology at the level of neuromuscular junctions as well. These mice present a modest loss of motor

neurons, around P13, and proprioceptive neurons but have a significant early impairment of motor behavior that precedes motor neuron loss; thus, the first behavioral abnormalities are most likely due to impairments in motor neuron function [40, 51, 55, 103]. They also show defects in synaptic transmission with an approximate 50% reduction in quantal content [30] along with a very drastic synapse number reduction in the sensory-motor connection between proprioceptive sensory neurons and motor neurons [51]. Ling *et al.* (2011) evaluated neuromuscular junctions in about 20 muscles of the SMAΔ7 mice and found that neuromuscular denervation in vulnerable muscles was widespread consistent with the expected pathology in SMA [104]. In this mouse model, the muscle that is most severely affected, in terms of functionality, is the transversus abdominis [9]. Interestingly, almost all the NMJs in the hindlimb muscles are innervated and capable of neurotransmitter release though some structural abnormalities are present; thus, part of the pathology observed in the SMA phenotype could instead be due to a significant reduction in central synapses, especially in proprioceptive inputs in L3-L5 innervating distal muscles [51]. Another characteristic of SMAΔ7 mice is that there is delay in the loss of polyneuronal innervation of some anterior muscles [40]. It is important to note that SMAΔ7 mice may suffer from bradycardia by P2 even before the onset of some neuromuscular symptoms [61].

A variation to SMAΔ7 is the SMAΔ7-like mouse. This mouse carries a conditional inducible mutant allele Smn^{res} floxed by Lox-P sites that can be reverted to a WT functional allele upon Cre-recombination. The Smn^{res} differs in that it has an inverted. 3' to 5', translationally silent, mouse *Smn* exon 7 in the intron between human

SMN2 exon 7 and 8. This mutant allele only produces transcripts coding for the truncated SMNΔ7 protein. SMAΔ7-like mice present many of the same pathological characteristics as the SMAΔ7 mice. They only survive 2 weeks on average, are unable to gain weight and thrive, have impaired motor behavior, structural and functional NMJ defects, NF accumulation, immature and small AChRs, progressive loss of motor neurons in the L1 segment (60% loss by end-stage of disease), small muscles and myofibers, NMJs with reduced evoked endplate current (EPC) amplitudes, reduction in the probability of synaptic vesicle release, and disruptions of central motor neuron synaptic inputs among others [56, 57]. SMAΔ7-like mice serve as a good model to determine cell-specific roles in SMA since the mutant allele can be conditionally reverted to WT in an individual subset of cells. This is the mouse model used in Aim 2 reported in Chapter III of this dissertation and will be explained in detail further along.

There is one type of mouse model that can survive much longer, even over a year, (average 227 days with one copy of the transgene) generated by Monani *et al.* in 2003 ($SMN2^{+/+}$; $Smn^{-/-}$; $SMN1(A2G)^{+/-}$). The authors used a cDNA carrying an A2G mutation under a 3.4-kb SMN promoter fragment that was later microinjected into fertilized mouse oocytes. The mice produced were crossed to low copy *SMN2*, $Smn^{-/-}$ mice. Double transgenic *SMN A2G*;$SMN2^{+/+}$;$Smn^{-/-}$ mice were interbred or crossed to $SMN2^{+/+}$;$Smn^{-/-}$ animals to obtain mice carrying 1 to 2 copies of *SMN2* plus the mutant transgene while lacking mouse *Smn* (*SMN A2G*;$SMN2^{+/+}$;$Smn^{-/-}$). The A2G transgene delays the onset of motor neuron loss thus rendering a milder phenotype. Their experiments demonstrated that mice of this genotype had the same phenotype as SMA

type III with muscle atrophy and motor neuron degeneration but with restored SMN in motor neurons, evidenced by immunocytochemical staining showing the presence of gems in the spinal cord. To note, mice with only one copy of *A2G* are significantly smaller than WT littermates and display a reduction in activity. Homozygosity of the *A2G* transgene renders a milder phenotype and has extended the survival of some mice up to at least 15 months. SMN A2G is unable to efficiently self-associate, the A2G transgene forms higher order SMN complexes only when it is in the presence of low levels of full-length SMN. However, the *A2G* mutant transgene was not capable of avoiding embryonic lethality in the absence of *SMN2* indicating that mutated SMN needs to be expressed in the presence of small amounts of FL-SMN to achieve phenotypic modification [37].

With one approach to reduce *Smn* levels, a mouse model was created by knocking-in the $Smn^{2B/-}$ allele, akin to *SMN2*, that disturbs endogenous *Smn* splicing resulting in the production of *Δ7Smn* mRNA. When the $Smn^{2B/-}$ allele is present with the null allele it gives rise to a mouse with a more moderate severity of SMA (mean lifespan of 28 days). The $Smn^{2B/-}$ allele has mutations (3 nucleotide substitutions) within the exonic splicing enhancer exon 7 of the endogenous *Smn* gene. Even though they are indistinguishable from controls at birth, by two weeks of age $Smn^{2B/-}$ mice start exhibiting symptoms of pathology and by the third week are significantly smaller than WT littermates. $Smn^{2B/-}$ mice present the characteristic pathological hallmarks of SMA observed in patients and mild mouse models such as muscle weakness (one study found that P9 TA muscle preparations produced 61% lower peak tetanic force than control

littermates, placing the weakness in evidence [100]), gait abnormalities, weight reduction, loss of lower motor neurons from the brain stem and spinal cord (around P21), pre-synaptic neurofilament accumulation, and denervation alongside post-synaptic shrinkage and abnormal endplate morphology. These mice have a significantly lower ratio of full-length *Smn/Δ7Smn* transcript while protein expression is reduced ubiquitously [96, 97, 105, 106]. There is a modification to this $Smn^{2B/-}$ allele, the Smn^{2B-Neo}, that when found homozygous causes embryonic lethality because of a *loxP*- flanked *neomycin (neo)* gene resistance cassette that impedes normal *Smn* expression. $Smn^{2B-Neo/2B-Neo}$ embryos die by E9 due to very low levels of SMN [107, 108]. In the presence of Cre recombinase, the embryonic lethality can be rescued by excision of the floxed neomycin cassette allowing for postnatal survival. Using a tamoxifen-inducible Cre line embryonic lethality can be rescued but only if it is early in gestation [108]. By breeding one copy of *SMN2* to an $Smn^{2B-Neo/2B-Neo}$ background protein levels were increased and embryonic lethality was prevented. However, these pups present a similar symptomatology as other severe SMA mouse models such as reduced survival and weight gain, diminished motor function with paralysis by P5, bradycardia, loss of sensory-motor synapses, motor neuron hyperexcitability and excess synaptic activity, and autonomic defects [107].

Frugier *et al.* (2000) from the Judith Melki Lab (France) generated mice carrying a deletion of *Smn* exon 7. The deletion was directed to neurons using the Cre–*loxP* system ($Smn^{f7}/Smn^{\Delta 7}$; $NSE\text{-}Cre^{+}$). These mutant mice exhibit a rapid motor deterioration and neurogenic atrophy of skeletal muscle leading to complete paralysis and death at ~ 4

weeks. They do, nonetheless, have a normal neuronal density in the spinal cord [109]. Cifuentes-Diaz *et al.* (2002) later used this neuronal mutant mouse model and observed a dramatic and progressive loss of proximal motor axons (up to 78% reduction) with only a mild loss of motor neuron cell bodies [58]. The Melki group also generated a muscle-specific Smn mutant ($Smn^{f7}/Smn^{\Delta 7}$; *HSA-Cre*$^{+}$). These are $Smn^{f7}/^{\Delta 7}$ mice with Cre-*loxP*-mediated deletion of *Smn* exon 7 in myoblasts and post-mitotic fused myotubes of skeletal muscle. *HSA-Cre*$^{+}$ mice survive approximately one month [54]. These two models from the Melki lab with tissue-specific complete ablation are not considered adequate SMA mouse models. Although muscle as well as neuronal knock-out mice do develop the SMA phenotype it is not surprising because SMN is essential to cell survival, and these mice were engineered so that the protein was abolished rather than reduced as it is in the human disease; SMN levels that are too low such as in the cases here induce cell death by disrupting the constitutive cellular function of SMN. Additionally, the nerve-targeting experiments abolished SMN indiscriminately in all neurons. In summary, these mice do not appropriately mimic the human SMA pathology nor provide complete or precise knowledge into motor neuron vulnerability [19, 96].

A potentially better mouse model was engineered later on by Park and collaborators (2010) in which endogenous *Smn* was conditionally depleted in motor neuron progenitor cells by *Cre-loxP* targeting of the *Smn* exon 7 in the spinal cord; the Cre cassette was knocked into the locus of the motor neuronal progenitor expressing *Olig2* gene. They used mice with the null *Smn* allele allowing them to produce heterozygotes with a floxed *Smn* allele on one chromosome and the null allele ($Smn^{F7/-}$)

on its homolog. SMN was not completely ablated because the mutant model includes copies *SMN2 (Olig2-Cre;SMN2;Smn$^{F7/-}$)*. Their experiments did confirm that *Olig2-Cre*-mediated recombination was specific to spinal motor and not sensory neurons. Through this approach about 70% of their mutant animals survived a year but were still clearly distinguishable from controls. By P2, these mice exhibited the SMA-like symptoms of reduced size and muscle mass, kyphosis of the spine, and significant weakness (determined by grip strength and the open field assay); however, some of these symptoms mitigated over time. By late-stage in the disease they observed a significant loss of cervical and lumbar spinal motor neurons. The authors concluded that SMA is likely a cell-autonomous consequence of reduced SMN in spinal motor neuron progenitors since depletion of SMN selectively in these cells was sufficient to cause SMA pathological hallmarks such as atrophic muscle fibers. The milder than expected phenotypes observed in these mice is probably due to the of the presence of SMN in tissues other than motor neurons thus lessening the phenotype directly or even indirectly by providing trophic support to the motor neurons slowing down disease progression [19].

1.7 RESTORATION HYPOTHESIS

Even though the role of SMN in assembly of the spliceosome has been extensively studied, the pathologically relevant cellular site of action is still unclear. A properly assembled spliceosome complex is vital for the normal functioning of all cells, thus it's puzzling why the SMA pathology is expressed more significantly in motor neurons and the skeletal muscles they innervate when the disruption of a housekeeping

gene should affect the entire organism and not so selectively. Extensive research has been performed attempting to elucidate which tissues are more directly susceptible to reduced levels of SMN and how that leads to the primary symptoms of SMA. The existing mouse models for SMA have been engineered to express the phenotype observed in patients. Nonetheless, it has not yet been elucidated whether the problem in SMA is cell autonomous or not. The main dogma in SMA research is that motor neurons are the cells most affected by the paucity of SMN because:

i) SMN might have a specific function in these cells that is not as essential in others. When said function is disrupted it could impair neuronal growth and differentiation [16].
ii) There is a very intrinsic property of motor neurons that makes them more susceptible.
iii) They have a higher demand for small nuclear ribonucleoprotein assembly and messenger RNA processing [41].
iv) Inefficient small nuclear ribonucleoprotein assembly could cause inappropriate splicing of vital motor neuron-specific messages.
v) Motor neurons lack a compensatory mechanism.

We have hypothesized that if motor neurons are indeed the key cells responsible for the SMA phenotype, then selective restoration specifically in these cells should have a critical impact on survival and ameliorate the characteristic symptoms.

1.8 JUSTIFICATION

It is widely known that different restoration efforts in mouse models have produced vast improvements in their SMA pathology and even increased lifespan significantly. For example, pan-neuronal expression of SMN in severe mutant mice (*Smn*$^{-/-}$; *SMN2*$^{+/+}$) increased the lifespan of mutant animals up to approximately 210 days [110]; SMAΔ7 mice treated with CNS or peripherally-directed viral vectors expressing SMN also greatly increased the lifespan between 50 to 200 days [78, 111]; and both CNS and peripherally-delivered oligonucleotides correcting the exon skipping defects in *SMN2* functioned to improve lifespan past 100 days [64, 72]. However, those approaches fail to elucidate precise cell specificity.

Patients have particularly low levels of spinal cord SMN [11] and motor neurons are the cells that exhibit vast pathology and appear most affected by the loss of this ubiquitous protein. Furthermore, muscle-specific SMN restoration does not improve lifespan [110] ruling it out as a primary target, and though the genetic reduction of SMN solely in motor neurons does not cause lethality it does yield the SMA pathology (such as NMJ structural and physiological abnormalities) [19, 55, 107]. Thus, motoneuronal-specific SMN restoration is a logical approach to both understand the basic mechanisms underlying SMA and to develop therapeutic strategies for site-specific delivery of SMN in motor neurons of SMA patients. However, it is important to highlight that during the course of this research, two independent groups attempted a motoneuron-specific restoration of SMN in SMA mouse models. These two groups reported on improvements or complete rescue of several signs of SMA pathology but achieved only a modest

increase in lifespan. These results contribute to the growing body of evidence that SMA may not be a cell-autonomous disorder and that motor neuron rescue is critical though not sufficient for significant increases in lifespan [57, 107].

In our study we have aimed at determining whether or not SMA is a cell-autonomous disease as well as to have a better understanding of the role that motor neurons have in the SMA pathology. We used two strategies, each with a different mouse model, to restore the SMN protein (exogenously or endogenously) selectively in α-motor neurons of the ventral horn of the spinal cord by means of the *Hb9* promoter. First, we tested restoring human SMN expression driven by the motor neuron specific promoter *Hb9* in transgenic animals generated in our lab. We determined whether crossing them to severe SMA mice, which die perinatally, would rescue survival. Our results indicate that in spite of detecting the presence of transgenic human SMN, inheritance of the transgene was insufficient to increase the survival of severe SMA mice (mean lifespan ~ 1 day). However, the transgene does allow for the expression of a stable SMN protein with a long turnover that was capable of significantly reducing neonatal mortalities in transgene-positive control mice and possibly improving motor function at an early time point. These experiments are described in Chapter II of this dissertation.

In the second approach we have attempted to restore endogenous motoneuronal-SMN expression following prenatal *Hb9*-dependent Cre recombination of a conditional hybrid mutant allele (Smn^{res}) in another severe SMA mouse model (SMAΔ7-like). Cre recombination irreversibly transforms the Smn^{res} allele to WT. We confirmed that

recombination of the conditional allele occurs exclusively in the spinal cord. Yet, mean lifespan, weight loss, and motor behavior did not significantly differ between our rescue and mutant mice. Another group performed similar motoneuron-selective rescue experiments of SMAΔ7-like mice. Though increase in lifespan was modest, they found improvements in SMA neuromuscular junction (NMJ) phenotypes by using a choline acetyltransferase *(ChAT)-Cre* driver to rescue the inducible allele [57]. We found that our *Hb9-Cre* driven SMN expression is significantly lower than the *ChAT-Cre* driven SMN in their rescue model, likely explaining the difference in phenotype between our and their mouse lines. However, like in ChAT(Cre^{+})SMA mice, we detected rescue of NMJ size and innervation status in denervation-susceptible muscles. Our results indicate that our *Hb9-Cre* driven SMN expression is insufficient to improve survival but sufficient to rescue two NMJ structural parameters very sensitive to changes in motoneuronal SMN levels. These experiments have been published (Paez-Colasante *et al.* (2013) [56]) and are described, with additional supporting results, in Chapter III of this dissertation.

CHAPTER II

RESCUE OF A SEVERE SMA MOUSE MODEL WITH TRANSGENIC HUMAN SMN RESTORATION DRIVEN BY THE MOTOR NEURON-SELECTIVE *HB9* PROMOTER

2.1 SYNOPSIS

Spinal muscular atrophy (SMA) is a common neuromuscular disorder in humans characterized by the loss of α-motor neurons and atrophy of their target muscles. SMA is caused by mutations in the *SMN1* gene that reduces the SMN protein to subnormal levels. Restoring levels of SMN in SMA animal models is perceived to be a viable therapeutic option. Since motor neurons are the cells most affected, we report on an attempt to restore human SMN selectively in motor neurons by driving its expression with the motor neuron-selective *Hb9* promoter. We have assessed whether their crossing into a severe SMA mouse model, which dies perinatally, could extend their survival and rescue their SMA-like phenotype. At the protein level, transgene expression was detected by immunostaining in embryos and until at least postnatal day (P) 6 in the ventral horn of the spinal cord. Expression of human SMN was specifically detected in spinal cord but not skeletal muscle by Western blot. Nonetheless, transgenic *hSMN mRNA* expression was undetected by late embryogenesis. Thus, slow protein turnover appeared to account for the detection of transgenic protein postnatally, despite the failure to detect transgenic mRNA prenatally. This result likely explains why hemizygous inheritance of the transgene was insufficient to increase the survival of severe SMA

mice, as both transgene-positive and transgene-negative animals survived only to P1 on average.

2.2 INTRODUCTION

SMA is a leading genetic cause of infant and early childhood mortality [2, 4, 5]. It is a recessive disorder resulting in degeneration of motor neurons and severe atrophy of their target muscle due to the paucity in SMN protein production [5, 28]. The protein SMN functions mainly in the assembly of the spliceosome in all cells [8, 103] and is encoded, in humans, by *SMN1* and *SMN2* [11]. These genes lie adjacent to each other and are almost identical except by one key nucleotide, a C-to-T transition in exon 7, which alters an exon splice modulator [1, 28, 33]. This single nucleotide causes the majority of the transcript from the *SMN2* gene to lack exon 7 (SMNΔ7), whereas *SMN1* produces full-length SMN transcripts [8, 28, 35]. Mutations in *SMN1* cause SMA, while the *SMN2* gene is retained [2, 8, 35, 37]. The protein SMNΔ7 does not oligomerize efficiently and is rapidly degraded, thus causing a reduction in SMN levels, which are insufficient for the correct function and survival of motor neurons [8, 28]. The phenotypic severity of SMA is modulated by how many copies of *SMN2* are present [14, 40, 44].

The existing mouse models for SMA have been engineered to express the phenotype observed in patients. Nonetheless, it has not yet been elucidated whether the problem in SMA is motor neuron-cell autonomous or not. Extensive research has been performed attempting to elucidate which tissues are more directly susceptible to reduced

levels of SMN and how that leads to the primary symptoms of SMA. For many years in the SMA field, the dogma has been that motor neurons are the most susceptible cells to the SMA pathology and thus are the first ones in need of rescue to ultimately stop the overt pathology progression. Reduction of SMN selectively in motor neurons is enough to yield some features of the SMA phenotype in mice [19]. If the dogma is accurate, selective SMN restoration in motor neurons should greatly ameliorate the pathological hallmarks. To test this hypothesis, we have attempted to restore human SMN expression driven by the motor neuron specific promoter *Hb9* in transgenic animals generated in our lab. We determined whether crossing them to severe SMA mice ($Smn^{-/-}$; $SMN2^{+/+}$), which die perinatally (described in Chapter I), would extend the survival of these short-lived animals.

Hb9 is a homeodomain transcription factor in the central nervous system vastly motoneuron specific [112]; it is composed of 3 exons (6 kb) with an open reading frame of 1206 nucleotides coinciding with a diverged homeodomain [113]. We are using an *Hb9* promoter because previous data has clearly demonstrated that *Hb9* is mostly specific to motor neurons and widely conserved in vertebrates, making it a useful marker for motor neuron phenotype and a tool to assess the function of motor neurons in SMA. The *Hb9* gene is properly activated in newly formed spinal motor neurons but not in adjacent cell populations in the developing spinal cord. *Hb9* functions to sort the different classes of motor neurons along the spinal cord and for their axons to extend to their appropriate pathways [114]. This transcription factor is also found in V2 interneurons though more modestly than in motor neurons. The progenitor cells of motor

neurons and V2 interneurons express a similar profile of genetic markers meaning that pathways in the specification of these neurons are closely related but *Hb9* serves to separate the identities of these two during development; furthermore, *Hb9* suppresses interneuron genetic programs and facilitates the development of normal patterns of motor neuron connectivity [114], thus it is useful to distinguish between motor neurons and interneurons [114, 115]. Mice and chick embryos with null mutants of *Hb9* have deficiencies in motor neuron development and these motor neurons aberrantly express genes ordinarily restricted to V2 interneurons. Also, proper cell fate specification in the spinal cord is dependent on the exclusion of *Hb9* from neighboring interneuron populations [114]. Boon *et al.* (2009) used zebrafish to test the role of motor neurons by restoring SMN specifically in these cells and determining if there was a rescue of phenotype in terms of synaptic vesicle protein, SV2, quantification. SMN was restored to motor neurons by expressing SMN through the *Hb9* promoter. Their experiments demonstrated that their mutant zebrafish with decreased SV2 expression were rescued when normal SMN levels were restored. Boon and co-authors not only demonstrated that SMN is vital for the maintenance of SV2 in presynaptic terminals, but most importantly that restoration of human SMN with an *Hb9* promoter is a viable strategy [7].

To exogenously restore SMN, transgenic mice were previously generated by our group to selectively express the human SMN (hSMN) protein in motor neurons by means of the motor neuron promoter *Hb9*. In the design, a murine *Hb9* promoter was inserted upstream of an expression cassette containing human *SMN1* cDNA, an internal ribosomal entry site (IRES), and enhanced green fluorescent protein (EGFP). The single

mRNA produced here yields hSMN and EGFP as separate proteins so the presence of EGFP indicates the existence of hSMN in tissues, *i.e.*, GFP is a marker or proxy gene (Fig. 2.1). The green fluorescent protein (GFP), from the jellyfish *Aequorea victoria*, is an autofluorescent protein that is a widely used reporter in gene expression and protein localization studies. The emission of GFP does not require any cofactors or substrates. The fluorescence of GFPs is dependent on the key sequence Ser-Tyr-Gly. Enhanced GFP (EGFP) contains mutations of Ser to Thr at amino acid 65 and Phe to Leu at position 64 and is encoded by a gene with human optimized codons [116]. The plasmid pHISG with the transgenic construct, denominated herein as *Hb9(hSMN/Gfp)*, was inserted into zygotes of an FVB background after three rounds of pronuclear injections yielding two transgenic lines, line 151 and line 4 (Rimer *et al*; unpublished).

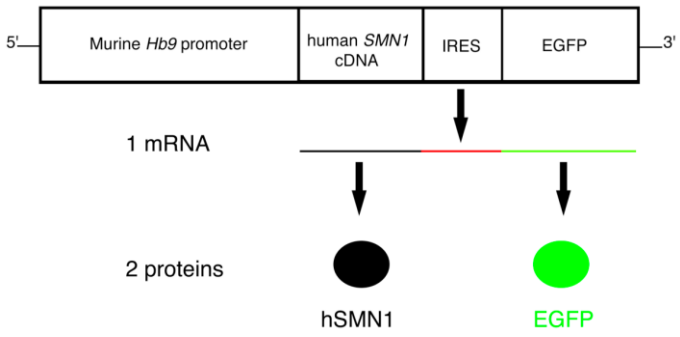

Fig. 2.1. Transgenic construct. Standard molecular cloning techniques were used to produce a transgenic construct with murine Hb9 promoter upstream of an hSMN1-IRES-EGFP expression cassette. This construct was introduced into zygotes of FVB background through pronuclear injection (Rimer *et al.*, unpublished).

Previous experiments performed by the lab (M.J. Rimer, *unpublished*) determined that only line 151 mice strongly expressed the *hSMN* transgene during embryogenesis (embryonic (E) day 13.5) and after birth. Expression was detected by immunostaining in embryos and until at least postnatal day (P) 6 in the ventral horn of the spinal cord. It was concentrated in motor neurons, with weaker staining in medial ventral interneurons (Fig. 2.2).

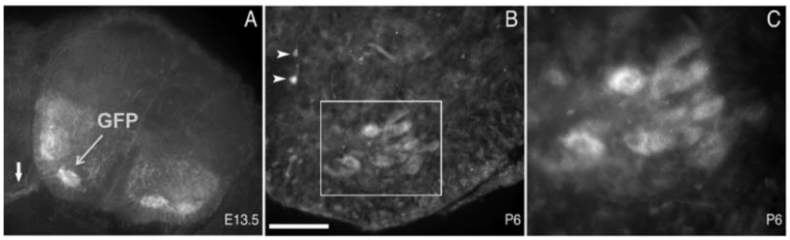

Fig. 2.2. GFP expression in the ventral horn of the spinal cord. Both transverse sections of whole E13.5 (**A)** embryos and spinal cords from P6 neonates (**B,C)** were fixed in PFA, blocked with goat serum and stained with a polyclonal antibody against GFP. **A.** GFP expression restricted to the ventral half of the cord. Short arrow points to staining in ventral roots. **B.** Staining was detected in large cells in the ventral horn (rectangle). Arrowheads point to two GFP^{+} interneurons **C.** Higher magnification of selected area (rectangle) in **B** (Rimer *et al*., unpublished).

To study the presence and localization of hSMN, a monoclonal antibody specific for hSMN (a kind gift from Drs. Adrian Krainer and Yimin Hua, Cold Spring Harbor laboratory, NY), along with anti-GFP, were used to label cross sections of P6 spinal cords of *Hb9-SMN1* mice. hSMN/GFP co-localized to the nuclei of spinal cord extracts in aggregates that are presumably the "gem" nuclear structures described by Liu and Dreyfuss 1996 [26]; Coady and Lorson, 2011 [8] (Fig. 2.3).

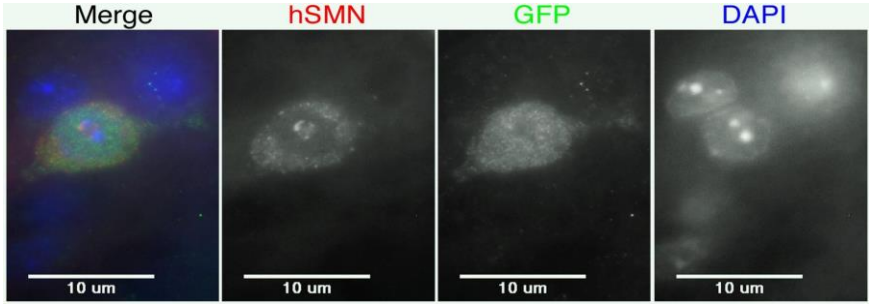

Fig. 2.3. Co-localization of hSMN and GFP proxy marker in motor neurons. Cross sections of P6 spinal cords were incubated ON in monoclonal Ab (1:50) anti-hSMN and in polyclonal Ab (1:500) anti-GFP. The secondary antibodies used were rhodamine-goat anti-mouse and fluorescein-donkey anti-goat to detect hSMN and GFP seen in the merge image as red and green, respectively.. GFP/hSMN co-localized to nuclei of one motor neuron in the ventral horn. Structures resembling gems within the nucleus are hSMN+. (Rimer *et al*., unpublished).

The transgene was indeed found to be selective for motor neurons. Co-localization of hSMN/GFP was found explicitly in the motor neurons of the ventral half of the spinal cord. SMN puncta, indicating gems, were also observed (Fig. 2.4).

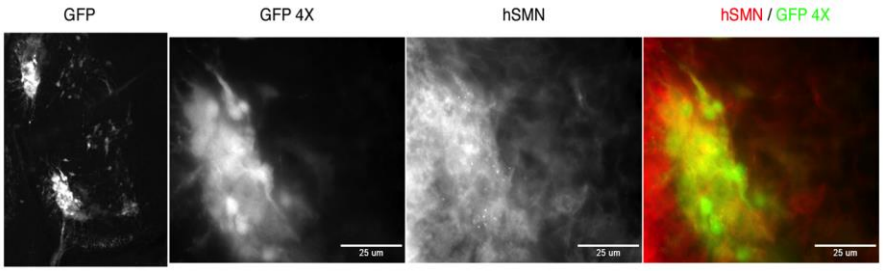

Fig. 2.4. hSMN and GFP expression in spinal cord from Hb9-SMN mice. Cross sections of E13 embryos stained with anti-human SMN monoclonal Ab (1:10) and in anti-GFP polyclonal Ab (1:500). Strong transgene expression in cells in the ventral horn observed. Human SMN puncta staining restricted to GFP-expressing cells seen in the color merge from the rightmost panel. The image from the leftmost panel was taken with a 10X objective and the images of the rest of the panels were taken with a 40X objective (scale bar: 25μm) (Rimer *et al*., unpublished).

Western blots were also used to determine the tissue specificity of SMN detected with the hSMN antibody in early postnatal tissue. The transgene was expressed in spinal cord but not skeletal muscle (Fig. 2.5).

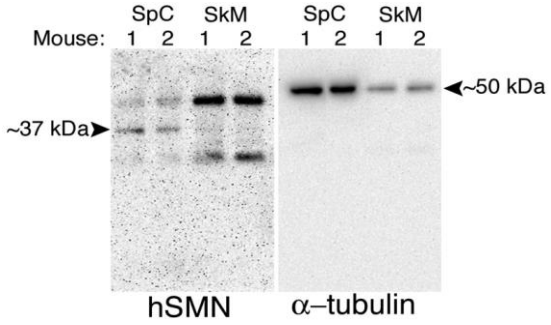

Fig. 2.5. Expression of hSMN in P6 spinal cord (SpC) and skeletal muscle (SkM) extracts from *Hb9(SMN/Gfp)* mice. Western blot: Equal amounts (50μg total protein) of extracts were fractionated in a 12.5% acrylamide gel, which was then transferred to a nylon membrane. *Left: Entire membrane blotted for hSMN shows essentially one band of the expected molecular weight (~37kDa) in spinal cord (SpC) but not in skeletal muscle (SkM) extracts. Two, non-specific bands were detected in SkM. *Right: The same membrane was stripped and re-probed for mouse α-tubulin to check for loading.

After confirming the presence and tissue specificity of the transgene, *Hb9(hSMN/Gfp)* mice were crossed to another set of mice carrying a mutation in *Smn* yielding a null allele ($Smn^{+/-}$). Homozygous inheritance of the null allele is embryonic lethal in mice [5, 40]. To prevent embryonic lethality, these mice harbor human *SMN2*, though the presence of *SMN2* is not enough to prevent the appearance of the SMA pathology. Thus, this is the most severe SMA mouse model (genotype: $Smn^{-/-};SMN2^{+/+}$), which dies perinatally due to the lack of functional full-length SMN (detailed in Chapter I) [44]. Mice from this cross that were heterozygous for both murine *Smn* and the *hSMN* transgene, (detected with a genomic PCR for *Gfp*), as well as homozygous for *SMN2*

(annotated as $Gfp^{+/?}$; $Smn^{+/-}$; $SMN2^{+/+}$) were crossed to transgene-negative mice ($Smn^{+/-}$; $SMN2^{+/+}$) to produce a fraction of progeny carrying the homozygous null *Smn* allele with our transgene (i.e., $Gfp^{+/?}$; $Smn^{-/-}$; $SMN2^{+/+}$).These were the experimental mice, used alongside controls, in our procedures.

Here, we aimed to rescue perinatal mortality and increase the lifespan of severe SMA mice. We assessed the survival of our experimental mice and the effects of the transgene on control animals as well. Our results indicate that hemizygous inheritance of the transgene was insufficient to increase the survival of severe SMA mice. We carried out these experiments because we detected transgenic protein at later times than P1, the mean survival time of the severe SMA mice used here (Figs. 2.2-2.5, above). However, on experiments conducted later on we were unable to detect transgenic mRNA at E18, just prior to birth. These results suggest that slow protein turnover may explain our transgene expression results.

2.3 MATERIALS AND METHODS

2.3.1 Ethics Statement

Care and treatments of all animals followed the National Institutes of Health Guide for the Care and Use of Laboratory Animals, and were approved by the Institutional Animal Care and Use Committee (IACUC) of Texas A&M University under animal use protocol 2010-0258.

2.3.2 Transgenic Mice

First, a line of transgenic mice (005024) was purchased from Jackson Labs (http://jaxmice.jax.org/strain/005024.html). These mice were produced thus: the endogenous *Smn* gene was disrupted in a set of mice and were then crossed to mice carrying an *SMN2* homozygous transgene, generated by Dr. Arthur Burghes, to prevent embryonic lethality. The final product was a mouse, of the genotype $Smn^{+/-}$, $SMN2^{+/+}$, that when intercrossed can yield a severe SMA mouse model $Smn^{-/-}$, $SMN2^{+/+}$. The Jackson 005024 mice were crossed to our mice expressing the *hSmn/Gfp* transgene. Several rounds of breeding were required to select for the $Gfp^{+/?}$; $Smn^{+/-}$; $SMN2^{+/+}$ mice. These mice were then intercrossed to produce the experimental animals. The genotype of each mouse was determined by standard PCR assays.

2.3.3 Genotyping

Upon either death or weaning of the experimental progeny, tail biopsies were obtained. DNA was extracted and amplified by PCR using REDExtract-N-Amp Hot start according to manufacturer instructions (Sigma-Aldrich, St. Louis, MO). Primers: *Smn* mutant: Forward 5'-CTT GGG TGG AGA GGC TAT TC-3', Reverse 5'-AGG TGA GAT GAC AGG AGA TC; *Smn* wild-type: Forward 5'-TTT TCT CCC TCT TCA GAG TGA T-3', Reverse 5'-CTG TTT CAA GGG AGT TGT GGC-3'; and Gfp^{+}: Forward 5'-ATG GTG AGC AAG GGC GAG GAG CT, Reverse 5'-TCG TTG GGG TCT TTG CTC AGG GC-3'. *SMN2* was detected with primers oIMR5065, oIMR5066, oIMR5067 (Jackson labs, Bar Harbor ME).

2.3.4 Western Blot

Western blots were performed on protein homogenates from P6 transgene-positive spinal cords and skeletal muscles. Samples were run on a 12.5% acrylamide gel. A monoclonal primary antibody specific for hSMN (provided by Drs. Krainer and Hua) was used to detect the ~37kD protein, followed by a secondary anti-mouse HRP antibody. The blots were also probed with an antibody against tubulin as a protein loading control.

2.3.5 Quantitative-Real Time-Polymerase Chain Reaction (qRT-PCR)

Adult female and male mice of the genotypes $Gfp^{+/?}$; $Smn^{+/-}$;$SMN2^{+/+}$ and $Gfp^{-/-}$; $Smn^{+/-}$;$SMN2^{+/+}$ were set up to breed overnight. The following day, females were evaluated for vaginal plugs and separated from their respective male partners. After 18 days following the presence of a plug and confirmation of pregnancy, the females were euthanized and all embryos were extracted *in utero.* The entire spinal cord along with a section of back skeletal muscle was removed separately from each embryo and flash frozen in liquid nitrogen and stored at -80^{o}C. Total RNA was extracted from E18 whole spinal cords and muscle samples using Trizol reagent according to manufacturer instructions (Life Technologies, Grand Island, NY) and stored at -80^{o}C until use. 0.5 µg of RNA per sample were reverse transcribed to cDNA using the High Capacity cDNA reverse transcription kit according to manufacturer instructions (Life Technologies, Grand Island, NY). Quantitative-RT-PCR for *hSMN* transcripts encoded by the transgene was performed according to the general guidelines of Taqman® Gene Expression Assays (Life Technologies, Grand Island, NY). *hSMN* primers: *SMN1* and

SMN2-fl transcripts were amplified by using the same primer pair (SMN_abs-F: 5'-TACATGAGTGGCTATCATACTGGCTA-3' and SMN_abs-R: 5'-AATGTGAGCACCTTCCTTCTTTTT-3', located in exons 6 and 7, respectively), obtaining 72 bp PCR products (Integrated DNA Technologies, Coralville, IA). Full-length transcripts of the two genes were differentiated by using two different Taqman MGB probes, labeled with different fluorochromes, on the basis of the C-T transition located in exon 7 (SMN1_abs: 5'-NEDTATGGGTTTCAGACAAA-NFQ-3' and SMN2_abs: 5'-VIC-ATATGGGTTTTAGACAAAA-NFQ-3') (Life Technologies, Grand Island, NY) [117]. These molecular probes are short oligonucleotides complimentary to the target sequence. A reporter fluorophore is attached to one end of the oligonucleotide and a non-fluorescent quencher moiety is attached to the other end of the oligonucleotide. In their stem-loop structure the fluorophore and quencher are in close proximity so that energy from the fluorophore can to be transferred directly to the quencher through contact quenching. Through binding with the target nucleic sequence, the probes undergo a conformational change that forces the stem-loop to dissociate and the fluorophore and the quencher are separated from each other, restoring fluorescence [118]. NED and VIC are *Life Technologies'* proprietary flourophores with excitations of ~550nm and ~540nm, respectively to be used with Taqman assays ([118] and personal communication *Life Technologies*). Non-fluorescent quenchers (NFQ) absorb excitation energy from the fluorophore and dissipate the energy. When the two are close together the fluorophore's emission is suppressed [118]. Murine *gapdh* served as a ubiquitous control to normalize the Cycle threshold (Ct) values (Taqman® Gene Expression Assays,

Life Technologies, Grand Island, NY). Primers for the amplification of mouse choline acetyltransferase (*chat*) were used as a control to ensure appropriate spinal cord dissection (Taqman® Gene Expression Assays, Life Technologies, Grand Island, NY). Samples were set up in triplicate using a Taqman® Master mix (Life Technologies, Grand Island, NY) and run for 52 cycles in an ABI Prism 7900HT Fast Real-Time PCR System (Life Technologies, Grand Island, NY). The ΔΔCt method [119] was used to determine changes in mRNA transcript expression levels between groups.

2.3.6 HeLa Cell Culture

In order to obtain a positive control for the qRT-PCR assay, the immortal human cell line *HeLa* was cultured until confluence with Dulbecco modified Eagle medium (DMEM) + sodium pyruvate (Life Technologies, Grand Island, NY) and horse donor serum. RNA was extracted using an RNeasy mini kit (Qiagen, Hilden, Germany) according to manufacturer's instructions and stored at -80^{o}C after determining the concentration with a Nanodrop.

2.3.7 hSMN Transgene

For another positive control used in the qRT-PCR assay, two different plasmids carrying cDNA for human *SMN1* were purified from DH5α *E. coli* host stocks. The bacteria were first plated on petri dishes with LB media agar and ampicillin and left to form colonies ON at 37^{o}C. The following day 3-4 colonies were picked and incubated ON in LB media with constant agitation. Subsequently, the plasmids were purified using Qiagen's mini prep kit according to the manufacturer's protocol (Qiagen, Hilden, Germany).

2.3.8 Survival Studies

The offspring of the experimental cross was expected to fall under the following proportions of genetic inheritance: ~20% *Gfp*$^{+/?}$; *Smn*$^{-/-}$; *SMN2*$^{+/+}$ (Hb9(Gfp^{+})SMA i.e. experimental animals), ~6% *Smn*$^{-/-}$; *SMN2*$^{+/+}$ (Hb9(Gfp^{-})SMA i.e. diseased mutant animals/negative controls), and ~56% *Gfp*$^{+/?}$; *Smn*$^{+/-}$; *SMN2*$^{+/+}$ or *Gfp*$^{+/?}$; *Smn*$^{+/+}$; *SMN2*$^{+/+}$ (WT/Controls). Progeny of these crosses were monitored daily for mortalities. Deceased mice were collected, date of death was recorded and a tail necropsy was taken for DNA extraction. Subsequently, PCR assays were performed for the alleles *Gfp, Smn* mutant and WT, and *hSMN2* as described in 2.3.2. Mice were grouped according to genotype and length of survival. Values were plotted on a Kaplan-Meier Survival Curve.

2.3.9 Motor Function Assays

Transgene positive and transgene negative, *Smn*$^{+/-}$ *or Smn*$^{+/+}$, (control) mice were evaluated using the hindlimb suspension (Tube) test and the righting reflex test was performed every three days after birth. The test consisted of placing the pup in supine position on a flat surface and measuring the time it took to turn over onto an upright position, or to "right" itself, by having all four paws simultaneously on the flat surface. This measurement was taken in duplicate and averaged. All animals assayed were grouped according to genotype and mean time to "right" for each time point was scored according to the following scale, modeled after Monani and co-workers [19]: 0-4s=5, 5-9s=4, 10-14s=3, 15-20s= 2, 21-49s=1, 50->60s=0. A score of 0 was considered a failed test. Scores were plotted using Prism5 (GraphPad Software, La Jolla, CA). A heat block was used while working with the pups to prevent hypothermia. The hindlimb suspension

(tube) test was performed according to El-Khodor and colleagues [120]. Each animal was suspended from an upright 50*ml* canonical tube by its hindlimbs. A cotton ball or tissue was placed inside the tube to prevent injury. The time it required for the mouse to fall into the tube (latency) was recorded from two consecutive trials. Values from the two trials were averaged. Only latency time to fall (up to 60s) was considered in the analysis.

2.3.10 Statistical Analysis

Quantitative data are expressed as mean ± SEM. Values for number of animals are given in the figures and/or figure legends. Kaplan-Meier survival curves were generated and tested for statistical significance using the log-rank test with Prism5 GraphPad Software®. Student's t-test, computed either with Microsoft Excel (Microsoft Corporation, Seattle, WA) was used to determine statistical significance in the expression assays. Microsoft Excel (Microsoft Corporation, Seattle, WA) or Prism5 GraphPad Software, along with Analysis of the Variance (ANOVA) through SAS software (SAS Institute, Cary, NC), was used to probe for statistical significance in motor function assays. Significance was set at $p \leq 0.05$ for all tests.

2.4 RESULTS

2.4.1 Survival of Hb9(Gfp$^+$)SMA Mice

To assess whether insertion of the transgene improved the survival length of the severe SMA mouse model, the progeny of our experimental crosses was evaluated daily, all mortalities collected, genotyped, grouped accordingly, and plotted on a Kaplan-Meier

Survival Curve. The severe SMA mouse model used here is reported to survive perinatally [44]. In our hands, median survival for Hb9(Gfp$^-$)SMA mice was 0.83±1.58 days (n=30) and for Hb9(Gfp$^+$)SMA was 0.71± 1.05 (p=0.92 log-rank test; Fig 2.6 and Table 2.1). The majority of control animals (n=139) survived well beyond weaning. Lifespan was not assessed after P21. The *Gfp* primer set used in our genotyping assay does not distinguish between homozygous and heterozygous inheritance of the transgene. To determine homozygosity, fourteen (14) *Gfp*$^{+/?}$ mice were crossed to transgene-negative C57/B6 mice. If homozygosity is plausible, then 1/4 of the breeders (~ 3-4 mice) would be expected to be homozygous, that when crossed to transgene negative mice would yield 100% *Gfp*$^{+/-}$ progeny. This was not the case for any of the 14 crosses indicating that homozygous inheritance of the transgene is likely embryonic lethal. Hence, heterozygous inheritance of the *Hb9*(*Gfp/hSMN)* transgene is insufficient to rescue the survival of severe SMA mice.

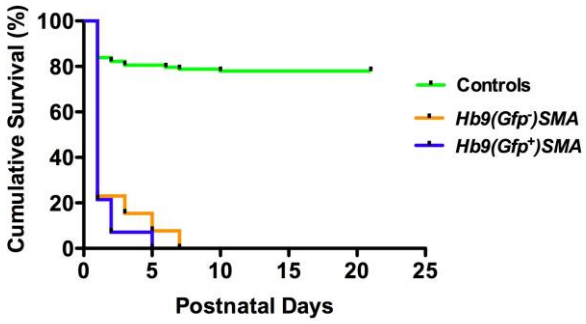

Fig. 2.6 Inheritance of the *Hb9(Gfp/hSMN)* transgene is insufficient to rescue severe SMA mice. Kaplan-Meier survival curves indicating the cumulative survival of the Hb9(Gfp$^+$)SMA, Hb9(Gfp$^-$)SMA, and control mice plotted with Prism 5 GraphPad software®. Transgene positive and transgene negative mice did not significantly differ in their lifespan (P = 0.92). Control animals were right censored in the analysis. No follow-up was performed after weaning (P21).

Table 2.1 Comparative survival between Hb9(Gfp$^+$)SMA and Hb9(Gfp$^-$)SMA mice.

Genotype	Mean lifespan (days)	n	*p* vs. control Hb9(Gfp$^-$)SMA mice Log-rank test
Hb9(Gfp$^-$)SMA	0.83±1.58	30	-
Hb9(Gfp$^+$)SMA	0.71±1.05	28	0.92
Controls	ND	139	<0.0001

2.4.2 Effect of the *Hb9(Gfp/hSMN)* Transgene on FVB/N Background Control Mice

To determine whether inheritance of the transgene had any beneficial or detrimental effects on the background of the experimental animals, a comparative survival analysis was performed on transgene-positive and transgene-negative control animals (*Gfp*$^+$;*Smn*$^{+/-}$;*SMN2*$^{+/+}$ or *Gfp*$^+$;*Smn*$^{+/+}$;*SMN2*$^{+/+}$ and *Smn*$^{+/-}$;*SMN2*$^{+/+}$ or *Smn*$^{+/+}$;*SMN2*$^{+/+}$, respectively). Hb9(Gfp$^+$)SMA mice had significantly less perinatal mortalities than Hb9(Gfp$^-$)SMA (p= 0.0040, Fig. 2.7) though the majority of animals in both groups survived to adulthood. These results indicate that, at least in control animals, insertion of the transgene does not interfere with normal progression and it could be providing beneficial effects during the first postnatal week.

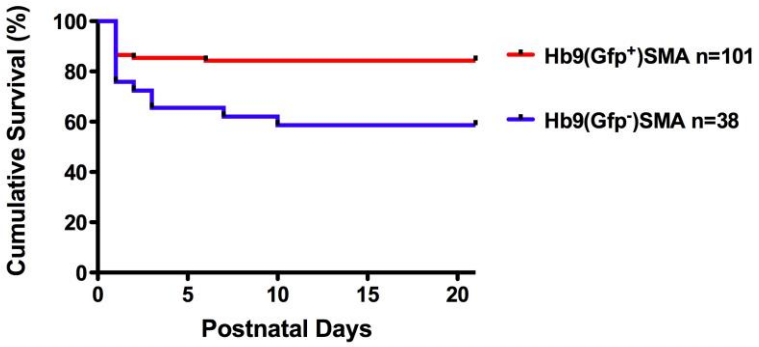

Fig. 2.7 The Hb9/hSMN transgene prevents early mortality in control mice. Kaplan-Meier curves demonstrate an overall increase in early survival ($p = 0.0040$, log-rank test). Mean lifespan is undetermined since subjects were not evaluated past weaning (P21) though the majority did survive to adulthood. Inheritance of the transgene may provide beneficial effects during the first days after birth reducing the chances of perinatal mortality.

Due to the tendency for improved survival rates during the first postnatal days in transgene-positive control mice, we proceeded to determine whether inheritance of the transgene had beneficial effects on motor behavior as well. Motor behavior was assessed using the righting reflex and the hindlimb suspension tests (Fig. 2.8). Both control groups displayed an age dependent improvement in motor behavior. Transgene-positive control mice [Hb9(Gfp^+), *Smn* WT or heterozygous, n=46] displayed a tendency to perform better than transgene-negative mice [Hb9(Gfp^-) *Smn* WT or heterozygous, n=25] on the righting reflex test during the first postnatal week (Fig 2.8.A), but this was only statistically significant at P3 ($p=0.05$). The overall performance until weaning did not differ significantly between the two groups. The opposite was found with the hindlimb suspension (Tube) test. In this case, the overall motor behavior did not differ significantly between Hb9(Gfp^+) control and Hb9(Gfp^-) control mice but we did find that Hb9(Gfp^-) controls scored better on their first measurement (P3) ($p=0.04$), Fig 2.8.B).

However, the Hindlimb Suspension test might not be the most adequate test for motor behavior in SMA mouse models. In at least two other studies that assessed motor function using motor neuron-rescued SMA mice, the results indicated that rescued animals performed worse than the diseased SMA animals by this test. On the other hand, rescued animals scored better than the disease ones in the Righting Reflex, which was more consistent with the overall improvements in SMA phenotype seen in their studies [57, 107].

With these data we conclude that insertion of the transgene does not cause any detrimental effects in heterozygous or WT mice, which also suggests that our breeding strategy did not alter the basic phenotype of the model mice. On the contrary, it is possible that inheritance of the transgene is providing beneficial effects during the first postnatal days as determined by the survival studies and one motor function assay.

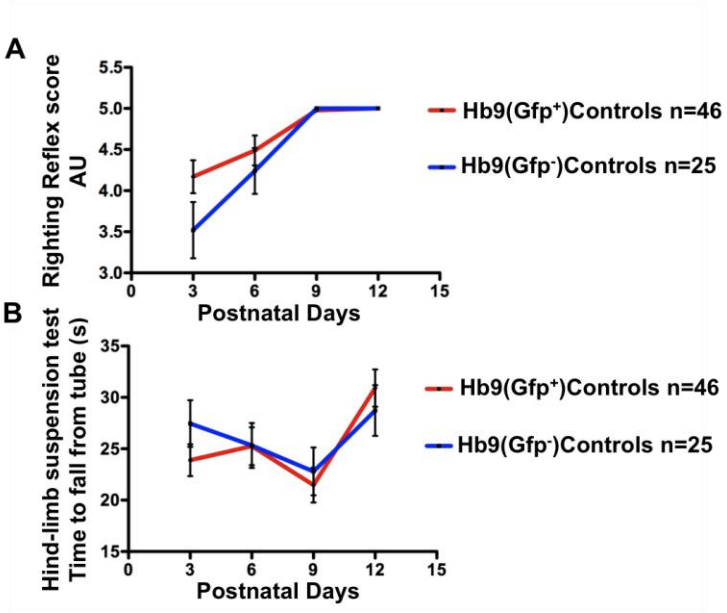

Fig. 2.8. Inheritance of the transgene does not improve the overall motor behavior. Comparative analysis of motor behavior between transgene-positive and transgene-negative control mice. Motor behavior was assessed by the righting reflex (**A**) and hindlimb (tube) suspension (**B**) tests. Only the latency to fall was recorded for the tube assays. Both controls groups improved their performance with age. There was no overall effect of genotype on motor function but in a point by point comparison we detected statistical difference between transgene-positive Hb9(Gfp^+) and Hb9(Gfp^-) control mice on both of these motor function assays at P3 only.

2.4.2 Expression of *Hb9(Gfp/hSMN)*

To restore SMN expression selectively in motor neurons, we have used an *Hb9* promoter to drive the exogenous expression of human SMN in a severe SMA mouse model. Homeobox gene *Hb9* is selectively expressed in spinal cord somatic and visceral motor neurons and Vx interneurons starting at E 9.5 [56]. Under normal conditions, SMN is strongly expressed in neurons in both fetal and postnatal spinal cord [17], thus we expected that our restored SMN would follow a similar pattern.

Given the transgene's failure to improve survival of severe SMA model mice despite its detection at the protein level, we sought to determine if the transgene was truly being expressed at sufficient quantities. We should have seen an improvement in the phenotype of our mutant mice, even a modest one if we are indeed restoring sufficient levels of SMN in motor neurons. For this, we used qRT-PCR to measure the levels of the hSMN transgene in E18 spinal cords and muscle from Hb9(Gfp^+)SMA and Hb9(Gfp^-)SMA mice. We followed the same methodology described by Paez-Colasante *et al.* [56]. The primers and probes tested were designed to specifically recognize *hSMN* and have been used previously by Tiziano *et al.* [117]. Cycle threshold (Ct) values obtained for murine *gapdh* RNA were used to equalize differences in total RNA per sample. Transcript level fold change was determined by the ΔΔCt method and values normalized to the Ct values obtained for Hb9(Gfp^-)SMA spinal cord samples. For positive controls, cDNA from human *HeLa* cells and two plasmids containing the *Hb9(Gfp/hSMN)* transgene were used. Surprisingly, we were unable to detect *hSMN* expression by quantitative RT-PCR in any of our spinal cord or muscle Gfp^+ or Gfp^- animals (Table 2.2). The *hSMN* primers did detect *HeLa* cell cDNA confirming primer efficacy (Table 2.2). The integrity of both spinal cord and muscle cDNA was confirmed since both *gapdh* and *SMN2* primers detected these samples and the Ct values obtained were consistent and within expected values (Table 2.2). The negative controls (no RT, no RNA, and water samples) were undetected by all three primer/probe sets used thus confirming the specificity of the assay.

Table 2.2. Quantitative RT-PCR data for expression of *SMN1, SMN2, gapdh* and *chat mRNA* transcripts in transgene-positive and negative spinal cord and skeletal muscle E18 samples

Mean ± SEM Cycle Threshold values				
	SMN1	*SMN2*	*gapdh*	*chat*
Hb9(Gfp$^-$)SMA spinal cord	UD	30.25 ± 0.32	20.51 ± 0.56	26.84 ± 1.02
Hb9(Gfp$^+$)SMA spinal cord	UD	29.81 ± 0.35	20.99 ± 0.27	28.71 ± 0.06
Hb9(Gfp$^-$)SMA skeletal muscle	UD	31.43 ± 0.33	20.33 ± 0.50	36.64 ± 0.52
Hb9(Gfp$^+$)SMA skeletal muscle	UD	30.29 ± 0.66	21.8 ± 0.40	35.85 ± 1.49
HeLa cells	24.71 ± 0.25	25.30 ± 0.02	UD	UD

UD: Undetected signal from transcript

As an additional control for the hSMN primer set, we assayed cDNA from the *HeLa* cell positive control, genomic DNA from two *Gfp*$^+$ and two *Gfp*$^-$ mice (same mice included in qRT-PCR assay), and two samples of plasmid DNA containing the *hSMN* transgene. Sample DNA was amplified via a PCR reaction using the *hSMN* primers and then run on a 2% agarose gel. A ~72bp band indicated the presence of the transgene in the plasmid DNA, the genomic *Gfp*$^+$, and *HeLa* cell cDNA samples but not the genomic *Gfp*$^-$ samples or water (negative control) (Fig 2.9). Thus, the *Hb9-hSMN1* mice we generated indeed carried the expected transgene in their genome.

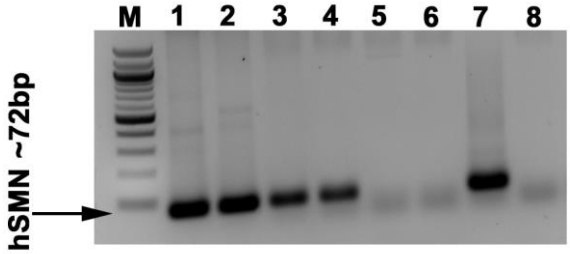

Fig. 2.9. *hSMN* qRT-PCR primer set accurately amplify the ~72bp band for *hSMN* in transgene-positive samples. 2% agarose gel. Lane description: (M) Marker of 100bp, (1) hSMN transgene-positive plasmid #1; (2) hSMN transgene-positive plasmid #2; (3) Gfp^+ genomic DNA sample #1; (4) Gfp^+ genomic DNA sample #2; (5) Gfp^- genomic DNA sample #1; (6) Gfp^- genomic DNA sample #2; (7) *HeLa* cell cDNA; (8) water, negative control.

To confirm tissue specificity and overall quality of the spinal cord extracts, the same samples (Gfp^+ and Gfp^- mutants) of both spinal cord and skeletal muscle used in the *hSMN* assay were tested by qRT-PCR for *ChAT* expression. This enzyme synthesizes the neurotransmitter acetylcholine and is found in high levels in the spinal cord but only modestly in muscle. We found that our E18 spinal cord samples express ~200-fold more *ChAT* than the E18 skeletal muscle samples (Fig. 2.10, Table 2.2.). This confirms that the samples used to test for hSMN expression are indeed extracts from spinal cord and RNA was efficiently extracted.

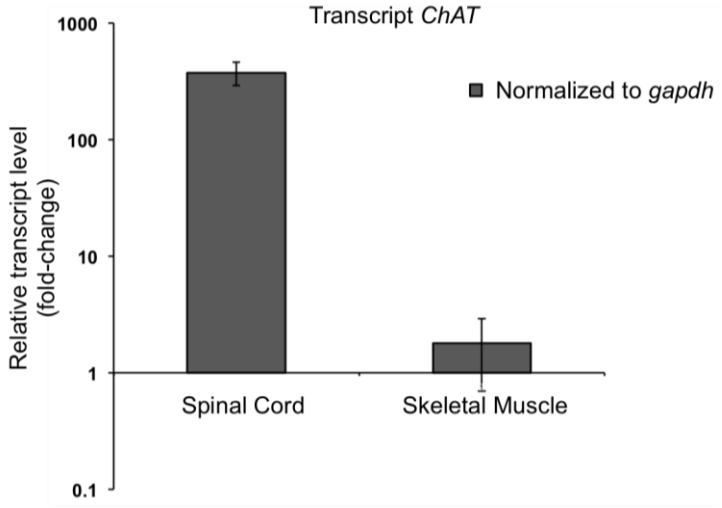

Fig. 2.10. Relative *chat* transcript expression in Hb9(Gfp^{+})SMA and Hb9(Gfp^{-})SMA E18 spinal cords. The ordinate, in log scale, shows *chat* expression in spinal cord normalized to levels in skeletal muscle samples of the same animals. Spinal cord samples displayed ~200-fold higher expression than Hb9(Gfp^{+})SMA and Hb9(Gfp^{-})SMA skeletal muscle samples. N= 4–5, per tissue group.

2.5 DISCUSSION

The *Hb9(Gfp/hSMN)* transgene is expressed early on and is vastly motor neuron-selective. Its expression was detected from embryogenesis through early postnatal days at the protein level in spinal cord and not in skeletal muscle thus confirming tissue specificity. However, transgene expression most likely drops to minimal levels during late embryogenesis and the first postnatal days when the presence of SMN is very critical to the survival of motor neurons. Therefore, hemizygous inheritance of the transgene was insufficient to extend survival of a severe SMA mouse model (*Smn*$^{-/-}$, *SMN2*$^{+/+}$) past P1.

Three groups performed different SMN restoration experiments using SMAΔ7 mice and determined that there are specific temporal requirements dictating when SMN restoration is most efficient to achieve the maximum overt rescue of the SMA

phenotype. These studies concluded that there is a neonatal period of time when high SMN levels are required. Early induction is the most efficacious [2, 28, 111] and even though improvements are found by increasing SMN at later stages of pathology, there is a window of time within which the protein must be restored for optimal effect by therapeutic efforts [2, 28]. Timely restoration of SMN may be capable of pausing the progression of the SMA pathology and serve as an effective post-symptomatic treatment [2]. Our experimental design is in agreement with this principle. In the spinal cord of mammals, motor neuron-specific-*Hb9* is expressed during early embryogenesis (E9) in newly formed embryonic motoneurons [121]. The important timing of expression and function of *Hb9* is in postmitotic motor neurons [122]. Thus in our transgene, *Hb9* drives the expression of hSMN very early on. This explains why the transgene was clearly detected by mid-embryogenesis (E13) in spinal cord cross sections with immunohistochemical staining. In theory if our experimental design is efficient then the transgene should be providing the developing motor neurons with the SMN protein that they are lacking. Nonetheless, this was not the case. It was very puzzling why expression was undetected at the mRNA level towards late embryogenesis. There is the possibility that the expression of *Hb9* peaks by late embryogenesis and then begins to decrease thus halting the expression of hSMN in transgene-positive animals at the time period when it is most needed. Hence, the timing and efficacy of *Hb9* as a driver for transgenic expression is not in line of what is expected from the endogenous *Smn* promoter likely explaining the lack of rescue in severe SMA mice. To circumvent this problem, motor neuron-restoration of SMN by *Hb9* should be continuous and permanent to prevent time-

related alterations in protein expression and meet the protein demands at the appropriate window.

There could also be a requirement for the transgene to be expressed from both alleles to produce enough SMN per cell to have a significant effect on the SMA phenotype. Nevertheless, since homozygous inheritance of the transgene seems to be embryonic lethal, perhaps due to its pattern of insertion in the genome, this was not be possible.

All the above could explain our lack of rescue except that the transgenic protein was detected up to several postnatal days. We have hypothesized that the extended half-life of both the hSMN and GFP proteins explain why mRNA was undetected as early as E18 but the protein was present postnatally. Though present, the concentration of hSMN is likely not high enough to produce significant rescue of motor neurons necessary for phenotypical improvements.

The stability of the SMN protein is modulated by complex formation; i.e., recruitment of SMN into large macromolecular complexes as well as increased association with several Gemin proteins increases its stability. This process is regulated by the cyclic AMP (cAMP)-dependent kinase, protein kinase A (PKA). A study by Burnett and collaborators (2009) found that SMN exists in at least two populations: a low-molecular-weight population consisting of SMN monomers with a relatively short half-life of a few hours and a high-molecular-weight population that consists of SMN in complex that is resistant to degradation with a half-life of several days. The fraction of SMN associated with Gemin 3, Gemin 5, and Gemin 6 is dramatically more stable

compared to total cellular SMN. Additional evidence found by this group is that mutations that inhibited SMN oligomerization and complex formation reduced SMN half-life [35]. A study by Garbes *et al.* (2009) showed that SMN is post-translationally stabilized via reduced ubiquitinylation in human SMA fibroblasts and upon its incorporation into the SMN complex [123]. Another study using normal and SMA patient fibroblasts determined that the half-life of FL- SMN messenger RNAs is approximately only 5 to 6 hours for both cells from patients with SMA and in unaffected cells [124].

According to Wahlers (2001), a factor that may influence conclusions about the potency of a given gene transfer vector is the use of a sensitive reporter with a long protein half-life, such as GFP [125]. GFP has a compact structure increasing its stability under a variety of conditions [116]. Both GFP and EGFP are indeed very stable proteins and very resistant to proteolysis, with a half-life exceeding 24 h; this has been found consistently in several studies both *in vivo* and *in vitro* with cultured mouse LA-9 cells [116, 125, 126]. The high stability means that once made, GFP will persist in a cell even after the promoter that drives its expression is shut down [127]. The stability of GFP limits its application in some studies, including transcriptional induction studies [116]. Thus, vectors that express stable proteins are not necessarily promising to express a given therapeutic protein to adequate levels in the cell type of interest [125].

The proteins produced from the *Hb9(Gfp/hSMN)* transgenic construct are thus detected postnatally due to their extensive half-life, a property conferred by their stability, but not at functional concentrations to optimally produce beneficial changes in

motor neuron pathology in severe SMA mice. However, the presence of the long-lived SMN protein was sufficient at reducing neonatal mortalities in transgene-positive control animals (Fig. 2.7). Consistent with this, transgene-positive control animals performed better on the Righting Reflex test during the first measurement (P3) than transgene-negative animals ($p=0.05$). If more time points would have been taken during the first week, we hypothesize that we would have observed a marked tendency for improved motor behavior during that period. The results obtained with the Hindlimb Suspension test were not in agreement with this. However, after performing this assay, we suggest that the Hindlimb Suspension test might not be the most accurate way to determine hindlimb strength or atrophy since we detected other influential factors. For example, we observed less willingness from the mice to cooperate on the Hindlimb Suspension test than with the Righting Reflex. From our observations, time of latency seemed to be affected by the animal's weight and size, as well as stress and fear. Even thought this assay has been used in several other studies [56, 57, 61, 107, 120], some of the results from the Hindlimb Suspension test differ from the motor behavior reported with the Righting Reflex test. For instance, Gogliotti *et al.* (2012) found that in the Hindlimb Suspension test SMA mice performed better than motoneuron-rescued mice until P6 when the former began to rapidly decline and the latter showed an age-dependent improvement. This datum differs from the results of the Righting Reflex test in which rescued animals performed much better than the mutant SMA animals [107]. A similar interpretation can be given to the motor behavior in another study that used a different inducible SMA line, $ChAT^{Cre}$ mice, to study motor neuronal-SMN rescue. With the

Hindlimb Suspension test, Martinez *et al.* (2012) observed that in the initial time points of the assay their rescue animals consistently outperformed the diseased $ChAT^{Cre-}$ mice but then at P8-10, the opposite occurred. Again, these results differed from the Righting Reflex test, in which $ChAT^{Cre+}$ rescue animals presented an age-dependent continuous improvement over the SMA mutant mice [57]. The improvements seen in rescue animals from both studies on the Righting Reflex assay were also more in line with the overall improvement in SMA pathology that these researchers found in each of their studies.

Our control group survival and Righting Reflex results are consistent with our expression analysis at the protein level showing that the transgenic construct yields a long-lived functional protein. The increase in survival in transgene-positive, control mice occurred during the critical neonatal window determined in the SMN restoration studies mentioned above [2, 28, 111]. We only observed these improvements in transgene-positive control animals and not severe SMA mutants because the severity of the SMA mouse model, demonstrated by their perinatal symptom onset and rapid deterioration, causes their rescue to be very difficult with such small increases in FL-SMN.

Amongst our possible explanations for the observed survival and motor function improvement in transgene-positive controls is the idea that the addition of small quantities of FL-SMN can compensate for the potentially detrimental effects of the additional SMNΔ7 protein present with the insertion of copies of human *SMN2* in this mouse model. Overexpression of SMAΔ7 is apoptotic for neurons [6] and SMN-deficient mice suffer from massive apoptosis during embryogenesis [128]. SMN and

SMNΔ7 form heterotopic complexes, which stabilize SMNΔ7, at least in transfected cultured cells. The presence of increased SMNΔ7 results in more oligomeric SMN-complex and a reduced phenotypic severity [6, 128]. The small increases in FL-SMN provided by the transgene along with the 10% of FL-SMN also produced by *SMN2*, may be able to overcome the pro-apoptotic toxic effects by SMNΔ7 because of possible anti-apoptotic properties of FL-SMN [6].

Since disease severity is inversely proportional to *SMN2* copy number, one would expect that SMNΔ7, the main product of *SMN2,* would have beneficial effects. Though it is possible that the protective effect of *SMN2* may only be coming from the 10% FL-SMN produced and not SMNΔ7 [6]. We can also hypothesize that the additional quantities of FL-SMN that the *Hb9(Gfp/hSMN)* transgene is providing to control mice can influence the competition for Gemin binding between SMN and SMNΔ7. When present, SMNΔ7 may be temporarily binding to the SMN-complex components before it is degraded due to its stability, thus preventing proper SMN binding to the complex. Additional SMN may be displacing the inefficient SMNΔ7 and restoring its proper place and function ultimately providing beneficial effects to transgene-positive control motor neurons.

Lastly, our group has not yet mapped the site of transgene insertion. This leaves open the possibility that the precise site may be located in such a way that it can influence a protective gene modifier of SMA. This could be something important to look into in future studies. One possibility is that our transgene has been inserted near *Plastin3*. *Plastin3* is a protective SMA modifier that is an isomer in the family of actin-

binding proteins involved in the stability and organization of actin F-filaments. In zebrafish motor neurons, it has been found to increase the amount of F-actin thus improving axon outgrowth. Yanyan *et al.* found that higher expression of Plastin3 in patients with SMA may act as a compensatory mechanism [129]. However, several other studies have found that this SMA modifier might be sex-dependent with mild SMA female patients having higher levels of *Plastin3* expression [130, 131]. We did not separate our experimental groups by sex so this cannot be easily demonstrated.

In conclusion, the *Hb9(Gfp/hSMN)* transgene from our experimental approach is being expressed in developing motor neurons during embryogenesis. The expression of the transgene is significantly reduced by late embryogenesis. Though, due to the stable properties, the early translated SMN protein appears to have a long enough half-life to functionally persist during the first postnatal days, when it is critically needed, and produce beneficial outcomes in transgene-positive control mice. Our experiments demonstrate that the transgene is indeed inherited and protein is both detectable and functional in motor neurons. Nonetheless, these increases in SMN are not sufficient to rescue the severe phenotype of our experimental mice, but they are indicators of the importance of motor neuronal-SMN restoration and that even small additions of the functional protein are enough to yield detectable improvements.

CHAPTER III

IMPROVEMENT OF NEUROMUSCULAR SYNAPTIC PHENOTYPES WITHOUT ENHANCED SURVIVAL OR MOTOR FUNCTION IN SEVERE SPINAL MUSCULAR ATROPHY MICE BY SELECTIVE SMN RESTORATION IN MOTOR NEURONS

3.1 SYNOPSIS

In the inherited childhood neuromuscular disease SMA, lower motor neuron death and severe muscle weakness result from the reduction of the ubiquitously expressed SMN protein. Although SMA mice recapitulate many features of the human disease, it has remained unclear if their short lifespan and motor weakness are primarily due to cell-autonomous defects in motor neurons. Using $Hb9^{Cre}$ as a driver, we selectively raised SMN expression in motor neurons in conditional SMAΔ7 mice. Unlike a previous study that used choline acetyltransferase ($ChAT^{Cre+}$) as a driver on the same mice, and another report that used $Hb9^{Cre}$ as a driver on a different line of conditional SMA mice, we found no improvement in survival, weight, motor behavior, endplate morphology, and presynaptic neurofilament accumulation. However, like in $ChAT^{Cre+}$ mice, we detected rescue of endplate size and mitigation of NMJ denervation status. The rescue of endplate size occurred in the absence of an increase in myofiber size, suggesting endplate size is determined by the motor neuron in these animals. Real time-PCR showed that the expression of spinal cord SMN transcript was sharply reduced in $Hb9^{Cre+}$ SMA mice relative to $ChAT^{Cre+}$ SMA mice. This suggests that our lack of

overall phenotypic improvement is most likely due to an unexpectedly poor recombination efficiency driven by $Hb9^{Cre}$. Nonetheless, the low levels of SMN were sufficient to rescue two NMJ structural parameters indicating that these motor neuron cell autonomous phenotypes are very sensitive to changes in motoneuronal SMN levels. Our results directly suggest that even those therapeutic interventions with very modest effects in raising SMN in motor neurons may provide mitigation of neuromuscular phenotypes in SMA patients. Most of the results from this chapter have already been published [56].

3.2 INTRODUCTION

SMA is an often fatal, childhood inherited neuromuscular disease caused by low levels of a ubiquitous protein required for spliceosome assembly, SMN. Reduction of SMN leads to loss of lower motor neurons, muscle denervation and atrophy. Humans harbor two genes encoding SMN, *SMN1* and *SMN2*. In SMA patients SMN production is drastically reduced by homozygous deletion/mutation of *SMN1*. In such patients SMN is solely derived from *SMN2*. *SMN2* is essentially identical to *SMN1* except for a C→T nucleotide change that causes exon 7 skipping in the splicing of ~90% *SMN2* RNA, leading to the synthesis of an unstable, minimally functional protein (SMNΔ7). Only ~10% of *SMN2* transcripts code for a full-length SMN protein and this reduced level is insufficient for motor neuron survival. *SMN2* can exist in multiple copies and SMA disease severity correlates inversely with *SMN2* copy number.

As detailed in Chapter I Introduction, mice only harbor one SMN gene, whose homozygous deletion (*Smn*$^{-/-}$) is embryonic lethal. *Smn*$^{-/-}$ mice with two copies of *SMN2* (i.e. *Smn*$^{-/-}$*; SMN2*$^{+/+}$) die perinatally and show features resembling the most severe human disease [44]. Addition of a transgene encoding the cDNA for SMNΔ7 to these mice (i.e. *Smn*$^{-/-}$*; SMN2*$^{+/+}$*; SMNΔ7*) improves survival to 14 days on average (SMAΔ7 mice), but they still display a severe SMA phenotype. Thus, among other features, they demonstrate impaired motor behavior, inability to thrive and gain weight, and structural and functional defects in their NMJs that include presynaptic accumulation of neurofilaments (NF), smaller and immature postsynaptic apparatus and diminished neurotransmission [6, 9, 30, 40, 61, 132]. A selective vulnerability to denervation of specific, clinically relevant muscles has also been reported for these animals [104].

Although SMA mice recapitulate many features of the human disease, it remains unclear if their short lifespan and SMA phenotype are primarily due to cell-autonomous defects in motor neurons. The general expectation in the field has been that selective SMN reduction in motor neurons should mimic the phenotype of the severe SMA model mice, and that conversely, selective restoration of SMN in motor neurons should dramatically rescue the phenotype of SMA model mice. These predictions have not been entirely borne out by the experiments. Thus, Olig2-Cre-driven conditional reduction of SMN in motor neuron precursors yields central and NMJ phenotypes in these animals that are present in the SMA mice, but the former animals have very mild SMA with a surprisingly long lifespan [19]. To conditionally restore SMN expression in motor neurons and other cells, two independent groups generated mice with inducible mutant

Smn alleles that can be reverted to functional, wild-type-like alleles after Cre recombination. These are the hybrid rescue allele, Smn^{Res} [2] (Fig. 3.2) and the $Smn^{2B\text{-}neo}$ allele [108]. Recently, *choline acetyltransferase-(ChAT)*-driven Cre was used to restore SMN expression in motor neurons of $Smn^{Res/Res}$ mice in the SMAΔ7 background [57], while *Hb9*-driven Cre was used to restore SMN expression in motor neurons of the $Smn^{2B\text{-}neo/2B\text{-}neo}$ SMA mice [107]. Mice rescued by both approaches showed measurable improvements in weight, motor behavior, central and neuromuscular phenotypes relative to diseased controls, but displayed a very modest increase in survival (8 and 5 days over diseased controls, respectively). These latter results contrast with the dramatic improvements, particularly in lifespan, produced by pan-neuronal expression of SMN in $Smn^{-/-}$; $SMN2^{+/+}$ mice (210 days) [110], or in SMAΔ7 mice treated with CNS or peripherally-directed viral vectors expressing SMN (50-200 days) [78, 111], or CNS and peripherally-delivered oligonucleotides that correct the exon skipping defects in *SMN2* (>100 days) [64, 72].

To better understand whether the SMA phenotype is primarily due to cell-autonomous defects in motor neurons and whether motor neuronal-selective SMN restoration is a viable strategy to rescue pathology we have used two approaches, each with a different severe SMA mouse model, to answer these questions. Chapter II of this dissertation details our initial efforts to rescue a very severe SMA mouse model by motor neuron-selective SMN restoration using *Hb9* to drive the expression of a transgene harboring cDNA for human SMN. However, we found that expression of *Hb9* peaks by mid to late embryogenesis halting the production of functional SMN at the

perinatal stage when SMN is most needed for motor neuron survival. Additionally, the severity of the SMA mouse model used, demonstrated by their perinatal symptom onset and rapid deterioration, caused both their rescue and assessment to be a challenging task. To circumvent the limitations of the very severe mouse model and the timing of expression for *Hb9*, we used a second approach that addressed both of these confinements by using a less severe mouse model with an average survival of ~14 days and a strategy in which SMN was to be restored permanently at embryogenesis. Thus, here we report on our attempt to restore SMN selectively in motor neurons of $Smn^{Res/Res}$ SMAΔ7 mice with the same *Hb9-Cre* driver used to rescue $Smn^{2B\text{-}neo/2B\text{-}neo}$ SMA mice. We found no improvement in survival, motor behavior, presynaptic NF accumulation, endplate morphology, and a marginal weight increase in our Hb9(Cre^{+})SMA mice relative to Hb9(Cre^{-})SMA mice. However, we detected rescue of endplate size and significant mitigation of NMJ denervation status in $Hb9^{Cre+}$ SMA mice. The rescue of endplate size was not a consequence of an increase in myofiber size. This pattern of mitigated peripheral structural phenotypes in $Hb9^{Cre+}$ SMA mice is similar to that in $Myf5^{Cre+}$ SMA mice [57], although the latter had restored SMN both in skeletal muscle and spinal cord, thus suggesting that this rescue in the $Myf5^{Cre+}$ SMA mice is due to neuronal and not muscle SMN restoration. Quantitative real time-polymerase chain reaction (qRT-PCR) showed that expression of the repaired Smn^{Res} allele (*SMN67m8h*, Fig. 3.2) was vastly lower in spinal cord in our $Hb9^{Cre+}$ SMA mice than in the spinal cord from $ChAT^{Cre+}$ SMA mice and this proportion remained regardless of varying the concentration of cDNA used in the assay. This suggests that our lack of overall

phenotypic improvement is most likely due to an unexpectedly poor recombination efficiency driven by $Hb9^{Cre}$. Nonetheless, our data show that specific structural NMJ phenotypes are very sensitive to small changes in SMN levels selectively in motor neurons and thus can be mitigated by very small increases in spinal cord SMN levels that fail at enhancing lifespan, weight and motor behavior. Although prior studies (e.g. [104, 133, 134]) have suggested that therapeutic interventions with very modest effects in raising SMN could potentially mitigate motor neuron-autonomous phenotypes in SMA patients, our results are the first to reach that conclusion directly based on an approach to selectively raise SMN levels in motor neurons. Additionally, we suggest that our experiments establish a threshold of SMN expression that distinguishes an order of SMN sensitivity for different SMA phenotypes.

3.3 MATERIALS AND METHODS

Note: a detailed description of the methods can be found in the Appendix A of this dissertation.

3.3.1 Ethics Statement

Care and treatments of all animals followed the National Institutes of Health Guide for the Care and Use of Laboratory Animals, and were approved by the Institutional Animal Care and Use Committee (IACUC) of Texas A&M University under animal use protocol 2010-0258.

3.3.2 Mice

Mice were housed in a vivarium at 25°C with a 12h light/dark cycle, fed *ad libitum* and monitored daily for health. Human alleles are referred in the text with the standard convention of capital letters in *italics*. Smn^{Res} carriers ($Smn^{Res/+}$; $SMN\Delta7^{+/+}$; $SMN2^{+/+}$, JAX stock #007951) and $Hb9^{Cre}$ carriers ($Hb9^{Cre+/-}$; $Smn^{+/-}$; $SMN\Delta7^{+/+}$; $SMN2^{+/+}$, JAX stock # 007022) were initially acquired from the Jackson Labs, Bar Harbor, ME. The $Hb9^{Cre}$ allele in 007022 came from JAX stock# 006600, the same Hb9-Cre line used by DiDonato and colleagues to rescue $Smn^{2B\text{-}Neo/2B\text{-}Neo}$ mice [107], and which has also been used by other groups in many developmental studies of motor neurons (e.g. [135, 136]). These lines were bred in our facility to generate $Hb9^{Cre+/-}$; $Smn^{Res/+}$; $SMN\Delta7^{+/+}$; $SMN2^{+/+}$ mice. For experiments, the latter were bred to Smn^{Res} carriers. The genotype for the rescued animals, designated as Hb9(Cre^{+})SMA, was $Hb9^{Cre+/-}$; $Smn^{Res/Res}$; $SMN\Delta7^{+/+}$; $SMN2^{+/+}$. The genotype for the disease animals, designated as Hb9(Cre^{-})SMA, was $Hb9^{Cre-/-}$; $Smn^{Res/Res}$; $SMN\Delta7^{+/+}$; $SMN2^{+/+}$. Controls were $Smn^{Res/+}$ or $Smn^{+/+}$ mice derived from the same crosses.

The initial design of the study assumed that precise measures of lifespan, from birth until death, were essential to determine the effects of the selective raising of SMN in motor neurons of SMA mice. Thus, the approved animal use protocol for this study allowed death without euthanasia as an endpoint for the survival analysis. This accommodation turned out to be critical as the results showed that our experimental manipulation had no effect on survival. Had the differences in lifespan been more clear between our rescued and diseased animals, it would have been possible for us to

establish a set of symptoms and criteria that would have allowed euthanasia before death without fear of changing or affecting the final results of the survival analysis. To minimize the number of SMA mice used in the study, animals that were followed for survival analysis were also used for longitudinal studies of weight progression and righting reflex. A separate set of control and SMA mice were used later to perform the hind-limb suspension test. This experiment was terminated at postnatal day (P) 12, before the SMA animals reached their mean lifespan of ~14 days. NMJ phenotypes were analyzed in P9-P11 animals.

3.3.3 Genotyping

Upon either death or weaning of the experimental progeny, tissue samples were obtained from tail, spinal cord, skeletal muscle, kidney, brain, heart and stomach. DNA was extracted and amplified by PCR using REDExtract-N-Amp Hot start according to manufacturer instructions (Sigma-Aldrich, St. Louis, MO). Primers: *Cre* was detected using the custom primers: Forward: 5'-CATTTGGGCCAGCTAAACAT-3', Reverse: 5'-CCCGGCAAAACAGGTAGTTA-3'. The product was 454 bp. Smn^- was detected with the following custom primers: Forward: 5'-CTTGGGTGGAGAGGCTATTC-3', Reverse: 5'-AGGTGAGATGACAGGAGATC-3'. Smn^+ was detected with primers oIMR7033 and oIMR7034 (Jackson labs, Bar Harbor, ME). *SMN2* was detected with primers oIMR5065, oIMR5066, oIMR5067 (Jackson labs, Bar Harbor ME).

3.3.4 Quantitative-Real Time-Polymerase Chain Reaction (qRT-PCR)

Total RNA was extracted from P4 whole spinal cords and hindlimb skeletal muscle using Trizol reagent according to manufacturer instructions (Life Technologies,

Grand Island, NY). 1µg of RNA per sample was reverse transcribed to cDNA using the High Capacity cDNA reverse transcription kit according to manufacturer instructions (Life Technologies, Grand Island, NY). Quantitative-RT-PCR for full length SMN transcripts encoded by the recombined Smn^{Res} allele (*SMN67m8h*, Fig. 3.2) was performed as described previously by Paez-Colasante *et al.* (2013) [56]. The 18S rRNA and *gapdh* 20X primers and probe were Taqman® Gene Expression Assays (Life Technologies, Grand Island, NY). Samples were set up in triplicate using a Taqman® Master mix (Life Technologies, Grand Island, NY) and run for 48-50 cycles in an ABI Prism 7900HT Fast Real-Time PCR System (Life Technologies, Grand Island, NY). The ΔΔCt method [119] was used to determine changes in mRNA transcript expression levels between groups.

3.3.5 Western Blot

Whole spinal cords from three Hb9(Cre^{+})SMA, three Hb9(Cre^{-})SMA and three WT control animals were dissected and frozen instantly in liquid nitrogen. Spinal cords were each homogenized and tissue was lysed with radioimmunoprecipitation assay (RIPA) buffer in order to extract proteins. Tail samples from P4 mice were taken for DNA extraction and genotyped with PCR assays. Samples were run on a 12.5% acrylamide gel and the membrane was incubated overnight in an anti-mouse SMN (1:3000) antibody, followed by a secondary anti-mouse HRP antibody. Same samples were incubated separately in α-Tubulin as a loading control. Levels of the ~37kD SMN protein were quantified against α-Tubulin and normalized to the WT control group. Protein bands were compared through band intensity analysis.

3.3.6 Survival Analysis

Our experimental litters were monitored twice daily for potential mortalities. As soon as death of an animal occurred, lifespan was recorded and samples of the above-mentioned tissues were taken for genotyping. All animals assayed (n= 187) were grouped according to genotype and lifespan (days). Survival data was plotted on Kaplan-Meier survival curves using Prism5 (GraphPad Software**,** La Jolla, CA).

3.3.7 Weight Progression

On P3, pups were tattooed with Indian black ink for identification purposes and henceforth weighed every three days to determine weight changes over the time course of 21 days (until weaning for controls and death for mutants). All animals assayed (n=150) were grouped according to genotype and mean weights for each time point were plotted using Prism5 (GraphPad Software**,** La Jolla, CA).

3.3.8 Motor Function

A righting reflex test was performed every three days on the same animals used for weight progression above. This measurement was taken in duplicate and averaged. All animals assayed (n=150) were grouped according to genotype and mean time to "right" for each time point was scored according to the following scale, modeled after Monani and co-workers [19]: 0-4s=5, 5-9s=4, 10-14s=3, 15-20s= 2, 21-49s=1, 50->60s=0. A score of 0 was considered a failed test. Scores were plotted using Prism5 (GraphPad Software, La Jolla, CA). The hindlimb suspension (tube) test was performed as described by El-Khodor and colleagues [120] except only latency time to fall (up to 60s) was used in the analysis (See Fig. 3.1, section and Appendix for details).

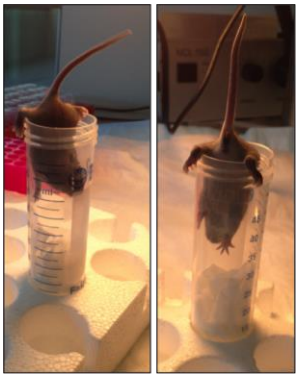

Fig. 3.1. Hindlimb suspension (tube) test. Mice are suspended from their hindlimbs onto a 50*ml* conical tube with a cotton ball or tissue at the bottom to prevent injury. Latency time is recorded up to 60s maximum.

3.3.9 Neurofilament (NF) Accumulation Assay

NMJ staining was performed on fixed whole mounts of P10-P11 tibialis anterior (TA) muscle. To label NF's, samples were incubated overnight at room temperature on a rocker with 2H3 monoclonal antibody (1:100, Developmental Studies Hybridoma Bank, Iowa City, IA). The following day, muscles were washed in PBS-T and then incubated in rhodamine goat anti-mouse secondary antibody (1:200, Jackson Immunoresearch, West Grove, PA) and fluorescein-conjugated α-bungarotoxin (BTX) (1:1000, Life Technologies, Grand Island, NY) to label acetylcholine receptors (AChRs). After washing, muscle bundles were separated and mounted on microscope slides using VectaShield (Vector Laboratories, Burlingame, CA). Slides were observed under an epifluorescence microscope fitted with a Z-motorized stage (Nikon Eclipse E1000, Nikon, Tokyo, Japan) with a 100X, 1.3 NA oil objective. Images of NMJs were taken with a CoolSNAP fx CCD camera (Photometrics, Tucson, AZ) and captured with MetaMorph (Molecular Devices, Downingtown, PA). An observer, blind to genotype,

initially classified NMJs as either NF accumulation positive (diseased) or negative (normal). NMJs were later grouped according to genotype for quantitative analysis.

3.3.10 Innervation Status

P9 triceps muscles were dissected, fixed and cryoprotected. Muscles were sliced in a cryostat into 40μm longitudinal sections. Free-floating sections were blocked in PBS + 10% normal goat serum. Sections were later incubated overnight in either an antibody to synaptophysin (1:300, Life Technologies, Grand Island, NY) or in a 2H3 monoclonal antibody (1:100, Developmental Studies Hybridoma Bank, Iowa City, IA). The following day all sections were washed and incubated either in rhodamine goat anti-rabbit antibody (1:1000, Jackson Immunoresearch, West Grove, PA) or in rhodamine goat anti-mouse secondary antibody (1:200, Jackson Immunoresearch, West Grove, PA) respectively. Fluorescein-conjugated α-bungarotoxin (BTX) (1:1000, Life Technologies, Grand Island, NY) was added to label acetylcholine receptors (AChRs). After washes in PBS-T, all free-floating sections were mounted on slides using VectaShield. A 40X, 1.3 NA oil objective was used to acquire wide field images of NMJs with MetaMorph Software. Endplates stained with synaptophysin were assessed blind to genotype for their innervation status by qualitatively classifying each junction into either fully-occupied (>75%), partially-occupied (25-75%) and unoccupied (<25%) depending on the relative proportion of synaptophysin staining versus the overall area of the AChR staining. NMJs stained for NF and BTX were assessed for status of innervation by categorizing them as innervated if there was any overlap between the two stains or denervated if NF was completely absent at the synaptic site.

3.3.11 Endplate Size

AChR area was calculated from the images of P9 TA whole mounts and from P9 triceps longitudinal sections using the MetaMorph software.

3.3.12 Endplate Morphology

AChR morphology was determined from the images of the same P9 triceps longitudinal sections described in 3.2.10 and 3.2.11 using the categories: 1) plaque, 2) perforated, 3) "C"-shape, and 4) complex. Plaque shape is the most immature stage of development and is characterized by an endplate without any perforations; perforated, as the name indicates, characterizes the receptors with one or more perforations; "C"-shape refers to an open and more mature configuration; and finally the complex shape is the most mature category and was assigned to highly branched receptors with numerous perforations and the typical "pretzel"-like shape. These categories were adapted from the ones previously described by Kummer *et al.* (2004) [137].

3.3.13 Myofiber Area and Diameter

P9 TA muscles were dissected and flash frozen with OCT medium (tissue tek) in an isopentane/liquid N_2 bath. 14μm-thick cross-sections were cut in a cryostat and mounted on a slide. Sections were fixed in 1% PFA then washed in PBS-T. The cross sections were blocked in PBS + 10% normal goat serum and then incubated overnight in a dystrophin antibody (1:300, Abcam, Cambridge, MA). The following day, muscle sections were incubated with a fluorescein-conjugated goat anti-rabbit secondary antibody (1:200). After washes, slides were mounted using VectaShield. A 20X, 0.5 NA oil objective (Nikon) was used to acquire wide field images of myofibers with

MetaMorph Software, taking as many images needed to encompass the entire area of a single whole muscle section avoiding overlapping myofibers. The dystrophin stained images were analyzed for myofiber area and diameter by first thresholding the calibrated image for dark objects and manually adjusting said threshold to fill the entire interior core surrounded by dystrophin staining of as many myofibers as possible per image. Next regions were drawn automatically around each individual fiber, and lastly the integrated morphometric analysis tool in MetaMorph was used to determine area and breath, which is the caliper width of the object perpendicular to the longest chord. This approach allows simultaneous accurate determination of myofiber size parameters in a large number of fibers. It is quicker than the traditional approach of measuring these parameters in single fibers at a time.

3.3.14 Statistical Analysis

Quantitative data are expressed as mean ± SEM. Values for number of animals and NMJs analyzed are given in the figure legends. Kaplan-Meier survival curves were generated and tested for statistical significance using the log-rank test with Prism5 GraphPad Software. Analysis of the Variance (ANOVA) was used to check for significance in weight and motor function data using SAS software (SAS Institute, Cary, NC). Student's t-test, computed either with Microsoft Excel (Microsoft Corporation, Seattle, WA) or Prism5 GraphPad Software, was used to probe for statistical significance in NF accumulation, innervation status and endplate size data. Significance was set at $p \leq 0.05$.

3.4 RESULTS

3.4.1 Spinal Cord-Specific Recombination of the *Smn^{res}* Allele

The hybrid *Smn^{Res}* allele has an inverted (i.e. 3'→5'), translationally silent mouse *Smn* exon 7 in the intron between human *SMN2* exon 7 and 8 (Fig. 3.2). Mutant (*lox71/lox66*) *loxP* sites in opposite orientation were engineered upstream of *SMN2* exon 7 and downstream of the inverted *Smn* exon 7, respectively. In this form, this allele potentially codes for transcripts containing *Smn* exons 1-6 and *SMN2* exons 7 and 8. However, it was found that in this configuration *Smn^{Res}* fails to encode transcripts for full-length SMN and only produces transcripts lacking *SMN2* exon 7 that code for SMNΔ7 protein (Fig. 3.2). Hence *Smn^{Res}* is functionally a null *Smn* allele [2]. Upon Cre recombination, *Smn* exon 7 5'→3' orientation is irreversibly restored so that transcripts containing *Smn* exons 1-7 and *SMN2* exon 8 *(SMN67m8h)* are generated, which encode full length SMN (Fig. 3.2). *Smn$^{Res/Res}$* mice are embryonic lethal, however, when *Smn^{Res}* replaces the *Smn* null allele in an SMAΔ7 background, the resulting *Smn$^{Res/Res}$* mice display essentially the same SMA phenotype as standard SMAΔ7 mice [2]. Thus, these mice are "conditional" SMAΔ7 mice. Repairing the *Smn^{Res}* allele using Cre-lines that express the recombinase ubiquitously from early development rescued the normal phenotype of the mice, validating the recombined, hybrid *Smn^{Res}* allele as a WT-surrogate *Smn* allele [2].

To restore SMN expression selectively in motor neurons, we sought to drive the repair of the *Smn^{Res}* allele with *Hb9*-Cre. The homeobox gene *Hb9* is selectively expressed in spinal cord somatic and visceral motor neurons and V_x interneurons starting

at embryonic (E) day 9.5 [122, 138]. In the *Hb9*^{Cre} allele an IRES-Cre cassette was knocked-in into the first exon of the *Hb9* gene. Thus, Cre expression under *Hb9* control follows the expression pattern of endogenous *Hb9*. *Hb9*^{Cre} is homozygous lethal thus only heterozygous animals survive past birth. The experimental crosses consisted of *Smn*^{Res} carriers (*Smn*$^{Res/+}$; *SMNΔ7*$^{+/+}$; *SMN2*$^{+/+}$, JAX stock #007951) bred to *Hb9*$^{Cre+/-}$; *Smn*$^{Res/+}$; *SMNΔ7*$^{+/+}$; *SMN2*$^{+/+}$ mice. The genotype for the rescued animals, designated as Hb9(Cre^{+})SMA, was *Hb9*$^{Cre+/-}$; *Smn*$^{Res/Res}$; *SMNΔ7*$^{+/+}$; *SMN2*$^{+/+}$. The genotype for the disease animals, designated as Hb9(Cre^{-})SMA, was *Hb9*$^{Cre-/-}$; *Smn*$^{Res/Res}$; *SMNΔ7*$^{+/+}$; *SMN2*$^{+/+}$. Controls were *Smn*$^{Res/+}$ or *Smn*$^{+/+}$ mice derived from the same crosses. Their precise genotypes were: *Hb9*$^{Cre?/-}$; *Smn*$^{Res/+}$; *SMNΔ7*$^{+/+}$; *SMN2*$^{+/+}$ and *Hb9*$^{Cre?/-}$; *Smn*$^{+/+}$; *SMNΔ7*$^{+/+}$; *SMN2*$^{+/+}$.

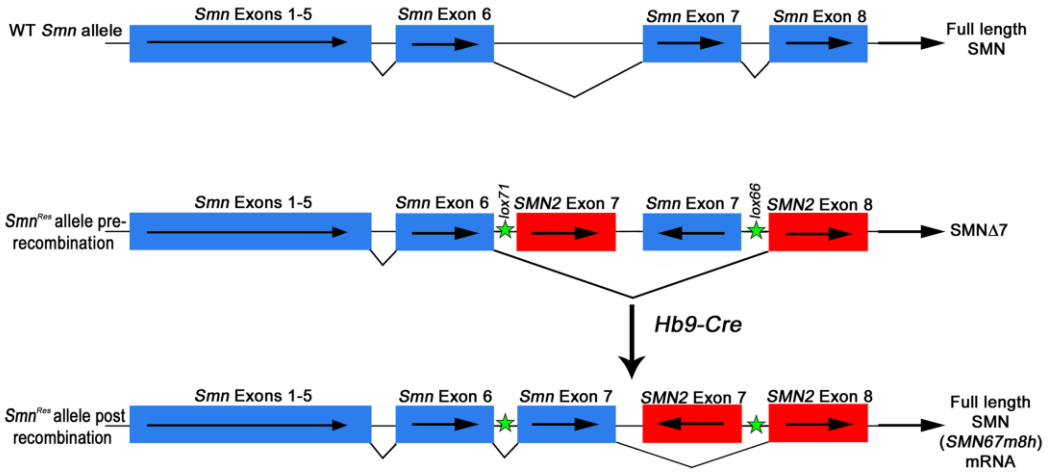

Figure 3.2. Schematic representation of the *Smn* WT allele and the *Smn*^{Res} conditional hybrid mutant allele before and after Hb9-Cre recombination. Blue boxes represent mouse Smn exons. Red boxes represent human *SMN2* exons. Arrows within boxes display orientation relative to transcription start. Green stars show approximate location of loxP sites (*lox71, lox 66*) in *Smn*^{Res}. Black lines connecting exons show splicing pattern for the predominant transcript encoded by each allele. Protein products are named to the right. *SMN67m8h* is the transcript encoded by the repaired *Smn*^{Res} allele. Not drawn to scale.

Genomic PCR confirmed spinal cord-selective, *Hb9*^{Cre} driven recombination of *Smn*^{Res} in our Hb9(Cre^{+})SMA mice as the repaired allele was only detected in spinal cord, but not in skeletal muscle, kidney (Fig. 3.3A), brain, heart or stomach (data not shown).

3.4.2 Comparison Between *Hb9*^{Cre} and *ChAT*^{Cre} Driven Repair of the *Smn*^{Res} Allele

We used quantitative RT-PCR to measure the levels of the recombined, repaired transcript *SMN67m8h*, which encodes full-length SMN (Fig. 3.2), in P4 spinal cord and muscle. We chose this early time point because disease symptoms were not overt at this stage. We used as controls P4 spinal cord and muscle tissue from *ChAT*$^{Cre+}$ and *Myf5*$^{Cre+}$ conditional SMAΔ7 mice [57]. Primers were designed to recognize the *SMN67m8h* transcript. The forward primer cut across *Smn* exons 6 and 7 exon/intron boundary and the reverse primer bound to *SMN2* exon 8 ([57] Fig. 3.2). For endogenous controls, we used primers for 18S rRNA and *gapdh*. Cycle threshold (Ct) values obtained for either 18S rRNA or *gapdh* were used to normalize the Ct values from the *SMN67m8h* transcript by equalizing differences in total cDNA per sample. The assays with each housekeeping gene were set up separately on different trials. Transcript level fold change was determined by the $2^{-\text{DeltaDeltaCt}}$ method [119] and values were normalized to the Ct values obtained for *ChAT*$^{Cre+}$*; Smn*$^{Res/Res}$ spinal cord samples in every case. In our hands, relative *SMN67m8h* expression levels for *ChAT*$^{Cre+}$*; Smn*$^{Res/Res}$ and *Myf5*$^{Cre+}$*; Smn*$^{Res/Res}$ samples were very similar to those reported before independently of the control primers used [57] (Fig. 3.3B). In fact, the Ct values obtained with these samples were almost

identical to the Ct values obtained previously with other samples with the same genotypes [57]. However, P4 *Hb9*$^{Cre+}$*; Smn*$^{Res/Res}$ spinal cord had approximately 100-fold lower levels of *SMN67m8h* transcript than *ChAT*$^{Cre+}$*; Smn*$^{Res/Res}$ spinal cord when using 18S rRNA primers as an endogenous control to normalize (Fig. 3.3B).

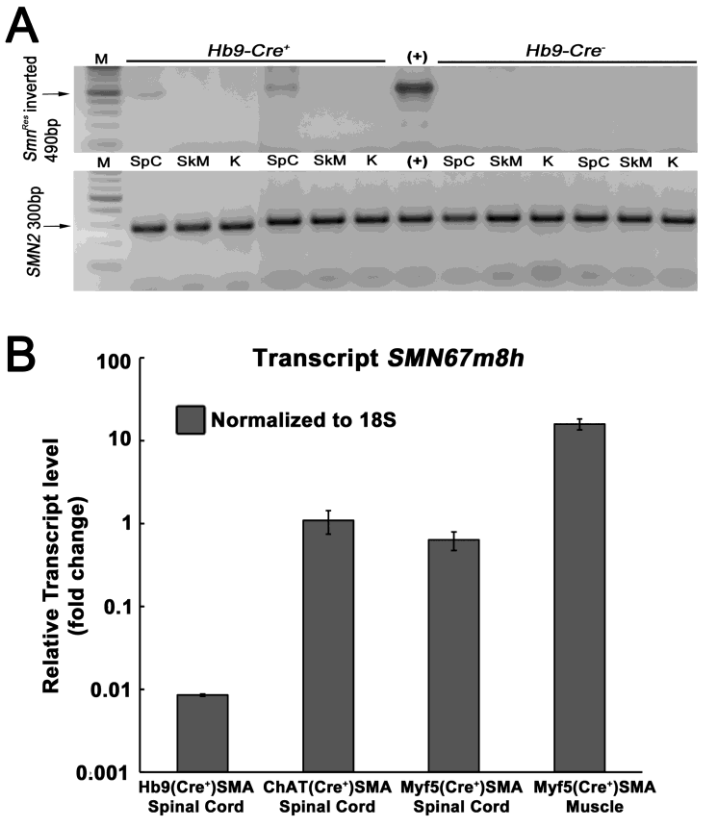

Fig. 3.3. A. Spinal cord-specific Cre recombination of the *Smn*^{Res} in Hb9(Cre+)SMA mice. Genomic DNA was prepared from spinal cord (SpC), skeletal muscle (SkM), and kidney (K) from 2 Hb9Cre^{+} and 2 Hb9Cre^{-} SMA animals postmortem. All animals died within the first two postnatal weeks suggesting they were *Smn*$^{Res/Res}$. Top panels: Genomic PCR specific for the inverted, recombined *Smn*^{Res} allele demonstrated its presence only in the spinal cord samples and not in the skeletal muscle or kidney samples. All these samples were positive for *SMN2*, which showed DNA integrity. Sizes of the expected DNA bands are indicated to the left of each panel. M: 100 bp ladder. (+): positive controls. Spleen DNA from a germline inverted *Smn*$^{Res/Res}$ animal was used as positive control for the recombined allele PCR. **B.** Relative *SMN67m8h* expression in *Hb9*^{Cre}, *ChAT*^{Cre} and *Myf5*^{Cre} SMA lines at P4. The ordinate, in log scale, shows SMN67m8h expression normalized to levels in ChATCre SMA spinal cord. Hb9Cre SMA spinal cord displayed ~100-fold lower expression than *ChAT*^{Cre} SMA spinal cord. N= 2–4, per genotype.

Subsequently, primers for *gapdh* were used to confirm the initial results normalized with 18S. On this other gene expression assay with the *SMN678* transcripts equalized to *gapdh* transcripts we obtained a ~70-fold change between Hb9(Cre^+) and ChAT(Cre^+) spinal cord samples (Fig. 3.4). We performed an additional experiment to validate our results. We altered the methodology of the qRT-PCR set-up by using 4X the concentration of cDNA. In this assay the Ct values obtained were also normalized to *gapdh* transcripts. As expected, Ct values lowered ~2-3 cycles for all of the groups yet the relative *SMN678* transcript expression levels remained very similar to initial results with a difference of ~70-fold between Hb9(Cre^+)SMA and ChAT(Cre^+)SMA spinal cords. The average Ct values were: Hb9(Cre^+)SMA spinal cord: 1X cDNA = 38.92 ± 0.41 vs. 4X 36.96 ± 0.33; ChAT(Cre^+) spinal cord: 1X cDNA = 34.56 ± 1.00 vs. 4X 31.39 ± 0.77; Myf5(Cre^+) spinal cord: 1X cDNA = 35.83 ± 0.32 vs. 4X 32.17 ± 0.26 and Myf5(Cre+)SMA muscle: 1X cDNA = 30.46 ± 0.23 vs. 4X cDNA 26.70 ± 0.05.

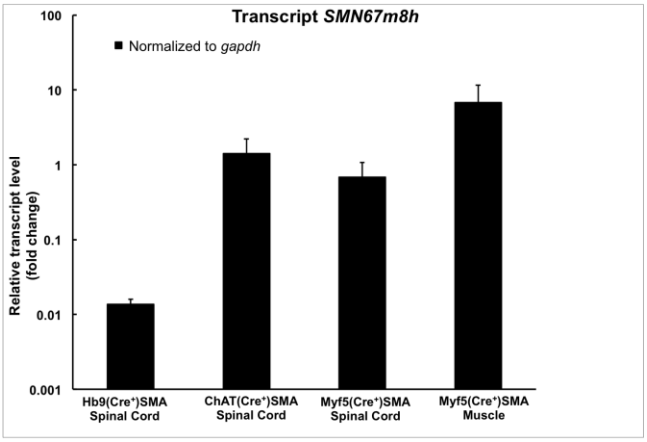

Fig. 3.4. Relative *SMN67m8h* expression in $Hb9^{Cre}$, $ChAT^{Cre}$ and $Myf5^{Cre}$ SMA lines at P4 normalized to *gapdh*. The ordinate, in log scale, shows *SMN67m8h* expression compared to levels in $ChAT^{Cre}$ SMA spinal cord. $Hb9^{Cre}$ SMA spinal cord displayed ~70-fold lower expression than $ChAT^{Cre}$ SMA spinal cord when equalized to *gapdh*. Thus confirming the results with 18S rRNA primers which indicate that the SMN transcript generated from Hb9(Cre^{+})SMA spinal cords is vastly lower than that produced in the spinal cords of ChAT(Cre^{+})SMA mice.

Consistent with our prior results at the genomic level (Fig. 3.3A), *SMN67m8h* transcript was undetectable in muscle samples from either $Hb9^{Cre+}$; $Smn^{Res/Res}$ or $Hb9^{Cre-}$; $Smn^{Res/Res}$ mice (data not shown). Nor was *SMN67m8h* detected in spinal cord from $Hb9^{Cre-}$; $Smn^{Res/Res}$ animals (data not shown). Thus, although these results confirm at the mRNA level the spinal cord specific recombination driven by $Hb9^{Cre}$ in conditional SMAΔ7 mice, they unexpectedly show that full length SMN expression in these mice is remarkably much lower than in $ChAT^{Cre+}$ conditional SMAΔ7 mice.

We failed to detect an increase in SMN protein levels by Western blot in spinal cord from $Hb9^{Cre+}$; $Smn^{Res/Res}$ animals relative to spinal cord from $Hb9^{Cre-}$; $Smn^{Res/Res}$ mice (Fig. 3.5) This is not surprising in light of the fact that this increase was not even observed when $ChAT^{Cre}$ drove the repair of Smn^{Res} in conditional SMAΔ7 mice [57],

which is probably due to the small proportion of motoneuron-derived material in lysates from whole spinal cord.

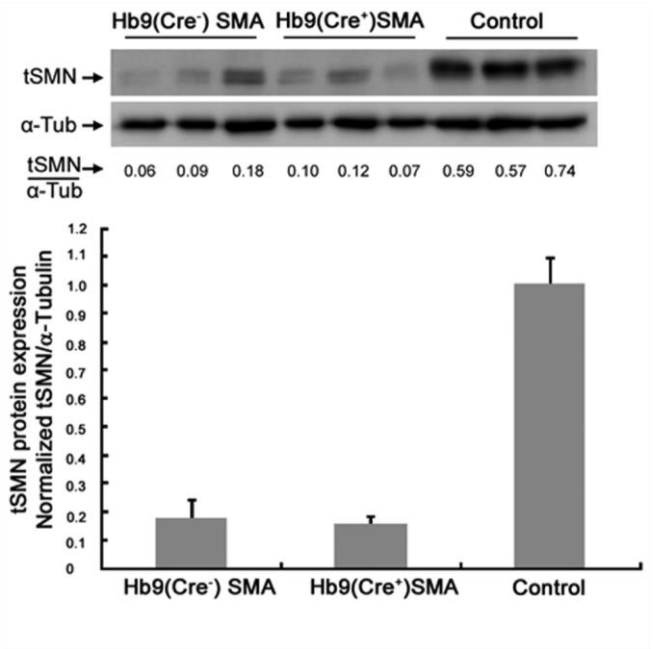

Fig. 3.5. SMN protein expression between Hb9(Cre$^+$)SMA and Hb9(Cre$^-$)SMA mice. Western blot analysis of SMN protein levels: Whole spinal cord protein samples from three Hb9(Cre$^+$)SMA, three Hb9(Cre$^-$)SMA and three WT control animals were incubated overnight in an anti-mouse SMN (1:3000) antibody. Same samples were incubated separately in α-Tubulin as a loading control. Levels of SMN were quantified against α-Tubulin and normalized to the WT control group. We found no significant increase in SMN levels between our Cre$^+$ and Cre$^-$ mice ($P > 0.05$).

3.4.3 Survival, Weight Progression and Motor Behavior in Hb9(Cre$^+$)SMA Mice

Having obtained evidence of spinal cord-selective recombination and expression, we next characterized the phenotype of Hb9(Cre$^+$)SMA mice. Figure 3.6A and B exemplifies the vast qualitative differences between P9 Hb9(Cre$^+$)SMA and WT control

littermate mice. These SMA mice are differentiated to controls by their visibly obvious small size and muscle atrophy that causes them to lose motor function.

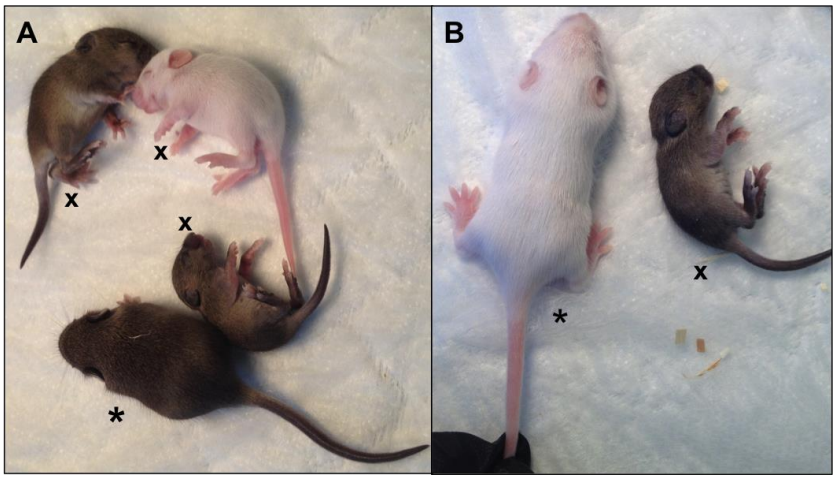

Fig 3.6. Images exemplifying phenotypical differences between P9 WT (*) and Hb9(Cre^{+})SMA (x) littermate mice. Images show both the size difference and the inability of mutant animals to stand up or "right" themselves. **A.** One WT mouse (*) is compared to two Hb9(Cre^{+})SMA mice (x, one very diseased brown mouse and one white mouse in the middle of the image), and one Hb9(Cre^{-})SMA mouse (x, brown mouse in the far upper left corner). **B.** Example of a very diseased mutant animal compared to a healthy control. The mutant animal was unable to stand on its own and had very limited limb movements, and was very lethargic with possible breathing difficulties. *Images not to scale.*

Median survival for Hb9(Cre^{-})SMA mice was 14.6 ± 2.64 days (n=20) (Fig. 3.7A). This value agrees very well with the mean survival reported by others for these mice [2, 57] and for the original SMAΔ7 animals [6], which suggests that our breeding strategy did not alter the basic phenotype of the mice. Hb9(Cre^{+})SMA mice displayed a statistically similar lifespan (Fig. 3.7A; 13.41 ± 3.73 days, n= 37, p = 0.6436, log-rank test). Both SMA lines were clearly unable to gain the weight that controls did (Fig. 3.7B and Fig. 3.6). *Hb9*$^{Cre+}$ and *Hb9*$^{Cre-}$ conditional SMAΔ7 mice gained some weight

between P3 and P9, but it declined steadily henceforth until time of death (Fig 3.7B). Hb9(Cre^{+})SMA mice tended to be a little heavier than Hb9(Cre^{-})SMA mice between P9 and P15, but this difference was statistically significant by ANOVA only at P12 ($F=9.78$; $p=0.004$).

Motor behavior was assessed using the righting reflex (Fig. 3.7C and Fig. 3.6B) and the hindlimb suspension tests (Fig. 3.7D). As expected heterozygous and WT controls performed much better than SMA mice in these tests. No statistical differences in motor function were apparent between Hb9(Cre^{+})SMA and Hb9(Cre^{-})SMA mice. Thus we failed to detect improvements in lifespan and motor behavior in Hb9(Cre^{+})SMA animals, even though there was a slight tendency for increased weight.

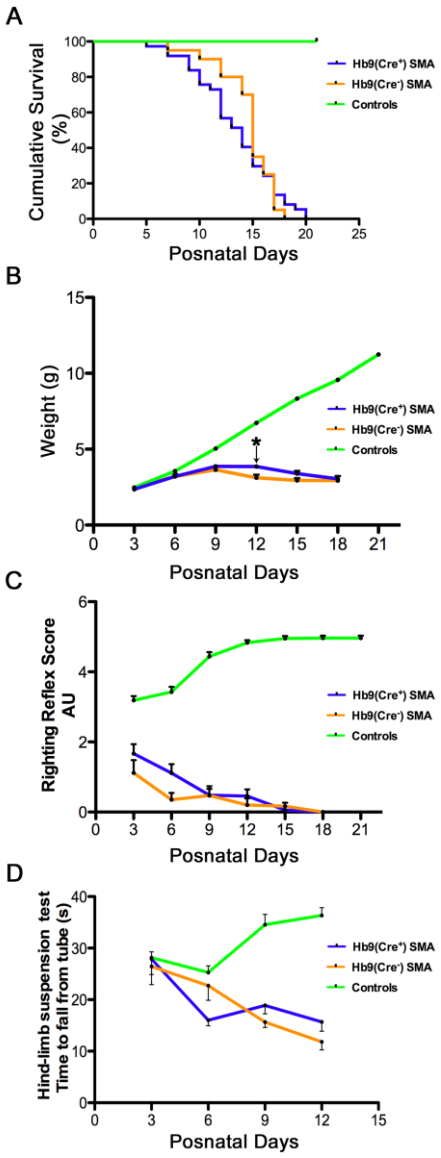

Figure 3.7. Hb9-Cre recombination fails to improve lifespan, weight gain and motor behavior in SMAΔ7 mice. A. Kaplan-Meier curves demonstrate no increase in survival, p = 0.6436, log-rank test. Mean life span: Hb9(Cre^{+})SMA: 13.41 ± 3.73 days, n=37. Hb9(Cre^{-})SMA mice: 14.6 ± 2.64 days; n=20. Controls: n=130. **B.** While controls (n=107) gained weight as expected, no statistical differences in weight were found during the lifespan of Hb9(Cre^{+})SMA and Hb9(Cre^{-})SMA mice except at P12 (*p=0.004, F=9.78, ANOVA). Hb9(Cre^{+})SMA: n=10-27 per time point. Hb9(Cre^{-})SMA: n=3-16 per time point. **C** and **D.** Motor behavior was assessed by the righting reflex (C) and hindlimb (tube) suspension (D) tests. Only the latency to fall was recorded for the tube assays. While controls improved their performance with age, SMA mice motor behavior deteriorated as they approached end stage. For the righting reflex assays: Controls: n=107 per time point. Hb9(Cre^{+})SMA: n=7-27 per time point. Hb9(Cre^{-})SMA: n=4-16 per time point. For the tube test: Controls: n=148 per time point. Hb9(Cre^{+})SMA: n=7-28 per time point. Hb9(Cre^{-})SMA: n=5-17 per time point.

3.4.4 Neuromuscular Phenotypes in Hb9(Cre^{+})SMA Mice

While Hb9-Cre-driven rescue of conditional SMAΔ7 mice had no apparent effect at the whole animal level, it was still possible that their NMJ pathology could be rescued by this approach. Accumulations of neurofilament (NF) staining at the nerve terminal are a hallmark pathological feature in SMA mice [30, 40, 132, 139], and they were reduced to control levels in *ChAT*$^{Cre+}$ conditional SMAΔ7 mice [57]. We stained whole mount preparations from P10 tibialis anterior (TA) muscle for NF and AChRs to mark NMJs. While about 10% of endplates had pre-synaptic NF accumulations in controls, over 80% of NMJs displayed them in Hb9Cre^{+} or Hb9Cre^{-} conditional SMAΔ7 preparations (Fig. 3.8). Thus, NF accumulations in nerve terminals persisted in Hb9(Cre^{+})SMA mice.

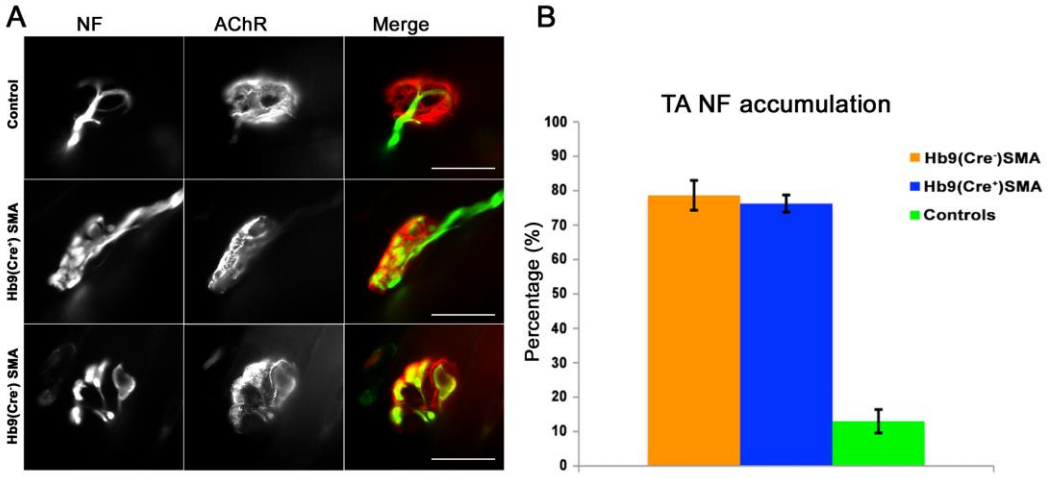

Fig 3.8. Neurofilament (NF) accumulation at nerve terminals fails to be rescued in Hb9(Cre^{+}) SMA mice. Whole mounts of P10 TA muscle stained for components of the NMJ. **A.** Representative images for each of the 3 genotypes assayed. Protuberances or "blebbing" of the nerve terminals (arrowheads) are distinct evidence of SMA pathology. Green: NF, Red: BTX. Scale bars: 20μm. **B.** Quantification of NF accumulation as seen in A. The ordinate plots the mean percentage of NMJs with NF accumulation per genotype. Most NMJs in Hb9(Cre^{+}) and Hb9(Cre^{-}) SMA mice had NF accumulations, while only a minority of endplates in controls showed so. Controls n=9 animals, 107 NMJs. Hb9(Cre^{+})SMA n=4 animals, 52 NMJs. Hb9(Cre^{-})SMA n=3 animals, 95 NMJs.

Endplate size in TA muscle, as measured by the area occupied by AChRs, was one of the synaptic phenotypes rescued in *ChAT*$^{Cre+}$ conditional SMAΔ7 mice [57]. We determined AChR area in whole mount TA preparations and in longitudinal sections of triceps muscles from P9 animals. To capture many NMJs per image and to ensure imagining of the entire junctional surface, wide field 3D images of the BTX-stained tissue were taken with an epifluorescence microscope fitted with a motorized Z-axis. Using Methamorph software, the Z-stacks were first flattened to the X/Y dimensions and endplate area was determined after thresholding of images. The average TA endplate areas for control (185.10 ± 6.87 μm^2) and Hb9(Cre$^-$)SMA (115 ± 0.94 μm^2) genotypes were very similar to those reported previously for P9 TAs in control and SMAΔ7 mice, respectively, which were imaged by confocal microscopy [132]. In Hb9(Cre$^+$)SMA mice average TA endplate area was 170.11 ± 7.08 μm^2. Figure 3.9 A,B shows that endplate area for both TA and triceps NMJs was restored to control values in Hb9(Cre$^+$)SMA mice. Thus, appendicular muscles innervated by pools of motor neurons in opposite ends of the spinal cord, cervical (triceps), lumbar/sacral (TA), had their average endplate area rescued in Hb9(Cre$^+$)SMA mice.

In normal animals endplate size correlates with myofiber size [140]. Following labeling of transverse sections for dystrophin to mark cell surface, we determined mean myofiber area and diameter in TA muscles from P9 controls, Hb9(Cre$^+$) and Hb9(Cre$^-$)SMA mice. We focused on this muscle because it was used previously by Martinez *et al.* (2012) [57] in their analysis of these parameters in *ChAT*^{Cre}-, *Myf5*^{Cre}- and *MyoD*^{iCre}-SMAΔ7 mice. Dystrophin staining was normal and qualitatively similar between

genotypes (Fig. 3.9C) despite the pronounced muscular atrophy in mutant animals. Thus, dystrophin is not altered in SMN-deficient spinal cords but is in SMN-deficient muscles as was observed by Cifuentes-Diaz et al. (2001) [54]. As expected, mean myofiber area and diameter were larger in controls than in SMA mice and were within the range reported previously [57, 132]. However, there were no differences in these parameters between Hb9(Cre^+) and Hb9(Cre^-)SMA mice (Fig. 3.9 D,E) (Control, area=449.4±44.94 μm^2; diameter=22.07±1.08 μm. Hb9(Cre^+)SMA, area=297.06±11.10 μm^2; diameter=17.53±0.37 μm. Hb9(Cre^-)SMA, area=268.05±32.49 μm^2; diameter=16.96±0.86 μm). Thus, the increase in endplate size in the TA muscle from Hb9(Cre^+)SMA mice was observed in the absence of a corresponding increase in myofiber area and diameter.

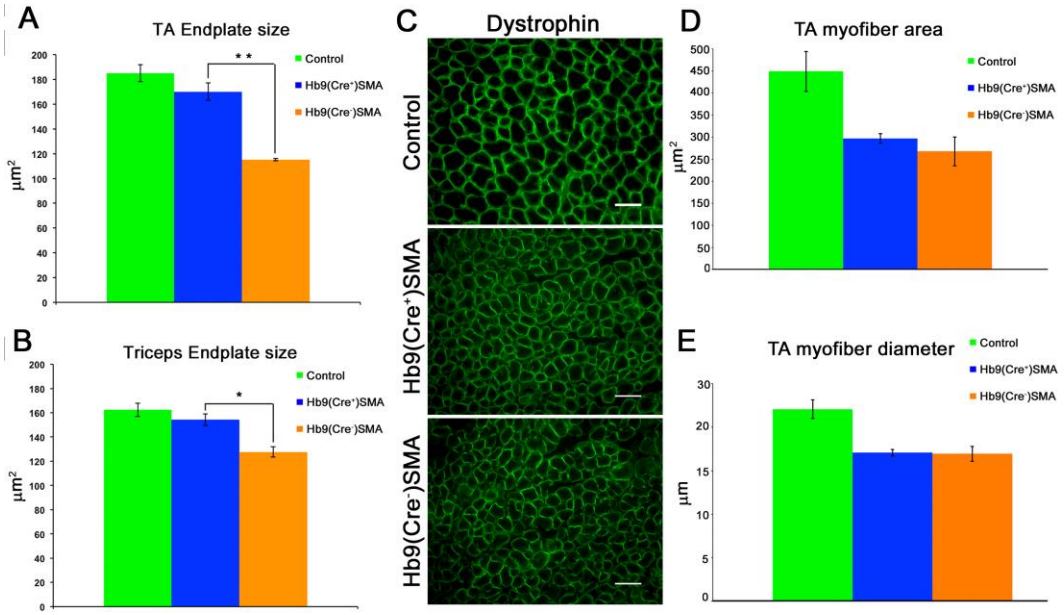

Fig. 3.9. Endplate size is rescued in Hb9(Cre+) SMA mice without change in myofiber size. **A.** and **B.** Quantification of endplate size in P9 TA and triceps muscles, respectively. TA endplate size was determined in whole-mount preparations. Triceps endplate area was determined in longitudinal sections from images such as that displayed in Fig. 3.11A. Endplate area was rescued in both muscles in Hb9(Cre^+)SMA mice. TA: Controls: n=5 animals, 512 NMJs. Hb9(Cre^+)SMA n=3 animals, 465 NMJs. Hb9(Cre^-)SMA n=3 animals, 303 NMJs. Triceps: Controls n=5 animals, 505 endplates. Hb9(Cre^+)SMA n= 3 animals, 524 endplates. Hb9(Cre^-)SMA n= 3 animals, 316 endplates. **p=0.002. *p=0.008 (t-test). **C.** Representative images of dystrophin stain for 14-µm-thick transverse sections of control and SMA P9 TA muscles. Dystrophin staining is qualitatively similar between genotypes but differences in fiber caliber between control and SMA muscles are evident. Scale bars: 50 µm. **D.** and **E.** Quantification of mean myofiber area and diameter of P9 TA muscles, respectively. Controls: n=2 animals, 3116 fibers. Hb9(Cre^+)SMA n=3 animals, 5729 fibers. Hb9(Cre^-)SMA n=3 animals, 4511 fibers.

We also assessed NMJ receptor morphology, similarly to what was done in Lee *et al*. (2011) [40] and Kummer *et al*. (2004) [137], to determine if we were able to rescue Hb9(Cre^+)SMA mice from an impairment of postsynaptic maturation. In developing and early postnatal mice, AChRs have an immature morphology appearing as even simple plaques. As the mouse matures, so does the endplate with its morphology evolving to more complex forms with perforations and branches, eventually resembling a "pretzel".

In SMA-like mutant mice the progression from a simple plaque to a complex form is severely delayed with the persistence of an immature plaque-like morphology in the majority of NMJs [40]. Sections of P9 triceps from Hb9(Cre^+)SMA, Hb9(Cre^-)SMA, and controls were observed and the postsynaptic AChR aggregates were classified into one of four different categories (plaque, perforated, C-shape or complex) . At P9, the triceps of Hb9(Cre^+)SMA mice had 80.51 ± 2.36 % of the endplates evaluated (n= 3 animals/ 190 endplates per animal) in the immature plaque-like stage. This was almost identical to what was observed for the Hb9(Cre^-)SMA in which 81.23 ± 3.56% of the endplates assessed (n= 3 animals/ 185.3 endplates/animal) were plaques as well (Fig. 3.10). However, this was not surprising in light that the control group also had the majority of its NMJs assessed in the immature plaque-like stage, likely due to the very young age (P9) at which the animals were evaluated (80.34 ± 2.61%, n= 4 animals/110.5 endplates per animal). The remaining percentages of receptors were classified between the categories perforated [Hb9(Cre^+)SMA = 9.37 ± 4.26%; Hb9(Cre^-)SMA = 12.10 ± 2.35%; Controls = 11.72 ± 2.24%], C-shape [Hb9(Cre^+)SMA = 4.67 ± 3.83%; Hb9(Cre^-)SMA = 5.85 ± 1.22%; Controls = 4.89 ± 1.65%], or complex [Hb9(Cre^+)SMA = 3.22 ± 1.61%; Hb9(Cre^-)SMA = 2.84 ± 0.47%; Controls = 3.00 ± 1.20%] (Fig. 3.10). We found no statistical difference between Hb9(Cre^+)SMA and Hb9(Cre^-)SMA mice ($p \geq 0.60$). Also, there was also no difference between either of these two and the control group for any of the categories ($p \geq 0.62$). Lee *et al.* observed open, more mature, configurations of control sternomastoid muscles starting at P12 but in the soleus and EDL muscles, most of the receptors were yet immature at this stage. This is consistent with the known rostral

to caudal pattern of maturation of the NMJ. In our case, we expected that a proximal muscle such as the triceps would present WT endplates at more mature stages. We suggest that this is due to the early stage at which the endplates were evaluated and thus, future studies should be conducted on older end-stage animals.

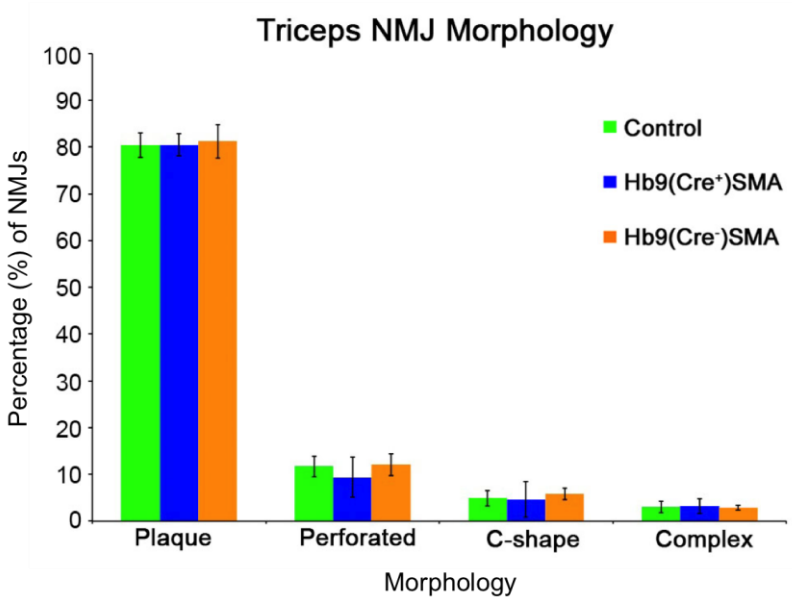

Fig. 3.10. AChR aggregate morphology. In P9 Hb9(Cre^{+})SMA, Hb9(Cre^{-})SMA and control triceps most of the AChR aggregates still remained in the plaque stage, while the few remaining receptors were distributed evently amongst the three groups into more mature stages of perforated, C-shape and complex morphological stages. We found no effect of genotype on receptor morphology and no significant difference between our P9 animal groups in any of the categories included in the assay at P9.

Ko and colleagues demonstrated a selective vulnerability to denervation of specific, clinically relevant muscles in SMAΔ7 mice [104]. Denervation of vulnerable muscles was restored to control values in *ChAT*$^{Cre+}$ conditional SMAΔ7 mice [57]. We determined the innervation status of NMJs in the triceps, one of the reported vulnerable appendicular muscles [104], by first co-staining longitudinal sections for AChRs and synaptophysin, a synaptic vesicle marker. While lack of synaptophysin staining may not

be indicative of structural denervation (i.e. absence of an axon terminal), increased synaptophysin coverage of an endplate is necessarily associated with axon terminal presence. Images were taken and processed as above. Endplates were classified as fully-occupied if at least ~75% of the AChR area was covered by synaptophysin staining. On the other hand, they were deemed as unoccupied if less than ~25% of the AChR area showed synaptophysin staining. Endplates with synaptophysin staining in between were categorized as partially occupied. We found a statistically significant improvement in the synaptophysin coverage of the P9 triceps endplates in Hb9(Cre^+)SMA mice (Fig. 3.11B). Thus, the fraction of fully-occupied synapses increased in $Hb9^{Cre+}$ SMAΔ7 mice over that in SMA mice [Hb9(Cre^+)SMA=57.47 ± 5.58%; Hb9(Cre^-)SMA= 23.00 ± 1.65%], while the fraction of unoccupied endplates decreased in the rescued animals relative to SMA mice [Hb9(Cre^+)SMA=25.97 ± 6.2%; Hb9(Cre^-)SMA=48.93 ± 3.37%]. Partially-occupied synapses also were reduced in numbers in Hb9(Cre^+)SMA mice [15.29 ± 0.86% vs. 29.46 ± 2.11% in Hb9(Cre^-)SMA animals]. However, the improvement in synaptophysin occupancy in the $Hb9^{Cre+}$ SMAΔ7 mice did not quite reach the levels observed in the control animals (Fig. 3.11B). To directly assess structural innervation, we co-stained serial triceps longitudinal sections for AChRs and neurofilament, a structural axonal marker. Synaptic sites labeled with BTX were considered innervated if there was overlap, however small, between NF and AChR staining, while complete lack of NF at synaptic sites categorized them as denervated (Fig. 3.11C). Innervation was also improved clearly in Hb9(Cre^+)SMA triceps using overlap between NF and BTX as scoring criterion (Fig. 3.11D). Thus, Hb9(Cre^-)SMA

triceps had 56.29±1.11% of innervated endplates, whereas Hb9(Cre^{+})SMA triceps displayed 86.36±2.6 % innervated synapses, a percentage similar to controls.

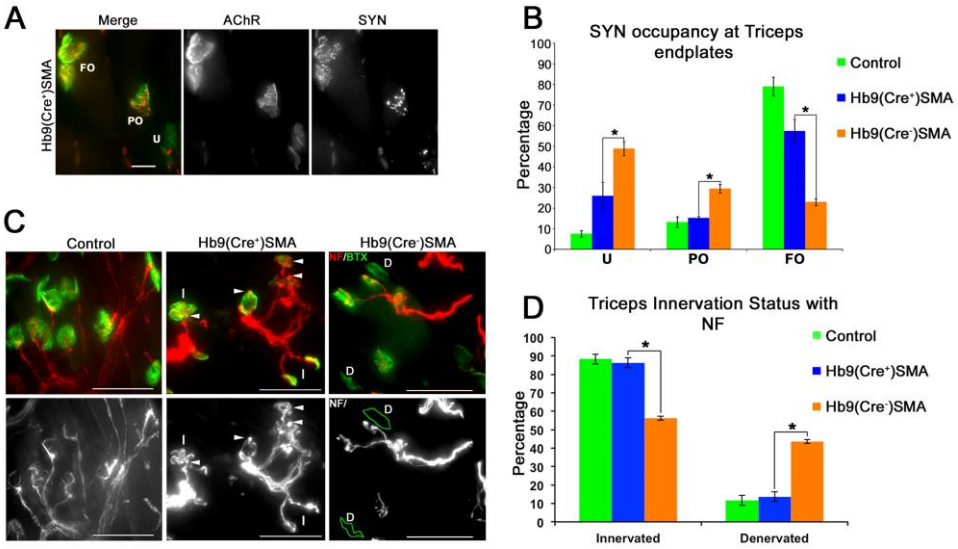

Fig. 3.11. Innervation status is improved in Hb9(Cre^{+}) SMA mice. A. A longitudinal section (40 µm-thick) from triceps muscle, from a P9 Hb9(Cre^{+})SMA animal, co-stained for synaptophysin (SYN) and BTX, to label nerve terminals and AChRs, respectively. A flattened 2D image derived from a wide field 3D stack for the fluorescein (AChR) and rhodamine (SYN) channels and their merge is shown. Two NMJs in the upper left have complete coverage of SYN staining over AChR staining, and are examples of fully-occupied (FO) NMJs. Two endplates in the bottom right (arrow), one sideways, one en face, lack detectable SYN staining, and are examples of unoccupied (U) endplates. The one endplate in the middle is partly covered by SYN staining and is an example of a partially-occupied (PO) NMJ. Scale bar: 20µm. **B.** Quantification of synaptophysin occupancy of triceps endplates. The percentage of fully-occupied NMJs was increased, and the percentage of partially- and unoccupied endplates were reduced in Hb9(Cre^{+})SMA mice relative to Hb9(Cre^{-})SMA animals (*p < 0.008, t-test). Controls: n=5 animals, 403 endplates. Hb9(Cre^{+})SMA: 3 animals, 394 endplates. Hb9(Cre^{-})SMA: 3 animals, 439 endplates **C.** Top panels: Representative merged images of P9 triceps longitudinal sections stained for NF (red) and BTX (green). Bottom panels: NF channel in black & white. In the top left panel (control) axons can be seen overlapping part of the BTX stain or barely entering the synaptic site (endplate on the lower right corner). Arrowheads in the middle panels indicate NF accumulations at synaptic sites on Hb9(Cre^{+}) SMA tissue. All the synapses in the middle panels were considered as innervated, three of them are indicated as (I). The right top panel (Hb9 (Cre^{-}) SMA) shows two examples of endplates completely lacking NF/BTX overlap and thus considered denervated (D). These two endplates have been outlined in green in the bottom right panel, to further clarify their lack of overlapping NF staining. Scale bars: 50 µm. **D.** Quantification of triceps innervation using NF/BTX overlap as criterion. The percentage of innervated endplates was increased and the percentage of denervated NMJs were reduced to control levels in Hb9(Cre^{+})SMA mice relative to Hb9(Cre^{-})SMA animals (*p = 0.0004, t-test). Controls: n=3 animals, 533 endplates. Hb9(Cre^{+})SMA: 3 animals, 478 endplates. Hb9(Cre^{-})SMA: 3 animals, 559 endplates.

Thus, of the three NMJ structural phenotypes that were different between WT and SMA mice, endplate area and innervation status, but not presynaptic NF accumulation showed significant improvements in Hb9(Cre^{+})SMA mice relative to diseased animals. Interestingly the increase in endplate size appeared to occur in the absence of an increase in myofiber size.

3.5 DISCUSSION

Compared to previous studies [57, 107, 141], ours seems to be the one in which restored spinal cord SMN levels are the lowest. Yet we were able to document full rescue of endplate size regardless of the susceptibility of a muscle to denervation and substantial recovery of innervation on a denervation vulnerable muscle. The increase in endplate size was not the result of an increase in muscle fiber size. The implication for therapeutics evaluation of this observation is that rescue of endplate size could be interpreted as a direct benefit on motor neurons rather than an indirect result of an increase in muscle fiber girth. Hence, our experiments uniquely highlight the exquisite sensitivity of these NMJ phenotypes to very small changes in SMN in spinal cords. These two phenotypes can be rescued by SMN levels that fail at reducing presynaptic NF accumulation, maturation of the endplate morphology, increasing animal weight and lifespan or improving overall motor performance. All of the above phenotypes were rescued or improved in $ChAT^{Cre+}$ conditional SMAΔ7 mice [57] , which our data imply display substantially more efficient Cre-mediated recombination in spinal cord than $Hb9^{Cre+}$ conditional SMAΔ7 mice. Thus, we suggest that our experiments establish a

threshold of SMN expression in motor neurons that distinguishes an order of SMN sensitivity for different SMA phenotypes.

Despite the inefficient restoration of motoneuronal SMN in *Hb9*$^{Cre+}$ conditional SMAΔ7 mice, the subclinical neuromuscular innervation improvements that can be measured in them raise the possibility that similar benefits could be seen in SMA patients even when the latter are under therapeutic interventions with known modest effects in raising SMN levels.

The pattern of structural neuromuscular phenotypes rescued in *Hb9*$^{Cre+}$ conditional SMAΔ7 mice was very similar to that in *Myf5*$^{Cre+}$ conditional SMAΔ7 mice [57]. Thus, TA endplate size and innervation status of a vulnerable muscle (the splenius capitis), but not levels of NF accumulation, were rescued in *Myf5*$^{Cre+}$ conditional SMAΔ7 mice. *Myf5*$^{Cre+}$ is strongly expressed in skeletal muscle but also weakly in spinal cord, including motor neurons (Fig. 3.3B [57]). Although whole spinal cord samples from *Myf5*$^{Cre+}$ and *ChAT*$^{Cre+}$ conditional SMAΔ7 mice seemed to have similar *SMN67m8h* levels (Fig 3.3B, [57]), it is important to point out that only a fraction of the full-length SMN expression in *Myf5*$^{Cre+}$ conditional SMAΔ7 mice may come from motor neurons themselves as *Myf5*$^{Cre+}$ was found strongly expressed in ChAT-negative ventral horn neurons and in dorsal root ganglia [57]. Thus, it is possible that expression of *Myf5*$^{Cre+}$ and *Hb9*$^{Cre+}$ in motor neurons may be more similar than suggested by our qRT-PCR in whole spinal cord samples. Our results with *Hb9*$^{Cre+}$ SMA mice strongly suggest that the rescue of endplate size and innervation status in *Myf5*$^{Cre+}$ SMA mice is explained by its expression in motor neurons and not in muscle. This is consistent with

the observation that these phenotypes were not rescued in *MyoD*$^{iCre+}$-expressing animals, which only had Cre expression in muscle but not spinal cord [57]. In normal animals, there is a direct correlation between muscle fiber girth and endplate size [140]. However, TA fiber diameter increased in *MyoD*$^{iCre+}$-expressing animals without a corresponding increase in endplate size [57] and the increase in P9 TA endplate size observed here occurred without a change in average muscle fiber size (Fig. 3.9 C-E). Thus, together these data suggest that endplate size, at least in SMA severe mice, is largely a motor neuron cell autonomous phenotype. While structural NMJ phenotypes, excluding NF accumulation, were improved in *Hb9*$^{Cre+}$- and *Myf5*$^{Cre+}$-conditional SMAΔ7 mice (this work and [57]), central structural phenotypes (i.e. loss of motor neuron numbers and of glutamatergic synapses onto their somas), which we did not analyze here, were not rescued in *Myf5*$^{Cre+}$-expressing animals [57]. They were mitigated in the higher SMN expressing *ChAT*$^{Cre+}$ conditional SMAΔ7 mice [57]. Together the above results suggest that peripheral structural phenotypes may be more sensitive to levels of SMN than central structural phenotypes.

The expression patterns for *ChAT* and *Hb9* largely overlap in that they both are present in motor neurons. *Hb9* may come up earlier during development than *ChAT*, but it is not surprising that the latter drives higher levels of transcription than the former, as transcription factor genes are generally expressed at lower level than other genes. Sets of non-overlapping interneurons in the spinal cord also express *Hb9* and *ChAT*. The former is expressed in glutamatergic V_x interneurons, while the latter is expressed in cholinergic $V0_c$ interneurons [138]. $V0_c$ interneurons are marked by expression of the Pitx2

transcription factor and interestingly modulate motor output amplitude [142]. It is a remote, though testable, possibility that restoration of SMN expression in $V0_c$ interneurons in *ChAT*$^{Cre+}$ conditional SMAΔ7 mice contributes to the difference between our results and those of Martinez and colleagues [57]. Much more likely is the possibility that recombination of the *Smn*^{Res} allele is more efficiently driven by *ChAT*^{Cre} than by *Hb9*^{Cre} simply because higher levels of the recombinase result from the former than the latter. Thus, one possibility is that recombination fails in many more motor neurons in Hb9(Cre^{+})SMA than in ChAT(Cre^{+}) SMA mice. This may be critical to mitigate whole animal phenotypes such as survival, weight and motor function but not NMJ phenotypes such as endplate size and innervation status as long as the endplates where these phenotypes are examined are innervated by motor neurons where Cre recombination occurred. Another possibility is that both *Smn*^{Res} alleles are repaired in more *ChAT*^{Cre}-expressing than *Hb9*^{Cre}-expressing motor neurons. This would translate into higher levels of SMN protein per motor neuron in *ChAT*^{Cre} animals. Thus, a combination of these non-exclusive alternatives may account for the higher *SMN67m8h* transcript levels in spinal cord from ChAT(Cre^{+})SMA mice, which lead to a more extensive rescue.

While our finding that spinal cord from *Hb9*$^{Cre+}$ conditional SMAΔ7 mice had remarkably much lower levels of full-length SMN transcript than spinal cord from *ChAT*$^{Cre+}$ conditional SMAΔ7 mice explains our results vis-à-vis those of Martinez and colleagues [57], it is more difficult to account for the results of Gogliotti and colleagues [107], who used the same *Hb9*^{Cre} line we used here, albeit to rescue a different

conditional *Smn* allele ($Smn^{2B\text{-}Neo}$). To generate $Smn^{2B\text{-}Neo}$, three nucleotide substitutions (GGA→TTT) were engineered in the exon splice enhancer within *Smn* exon 7 and a *pgk-neo* cassette, flanked by WT *loxP* sites, was inserted downstream in the intron between *Smn* exons 7 and 8 [108]. Upon Cre recombination, *the pgk-neo* cassette is excised, and the allele becomes Smn^{2B} [106, 108]. $Smn^{2B/2B}$ mice show no signs of SMA phenotype and have a normal lifespan, despite ~66% decrease in SMN protein in spinal cord [106]. Contrary to Smn^{Res} [2], the $Smn^{2B\text{-}Neo}$ allele yields transcripts encoding full-length SMN prior to Cre recombination (~7.5% WT allele levels [108]), although like *SMN2*, the majority of its transcripts encode SMNΔ7 [108]. $Smn^{2B\text{-}Neo/2B\text{-}Neo}$ mice are embryonic lethal that die between E9.5-E12.5, later than $Smn^{-/-}$ embryos, which die at E7.5 [108]. Full length SMN protein could be detected in $Smn^{2B\text{-}Neo/2B\text{-}Neo}$ embryos at 1-3% WT levels, somehow lower than predicted by the levels of transcript [108]. This embryonic lethality can be rescued in $Smn^{2B\text{-}Neo/2B\text{-}Neo}$; $SMN2^{+/-}$ mice, which die perinatally around P7 [107]. Like us, Gogliotti et al. used $Hb9^{Cre}$ to selectively restore SMN in motor neurons of $Smn^{2B\text{-}Neo/2B\text{-}Neo}$; $SMN2^{+/-}$ mice [107]. However, unlike results reported here with conditional SMAΔ7 mice, they found improvements in lifespan (to just P12 on average), weight, and motor behavior assayed by the righting reflex and hindlimb suspension tests, the same tests used here. NMJ pathology also improved in $Hb9^{Cre+/-}$; $Smn^{2B\text{-}Neo/2B\text{-}Neo}$; $SMN2^{+/-}$ mice. We propose that their more extensive rescue was due to the endogenous low levels of full length SMN protein afforded by the $Smn^{2B\text{-}Neo}$ allele, that together with those provided by the Smn^{2B} allele (i.e. after recombination) yielded higher overall levels of SMN in motor neurons. This interpretation assumes that

the recombination efficiency of Smn^{Res} and $Smn^{2B\text{-}Neo}$ was the same in the two experiments as both used the same $Hb9^{Cre}$ line. However, the recombination efficiency may not only depend on the levels of Cre but also on the nature of the two conditional alleles. Hence, to be repaired $Smn^{2B\text{-}Neo}$ requires the excision of the *pgk-neo* cassette, while Smn^{Res} requires the inversion of the 3'→5' *Smn* exon 7 (Fig. 3.2). The *pgk-neo* cassette in $Smn^{2B\text{-}Neo}$ is flanked by WT *loxP* sites, while the inversion cassette in Smn^{Res} is flanked by mutant *lox66/lox71* sites, which ensures the irreversibility of the inversion reaction [143]. To reach comparable levels of recombination efficiency in vitro, Cre-mediated inversion of *lox66/lox71*-flanked DNA regions requires 2-3 fold more Cre than Cre-mediated excision of WT *loxP*-flanked DNA regions [143]. In vivo, the same study showed that *lox66/lox71* inversion was slightly less efficient than WT *loxP* excision [143]. Thus, it is possible that the $Hb9^{Cre}$-driven recombination efficiency of $Smn^{2B\text{-}Neo}$ is higher than that for Smn^{Res}. This, together with the likely higher basal levels of full-length SMN in $Smn^{2B\text{-}Neo/2B\text{-}Neo}$; $SMN2^{+/-}$ mice relative to conditional SMAΔ7 mice, may account for the amelioration of less SMN-sensitive phenotypes observed by Gogliotti *et al.* [107], which we failed to observe in our experiments. Recent experiments by others indicate that pathology in cells other than motor neurons critically underlie the short lifespan of severe SMA mice (for review see [144]). As the two lines carrying the inducible conditional *Smn* alleles, Smn^{Res} and $Smn^{2B\text{-}Neo}$, continue to be used to determine the contribution of other cell types to the SMA phenotype and lifespan, it will be important that the research community be aware of the differences between these two conditional lines regarding their endogenous SMN levels and their differential demand

for Cre drivers. While used successfully by many for excision of floxed alleles (e.g. references in http://jaxmice.jax.org/strain/006600.html), our results raise the possibility that *Hb9*^{Cre} might not be a robust Cre driver for inversion of floxed alleles in general.

Notwithstanding the involvement of other cell types suggested by animal models, survival and other defects in motor neurons are still expected to be hallmark features of the human disease. Having biomarkers that directly reflect changes in motor neuron phenotypes following a therapeutic approach is still very important. The apparent higher SMN sensitivity and the easier experimental accessibility of the NMJ better position peripheral structural phenotypes to serve as biomarkers for testing therapeutic interventions than central structural phenotypes. Indeed, Ko and colleagues already demonstrated that denervation of vulnerable muscles can serve as a very sensitive biomarker to evaluate pharmacological interventions in SMAΔ7 mice [104]. Results of the present study further support this conclusion. Our analysis of endplate area in one denervation-vulnerable (triceps) and one denervation-resistant (TA) muscle, innervated by motor neuron pools located in opposite ends of the spinal cord, indicates that this phenotype could also be used as a sensitive motoneuron-autonomous marker to evaluate drug therapies in SMAΔ7 mice. Although both parameters appear equally sensitive to small increases in SMN levels, endplate size has the potential advantage of applying to all muscles, regardless of their vulnerability to denervation. An additional important conclusion derived from our study is that both endplate area and denervation status can be mitigated without impact on motor behavior. This suggests that in order to properly

evaluate drug efficacy the improvement of these sensitive parameters has to be considered in the context of parallel changes in motor function.

CHAPTER IV

DISCUSSION AND CONCLUSIONS

Autosomal recessive SMA is characterized by the paucity in production of the SMN protein, which leads to loss of motor neurons causing muscle atrophy, paresis, and in the most severe cases infantile death (Type I and II SMA) [5, 36, 56]. A minimal level of SMN protein is essential for cell survival, regardless of cell type, and this is consistent with its essential housekeeping functions in spliceosome assembly. Nevertheless, motor neurons are the cells most severely and consistently affected by the reduction of SMN [41]. The pathology seen after SMN reduction could be due to altered splicing of a select group of genes important in motor neuron circuitry by the disruption of snRNP formation, alterations to the axonal functions for SMN, or both [5]. A recent transcriptome study by Zhang *et al.* (2013) has demonstrated that a significant contributor to the SMA pathology is the dysregulation of key mRNAs in motor neuron synaptogenesis that lead to motor neuronal impairments. This was found in motor neurons and surround glial cells in the spinal cords of SMAΔ7 mice by P1, before any overt pathology is observed. Amongst the mRNA found to be altered were agrin's Z exons that are critical for NMJ maintenance, a synapse pruning-promoting complement factor (C1q), and a transcription factor required for establishing sensory-motor circuitry (Etv1/ER81) [145]. These results directly link SMN's general function in RNA metabolism with SMA pathogenesis in motor neurons. Extensive research has been performed attempting to elucidate whether SMA is a cell-autonomous disease, with

motor neurons as the primary target, or a non-cell-autonomous disease in which other cells are just as susceptible to low levels of SMN needing be rescued in conjunction.

Patients have particularly low levels of spinal cord SMN [11] and a direct implication of the phenotype is that correcting motor neuron insults should be the natural target of treatment development [36]. Additionally, neurons have a remarkable resilience towards some genetic insults that allows for their rescue making them a viable target [2]. Although the genetic reduction of SMN solely in motor neurons does not cause lethality it is enough to yield some features of the SMA phenotype in mice (such as NMJ structural, and electrophysiological abnormalities) [19, 55, 107]. SMN-deficient motor neurons and/or muscle fibers lead to SMA. Thus, it would be expected that restoration specifically in these tissues would bring forth conspicuously positive results. Yet, this has not been the case [56, 57, 107, 110]. Many questions remain unanswered regarding disease pathology and the causative pathways. Resolution of such enigmas is key for the development and optimization of therapeutic strategies [96]. In an attempt to address these key questions we focused on selectively raising SMN expression in motor neurons using two approaches with two different severe SMA models. First, we exogenously restored human SMN, driving its expression selectively in motor neurons with an *Hb9* promoter, in severe SMA mice that die perinatally, to assess whether their survival could be extended. We determined that hemizygous inheritance of the transgene was insufficient to increase survival of SMA animals. At the protein level, transgene expression was detected by immunostaining in embryos and until the first postnatal week in the ventral horn of the spinal cord. Expression of human SMN was solely

detected in spinal cord. Nonetheless, transgenic *hSMN mRNA* expression was undetected by late embryogenesis likely due to the timing of expression of the *Hb9* promoter, which decreases by this developmental stage. A slow hSMN and GFP turnover may explain the detection of transgenic protein postnatally. Transgene-positive control mice were found to have improvements in motor behavior, when determined by the Righting Reflex test, as well as significantly fewer neonatal mortalities than transgene-negative control mice. These benefits granted by the motor neuronal-restoration of low levels of SMN through the *Hb9(Gfp/SMN)* transgene are consistent with the idea that motor neurons are a necessary target in SMA rescue efforts.

In our second approach, we restored endogenous motor neuronal-SMN expression following prenatal *Hb9*-dependent Cre recombination of a conditional hybrid mutant allele (Smn^{res}) in another severe SMA mouse model (SMAΔ7-like). Cre recombination irreversibly transforms the Smn^{res} allele to WT. Unlike a previous study that used choline acetyltransferase ($ChAT^{Cre+}$) as a driver on the same mice, we found no improvement in survival, weight, motor behavior, endplate morphology, and presynaptic neurofilament accumulation. All of the above were improved or mitigated in $ChAT^{Cre+}$ SMA mice. We did, nonetheless, rescue endplate size and mitigate NMJ denervation status. The rescue of endplate size occurred in the absence of an increase in myofiber size, suggesting endplate size is determined by the motor neuron in SMAΔ7-like mice. Real time-PCR showed that the expression of spinal cord SMN transcript was sharply reduced in $Hb9^{Cre+}$ SMA mice relative to $ChAT^{Cre+}$ SMA mice. This suggests that our lack of overall phenotypic improvement is most likely due to an unexpectedly poor

recombination efficiency driven by $Hb9^{Cre}$. However, from our results we can infer that endplate area and status of innervation may be NMJ parameters highly sensitive to low increases in SMN that can serve as biomarkers in SMA research. Furthermore, therapeutic interventions with very modest effects in raising SMN in motor neurons may still provide mitigation of neuromuscular phenotypes in SMA patients. Also, using a combination of dystrophin staining with imaging processing with the Metamorph sorftware, we devised a new method to measure myofiber size that is very fast, practical and allows for a large number of fibers to be measured simultaneously.

Though the results were not what we had hoped to find, we were able, through both approaches, to provide data that supports the notions that motor neurons are key in pathology and a necessary target (among others) for future therapy development. This is in line with past studies, which demonstrated that some motor neuron-SMN restoration is necessary to improve the phenotype though not sufficient to achieve a complete correction and suggest that increased levels of SMN are also required in other tissues including those in the autonomic nervous system [36].

It is unclear if there is a differential necessity for SMN expression levels in different cell types. A critical threshold for SMN that dictates the onset of SMA pathology has been derived from studies in the Smn^{2B} mouse model. The presence of one or two Smn^{2B} alleles is enough to reduce protein expression but these mice have a normal lifespan and physiology. When SMN levels are further reduced in Smn^{2B-} mice (10% and 15% less than WT in spinal cord and brain respectively) the phenotype begins to resemble that of SMA [106]. Bowermann *et al.* (2012) suggest that the severity of

SMA is more dependent on a narrow threshold for SMN levels of expression rather than a linear function of pathology [106]. This is most likely because different cell populations have different needs of SMN levels, and as more cells reach their limit of functionality with low SMN, the overt pathology appears. Equally, small increases of SMN past the required threshold will be enough to improve the phenotype. Additionally, mice with 4 ≥ copies of *SMN2* show complete rescue and a normal lifespan. This means that modestly enhanced ubiquitous expression of FL-SMN from the *SMN2* gene can prevent SMA [96]..

Muscles may require a very high amount of SMN increase to rescue muscle-related symptoms. Martinez *et al.* (2012) selectively restored SMN expression solely in skeletal muscle, using a *MyoD* promoter to drive Cre recombination of the same Smn^{res} allele used by us. They found that a vast increase of almost 500% in FL-SMN protein was enough to restore myofiber size but only modestly improve lifespan (5-6 days) with no improvements in any of the NMJ phenotypes assayed [57]. This may suggest that muscle fibers are less sensitive to SMN levels and would require additional protein restoration.

It is also unclear whether there is a differential necessity for SMN expression during all stages of development. Early postnatal induction of SMN has been determined as the most efficacious [2, 28, 111] and if SMN is indeed restored in a timely manner, the progression of the pathology could be halted. Even though improvements are found by increasing SMN at later stages of pathology, it is becoming quite clear that, at least in SMA model mice, there is a window of time within which the protein must be restored

for optimal effect by therapeutic efforts [2, 28, 68]. The experimental approach of our first aim, described in Chapter II, has managed this. We found that *Hb9* did drive the expression of exogenous human SMN from very early on as it was detected by E13 in immunohistochemical assays. Yet, the transcriptional activity of *Hb9* is reduced by late embryogenesis since we were unable to detect the *mRNA* expression from the *Hb9(Gfp/hSMN)* transgene at E18 in transgene-positive spinal cords by qRT-PCR. This most likely accounts for the failure to increase lifespan in the severe SMA mouse model used. Nonetheless, this early restoration of SMN in motor neurons proves efficacious to improve neonatal survival and motor behavior in transgene-positive *Smn* heterozygous or WT littermates. Thus, our results further support the notion that early restoration proves beneficial. However, if the early restoration is not maintained to at least the perinatal stage there will not be a clear rescue.

To bypass the issues of SMN-restoration timing from our first approach, we moved forward with the second approach (described in Chapter III and Paez-Colasante *et al.* (2013) [56]). In this second study, SMN was restored by $Hb9^{Cre}$-mediated recombination of the conditional Smn^{res} allele in a permanent manner during early embryogenesis using the mouse's own *Smn* promoter as opposed to the first approach in which an exogenous *Hb9* promoter drove human SMN expression. If the $Hb9^{Cre}$ driven recombination were efficiently producing high enough levels of endogenous SMN, significant positive results over the phenotype were to be expected since this approach of protein restoration would be the most similar to the naturally occurring process in WT mice.

Another question that remains is whether SMN is required in adult motor neurons to survive. We have not addressed this but it would be important because if SMN is indeed a survival factor for motor neurons during adulthood, it could be used as a therapeutic option for Amyotrophic lateral sclerosis (ALS) patients as well [96]. ALS is the most common adult-onset fatal neurodegenerative disease in which upper and lower motor neurons are lost. There is a lot of crossover between ALS and SMA pathologies [146], for example, gem depletion and similar patterns of neuroinflammation have been observed in both diseases [147, 148]. Copy number abnormalities of *SMN* have been reported in sporadic ALS. Expression of SMN in spinal anterior horn cells is significantly associated with cell size and may be reduced when these cells are atrophic. However, unlike in SMA, decrease of SMN in spinal anterior horn cells in ALS patients may be a secondary phenomenon in this disease [149]. Therefore, ALS patients could benefit from SMA-directed therapeutics currently in the pipeline.

Furthermore, an additional question that remains to be addressed is whether different severities of SMA will require differential levels of SMN, especially because the time frame when motor neurons are lost in milder types is not well known. It is proven that increases of SMN early on in life are needed to rescue severe SMA mice, but what if SMN is increased later on in life for type II or III patients in the more symptomatic stages? It might be possible that this would allow the remaining motor neurons to perform better according to Arnold *et al.* (2013) [68]. A future step will be to address this through clinical trials with patients of various types of SMA.

Despite the standing motor neuron dogma, research is now deviating towards

considering SMA as a non-cell autonomous disease with other important targets as key in pathology and therapy. Motor neuron cell loss has not been detected before postnatal P4 in SMAΔ7 mice and is not significant towards the end-stage of survival [6], while muscle weakness is evident as early as P2 [30]. Thus, the first behavioral abnormalities are due to impairments in motor neuron function [6]. If motor neurons are lost, it can be in a similar amount between mice of ranging severity and produce very different outcomes. For example, even a 50% loss of motor neurons can still result in viable year-old *Smn* heterozygous mouse as long as the remaining motor neurons are healthy [150], while just ~30% cell loss at the end-stage of severe SMA mice is lethal [30], indicating that the number of motor neurons lost is not as determinant of pathology but rather the time when these cells are lost and the state of the remaining motor neurons that can compensate may be the determinant [37]. We did not study motoneuron loss in our experiments with either of our two models.

If SMA, at least in SMAΔ7 mice, is in fact a disease of motor neurons, it can act in a manner that does not result in their death or disconnection [40]. Motor neurons seem to be well connected to their targets except for the denervation-vulnerable muscles [104]. A group led by Dr. Ko has determined which muscles are most likely to suffer from denervation. The triceps was one of the appendicular muscles determined as denervation-vulnerable in SMAΔ7 mice [104], therefore it was the muscle we assayed for status of innervation (Chapter II and Paez-Colasante *et al.* (2013) and found a significant improvement in Hb9(Cre^{+})SMA mice. Nonetheless, even with this parameter rescued and the fact that several important hindlimb muscles are not typically

denervated, the reduction of SMN still alters many aspects of neuromuscular development [40] and produces a reduction of synaptic vesicle release (~50% in quantal content) [132]. Consequently, it is unlikely that these abnormalities can account for the impairments of motor behavior, thus muscle weakness and motor dysfunction might be the result of alterations in spinal circuit function [55].

It is possible that other neurons besides motor neurons are contributing to the motor impairments seen in SMA. Several studies have described pronounced early deficits of spinal reflexes and reduced numbers of proprioceptive synaptic inputs onto motoneurons of SMAΔ7 mice. Ling *et al.* (2010) studied the spinal and neuromuscular circuitry of motor behavior in SMAΔ7 mice. In the spinal circuitry they determined an approximate 30% loss of synapses onto lumbar motor neurons and a significant reduction in proprioceptive sensory neurons [51]. Proprioceptive neurons provide essential inputs to motor circuits and can serve as potential targets [50]. This group has inferred that synaptic defects may occur at multiple levels of the spinal and neuromuscular circuitry [51]. Another group's findings indicate that profound spinal circuit dysfunction occurs very early on generating impairments in motor function. They have demonstrated, in the SMAΔ7 mouse as well, that the strength of the monosynaptic connection between primary proprioceptive afferents and motor neurons is reduced and this occurs before detectable motor neuron cell loss [55]. Similar results are found in *smn* null *Drosophila* [50] though the differences between *Drosophila* and mammalian motor circuits limit the extrapolation of those results towards what may occur in SMA patients. Imalach *et al.* (2012) found that motor neuron-SMN restoration did not produce

great positive results but rather SMN is required in both proprioceptive and central cholinergic neurons to rescue defect in motor neurons and muscles, at least in the fruit fly *smn* mutants [50]. Though proprioceptive and central cholinergic neurons need to be rescued, they will most likely not be the only cell populations that require SMN restoration. Martinez *et al.* (2012) and Gogliotti *et al.* (2012) did rescue the loss of proprioceptive innervation to motor neurons in their experiments of motor neuron-selective SMN restoration. Yet, they only achieved a modest increase in survival via their approaches. Other cell types in the spotlight for SMA research are glial cells. Reactive astrocytosis or gliosis are hallmarks of neurodegenerative diseases such as SMA or ALS. Gliosis in the spinal cord is associated with a severe reduction of motor neuron number and oxidative stress-related products that are deposited into the remaining atrophic motor neurons [148]. Increases in glial cell-derived neurotrophic factor levels have been detected in the cerebrospinal fluid of SMA patients. Glial cell-derived neurotrophic factor is one of the most powerful survival factors for motor neurons [151].

Under healthy conditions, astrocytes are critical for maintenance of the blood brain barrier, nourishment, regulation of synapse formation and function, ion uptake, clearing of excess glutamate from the synaptic clefts, and growth factor secretion, among others [152, 153]. One very recent study has demonstrated that there are morphological, cellular, and activation state changes in astrocytes in SMAΔ7 murine spinal cords seen prior to overt motor neuron loss [152]. McGivern *et al.* (2013) also observed increases in basal intracellular calcium levels and a reduced calcium response

to ATP in iPSC-derived astrocytes from two SMA patients [152]. Astrocytes should be considered as an additional target for therapeutic efforts. Low levels of SMN have been detected in Schwann cells and this has been linked to the induction of primary intrinsic changes. In Schwann cells, the SMN protein is required either to regulate translational control of key myelin proteins and/or to modulate protein turnover [154]. Schwann cells from SMA mouse models fail to respond normally to myelination cues in culture, therefore they are unable to myelinate healthy motor neurons efficiently and thus are detrimental to their stability. Cellular and molecular aspects of myelination are affected in peripheral nerves with a delay in maturation of axo–glial interactions at paranodes; for example, myelination in intercostal nerves was perturbed at early- and late-symptomatic stages of disease in two SMA mouse models. Also, apoptotic pathways are initiated in Schwann cells when they are directed towards a myelinating phenotype [154]. In a study by Hunter *et al.* (2013) myelin protein expression was restored in SMA Schwann cells following transfection with an SMN construct. By performing this experiment, the group demonstrated that the defects observed in Schwann cells/neuron co-cultures were due to deficiencies of Schwann cells themselves and that this process was SMN-dependent and reversible [154].

Pan-neuronal SMN restoration seems to be the most promising strategy. Further evidence that other neuronal cell populations besides motor neurons are important in SMA and that pan-neuronal expression of SMN is efficient at increasing lifespan is a study by Gavrilina *et al.* (2008). Here, SMN expression was mediated by the prion promoter PrP^{92} which accomplished to increase the lifespan of SMA model mice

significantly (~200 days) and rescued several aspects of pathology such as the number of motor neurons [110]. The prion protein promoter is expressed abundantly throughout the nervous system but also at very low levels in muscles [110], therefore it cannot be easily concluded that muscles are not important in restoration efforts in these experiments Another group determined that expression of transgenic SMN in the CNS by viral vectors is also able to rescue the survival and motor behavior of SMAΔ7 mice [78, 110].

Increasing awareness of how low levels of SMN affect a wide range of cells has broadened the understanding of the contribution that non-neuronal cells have in the pathogenesis of SMA. Because of the observed abnormalities in non-motor neurons in severe SMA models, such as reduction of synaptic bouton area, sensory projection dysfunctions, central synaptic defects, affected neurogenesis and neuritogenesis, general pathological changes in brain including weight and size, one can conclude that other cells are affected by the reduction of SMN as well but with differential sensitivity to lesser SMN. There seems to be a gradient of susceptibility to SMN reduction in the nervous system in which motor neurons might be at one extreme of the spectrum having the highest susceptibility [96].

In conclusion, though we were unable to achieve vast improvements in lifespan and pathology of SMA model mice using two approaches to selectively restore SMN in motor neurons, we did find improvements or complete rescue of certain parameters such as NMJ endplate size and status of denervation in the second approach and prevention of neonatal mortalities and improved motor behavior in transgene-positive control animals in the initial study. These improvements by early induction of low increases of SMN

solely in motor neurons indicate that the importance of motor neurons in the causative pathways of SMA and as targets for therapy. Therefore, motor neurons cannot be ruled out as key players even though it is very likely that SMA is not a motor neuron-cell-autonomous disease since genetic restoration of SMN in these cells alone has proven inefficient to rescue mutant lethality [56, 57, 107]. Evidence from our study and the current literature suggests a possible relative, rather than absolute, selective vulnerability of motor neurons to the loss of normal SMN levels [96] indicating that multiple SMN-decreased cell populations are responsible for the progression of pathology. Most likely, therapies aimed at elevating SMN levels will need to be delivered systemically.

4.1 FUTURE STUDIES

The results presented in Chapter II, indicate that hemizygous inheritance of the *Hb9(Gfp/SMN)* transgene, while insufficient to extend the lifespan of a severe SMA mouse model, was capable of clearly reducing perinatal mortality in transgene-positive control mice. The complete extent of this benefit was not assayed in these mice. Other motor function tests could be performed, such as the grip-assay or rotorod test on adult control mice, to determine if the improvements we observed with the Righting Reflex might be observed using other tests. These control animals could also be evaluated for differences in NMJ maturation in comparison to transgene-negative mice. If endplate size and status of innervation are very sensitive to small changes in SMN expression and can serve as biomarkers, then we can expect to see improvements in transgene-positive control animals as well at this level. This analysis should be done in those muscles

already known to be the most sensitive to diminished SMN such as levator auris longus, abductor auris longus, and auricularis superior [155]

We did not determine if there was any differential motor neuron loss between Hb9(Cre^{+}) and Hb9(Cre^{-})SMA mice. This would be another interesting aspect to evaluate since low levels of SMN might be neuroprotective aiding motor neurons to survive longer towards the end-stage of SMAΔ7-like mice even though the rescue does not translate into an increase of overall lifespan. Also interesting to look into would be to determine the exact levels of SMN per motor neuron restored by $Hb9^{Cre}$-mediated recombination or the number of motor neurons in which recombination is occurring. This would allow setting a threshold of minimum levels of SMN expression needed to rescue NMJ parameters. Accurately setting this threshold in the context of an animal with a null *Smn* allele, like the one carried by the human patients, would be more relevant for therapy than the threshold that was derived from the Smn^{2B} allele (see above, [106]), which is not a null allele nor is found in human patients. Furthermore, apart from the muscles (TA and triceps) used in our study to determine NMJ characteristics rescued by SMN restoration, a future approach would be to assess other denervation-vulnerable muscles such as the masseter, SPI, and longissimus capitis, which are axial muscles with a very high susceptibility for denervation, as well as the FBD-2, FDB-3, and biceps brachii, which are appendicular muscles [104].

REFERENCES

1. Farooq, F., et al., *Prolactin increases SMN expression and survival in a mouse model of severe spinal muscular atrophy via the STAT5 pathway.* The Journal Of Clinical Investigation, 2011. **121**(8): P. 3042-50.

2. Lutz, C.M., et al., *Postsymptomatic restoration of SMN rescues the disease phenotype in a mouse model of severe spinal muscular atrophy.* The Journal Of Clinical Investigation, 2011. **121**(8): P. 3029-41.

3. Czeizel, A. and J. Hamula, *A hungarian study on Werdnig-Hoffmann disease.* Journal Of Medical Genetics, 1989. **26**(12): p. 761-3.

4. Lefebvre, S., et al., *Identification and characterization of a spinal muscular atrophy-determining gene.* Cell, 1995. **80**(1): p. 155-65.

5. Burghes, A.H. and C.E. Beattie, *Spinal muscular atrophy: why do low levels of survival motor neuron protein make motor neurons sick?* Nature reviews. Neuroscience, 2009. **10**(8): p. 597-609.

6. Le, T.T., et al., *SMNDelta7, the major product of the centromeric survival motor neuron (SMN2) gene, extends survival in mice with spinal muscular atrophy and associates with full-length SMN.* Human Molecular Genetics, 2005. **14**(6): p. 845-57.

7. Boon, K.L., et al., *Zebrafish survival motor neuron mutants exhibit presynaptic neuromuscular junction defects.* Human Molecular Genetics, 2009. **18**(19): p. 3615-25.

8. Coady, T.H. and C.L. Lorson, *SMN in spinal muscular atrophy and snRNP biogenesis.* Wiley Interdisciplinary Reviews. RNA, 2011. **2**(4): p. 546-64.

9. Torres-Benito L., R.R., Tabares L. , *Synaptic defects in spinal muscular atrophy animal models.* Developmental Neurobiology, 2011. **72**(1)**:126-33**.

10. Fallini, C., G.J. Bassell, and W. Rossoll, *Spinal muscular atrophy: the role of SMN in axonal mRNA regulation.* Brain Research, 2012. **1462**: p. 81-92.

11. Monani, U.R., et al., *A single nucleotide difference that alters splicing patterns distinguishes the SMA gene SMN1 from the copy gene SMN2.* Human Molecular Genetics, 1999. **8**(7): p. 1177-83.

12. Srivastava, S., et al., *SMN2-deletion in childhood-onset spinal muscular atrophy.* American Journal of Medical Genetics, 2001. **101**(3): p. 198-202.

13. Monani, U.R., D.D. Coovert, and A.H. Burghes, *Animal models of spinal muscular atrophy.* Human Molecular Genetics, 2000. **9**(16): p. 2451-7.

14. Swoboda, K.J., et al., *Natural history of denervation in SMA: relation to age, SMN2 copy number, and function.* Annals of Neurology, 2005. **57**(5): p. 704-12.

15. Coovert, D.D., et al., *The survival motor neuron protein in spinal muscular atrophy.* Human Molecular Genetics, 1997. **6**(8): p. 1205-14.

16. Zhang, H.L., et al., *Active transport of the survival motor neuron protein and the role of exon-7 in cytoplasmic localization.* The Journal of Neuroscience : the Official Journal of the Society for Neuroscience, 2003. **23**(16): p. 6627-37.

17. Boda, B., et al., *Survival motor neuron SMN1 and SMN2 gene promoters: identical sequences and differential expression in neurons and non-neuronal cells.* European Journal of Human Genetics : EJHG, 2004. **12**(9): p. 729-37.

18. Schmid, A. and C.J. DiDonato, *Animal models of spinal muscular atrophy.* Journal of Child Neurology, 2007. **22**(8): p. 1004-12.

19. Park, G.H., et al., *Reduced survival of motor neuron (SMN) protein in motor neuronal progenitors functions cell autonomously to cause spinal muscular atrophy in model mice expressing the human centromeric (SMN2) gene.* The Journal of Neuroscience : the Official Journal of the Society for Neuroscience, 2010. **30**(36): p. 12005-19.

20. Yong, J., L. Wan, and G. Dreyfuss, *Why do cells need an assembly machine for RNA-protein complexes?* Trends in Cell Biology, 2004. **14**(5): p. 226-32.

21. Buhler, D., et al., *Essential role for the tudor domain of SMN in spliceosomal U snRNP assembly: implications for spinal muscular atrophy.* Human Molecular Genetics, 1999. **8**(13): p. 2351-7.

22. Pellizzoni, L., et al., *A novel function for SMN, the spinal muscular atrophy disease gene product, in pre-mRNA splicing.* Cell, 1998. **95**(5): p. 615-24.

23. Winkler, C., et al., *Reduced U snRNP assembly causes motor axon degeneration in an animal model for spinal muscular atrophy.* Genes & Development, 2005. **19**(19): p. 2320-30.

24. Vyas, S., et al., *Involvement of survival motor neuron (SMN) protein in cell death.* Human Molecular Genetics, 2002. **11**(22): p. 2751-64.

25. Pellizzoni, L., J. Yong, and G. Dreyfuss, *Essential role for the SMN complex in the specificity of snRNP assembly.* Science, 2002. **298**(5599): p. 1775-9.

26. Liu, Q. and G. Dreyfuss, *A novel nuclear structure containing the survival of motor neurons protein.* The EMBO Journal, 1996. **15**(14): p. 3555-65.

27. Paushkin, S., et al., *The SMN complex, an assemblyosome of ribonucleoproteins.* Current Opinion in Cell Biology, 2002. **14**(3): p. 305-12.

28. Le, T.T., et al., *Temporal requirement for high SMN expression in SMA mice.* Human Molecular Genetics, 2011. **20**(18): p. 3578-91.

29. Tisdale, S., et al., *SMN Is Essential for the Biogenesis of U7 Small Nuclear Ribonucleoprotein and 3'-End Formation of Histone mRNAs.* Cell Reports, 2013. **5**(5): p. 1187-95.

30. Kariya, S., et al., *Reduced SMN protein impairs maturation of the neuromuscular junctions in mouse models of spinal muscular atrophy.* Human Molecular Genetics, 2008. **17**(16): p. 2552-69.

31. Fallini, C., G.J. Bassell, and W. Rossoll, *High-efficiency transfection of cultured primary motor neurons to study protein localization, trafficking, and function.* Molecular Neurodegeneration, 2010. **5**: p. 17.

32. Burglen, L., et al., *Structure and organization of the human survival motor neurone (SMN) gene.* Genomics, 1996. **32**(3): p. 479-82.

33. Lorson, C.L., et al., *A single nucleotide in the SMN gene regulates splicing and is responsible for spinal muscular atrophy.* Proceedings of the National Academy of Sciences of the United States of America, 1999. **96**(11): p. 6307-11.

34. Lorson, C.L., H. Rindt, and M. Shababi, *Spinal muscular atrophy: mechanisms and therapeutic strategies.* Human Molecular Genetics, 2010. **19**(R1): p. R111-8.

35. Burnett, B.G., et al., *Regulation of SMN protein stability.* Molecular and Cellular Biology, 2009. **29**(5): p. 1107-15.

36. MacKenzie, A., *Sense in antisense therapy for spinal muscular atrophy.* The New England Journal of Medicine, 2012. **366**(8): p. 761-3.

37. Monani, U.R., et al., *A transgene carrying an A2G missense mutation in the SMN gene modulates phenotypic severity in mice with severe (type I) spinal muscular atrophy.* The Journal of Cell Biology, 2003. **160**(1): p. 41-52.

38. Corti, S., et al., *Embryonic stem cell-derived neural stem cells improve spinal muscular atrophy phenotype in mice.* Brain : a Journal of Neurology, 2010. **133**(Pt 2): p. 465-81.

39. Frugier, T., et al., *The molecular bases of spinal muscular atrophy.* Current Opinion in Genetics & Development, 2002. **12**(3): p. 294-8.

40. Lee, Y.I., et al., *Muscles in a mouse model of spinal muscular atrophy show profound defects in neuromuscular development even in the absence of failure in neuromuscular transmission or loss of motor neurons.* Developmental Biology, 2011. **356**(2): p. 432-44.

41. Sumner, C.J., *Molecular mechanisms of spinal muscular atrophy.* Journal of Child Neurology, 2007. **22**(8): p. 979-89.

42. Schwartz, M., et al., *Quantification, by solid-phase minisequencing, of the telomeric and centromeric copies of the survival motor neuron gene in families with spinal muscular atrophy.* Human Molecular Genetics, 1997. **6**(1): p. 99-104.

43. Rochette, C.F., N. Gilbert, and L.R. Simard, *SMN gene duplication and the emergence of the SMN2 gene occurred in distinct hominids: SMN2 is unique to Homo sapiens.* Human Genetics, 2001. **108**(3): p. 255-66.

44. Monani, U.R., et al., *The human centromeric survival motor neuron gene (SMN2) rescues embryonic lethality in Smn(-/-) mice and results in a mouse with spinal muscular atrophy.* Human Molecular Genetics, 2000. **9**(3): p. 333-9.

45. Wirth, B.B., L., Schrank, B., Lochmuller, H., Blick, S., Baasner, A., Heller, R., *Mildly affected patients with spinal muscular atrophy are partially protected by an increased SMN2 copy number.* Human Genetics, 2006. **119**: p. 422-428.

46. Hsieh-Li, H.M., et al., *A mouse model for spinal muscular atrophy.* Nature Genetics, 2000. **24**(1): p. 66-70.

47. Feldkotter, M., et al., *Quantitative analyses of SMN1 and SMN2 based on real-time lightCycler PCR: fast and highly reliable carrier testing and prediction of severity of spinal muscular atrophy.* American Journal of Human Genetics, 2002. **70**(2): p. 358-68.

48. Moulard, B., Salachas, F., Chassande, B., Briolotti, V., Meininger, V., Malafosse, A., Camu, W., *Association between centromeric deletions of the SMN gene and sporadic adult-onset lower motor neuron disease.* Annals of Neurology , 1998. **45**: p. 640-644.

49. Monani, U.R., De Vivo D. C, *Neurodegeneration in Spinal Muscular Atrophy: disease phenotype, animal models, therapies, and beyond: executive summary.* Future Neurology, 2014. **9**(1): p. 49-65.

50. Imlach, W.L., et al., *SMN is required for sensory-motor circuit function in Drosophila.* Cell, 2012. **151**(2): p. 427-39.

51. Ling, K.K., et al., *Synaptic defects in the spinal and neuromuscular circuitry in a mouse model of spinal muscular atrophy.* PloS One, 2010. **5**(11): p. e15457.

52. Mercuri, E., E. Bertini, and S.T. Iannaccone, *Childhood spinal muscular atrophy: controversies and challenges.* Lancet Neurology, 2012. **11**(5): p. 443-52.

53. Nadeau, A., et al., *A newborn with spinal muscular atrophy type 0 presenting with a clinicopathological picture suggestive of myotubular myopathy.* Journal of Child Neurology, 2007. **22**(11): p. 1301-4.

54. Cifuentes-Diaz, C., et al., *Deletion of murine SMN exon 7 directed to skeletal muscle leads to severe muscular dystrophy.* The Journal of Cell Biology, 2001. **152**(5): p. 1107-14.

55. Mentis, G.Z., et al., *Early functional impairment of sensory-motor connectivity in a mouse model of spinal muscular atrophy.* Neuron, 2011. **69**(3): p. 453-67.

56. Paez-Colasante, X., et al., *Improvement of neuromuscular synaptic phenotypes without enhanced survival and motor function in severe spinal muscular atrophy mice selectively rescued in motor neurons.* PloS One, 2013. **8**(9): p. e75866.

57. Martinez, T.L., et al., *Survival motor neuron protein in motor neurons determines synaptic integrity in spinal muscular atrophy.* The Journal of Neuroscience : The Official Journal of the Society for Neuroscience, 2012. **32**(25): p. 8703-15.

58. Cifuentes-Diaz, C., et al., *Neurofilament accumulation at the motor endplate and lack of axonal sprouting in a spinal muscular atrophy mouse model.* Human Molecular Genetics, 2002. **11**(12): p. 1439-47.

59. Liu, Q., et al., *Neurofilament proteins in neurodegenerative diseases.* Cellular and molecular life sciences : CMLS, 2004. **61**(24): p. 3057-75.

60. Shababi, M., et al., *Cardiac defects contribute to the pathology of spinal muscular atrophy models.* Human Molecular Genetics, 2010. **19**(20): p. 4059-71.

61. Heier, C.R., et al., *Arrhythmia and cardiac defects are a feature of spinal muscular atrophy model mice.* Human Molecular Genetics, 2010. **19**(20): p. 3906-18.

62. Shababi, M., et al., *Partial restoration of cardio-vascular defects in a rescued severe model of spinal muscular atrophy.* Journal of Molecular and Cellular Cardiology, 2012. **52**(5): p. 1074-82.

63. Bevan, A.K., et al., *Early heart failure in the SMNDelta7 model of spinal muscular atrophy and correction by postnatal scAAV9-SMN delivery.* Human Molecular Genetics, 2010. **19**(20): p. 3895-905.

64. Hua, Y., et al., *Peripheral SMN restoration is essential for long-term rescue of a severe spinal muscular atrophy mouse model.* Nature, 2011. **478**(7367): p. 123-6.

65. Hua, Y., et al., *Antisense correction of SMN2 splicing in the CNS rescues necrosis in a type III SMA mouse model.* Genes & Development, 2010. **24**(15): p. 1634-44.

66. Sivanesan, S., et al., *Antisense oligonucleotide mediated therapy of spinal muscular atrophy.* Translational Neuroscience, 2013. **4**(1).

67. Singh, N.K., et al., *Splicing of a critical exon of human Survival Motor Neuron is regulated by a unique silencer element located in the last intron.* Molecular and Cellular Biology, 2006. **26**(4): p. 1333-46.

68. Arnold, W.D. and A.H. Burghes, *Spinal muscular atrophy: development and implementation of potential treatments.* Annals of Neurology, 2013. **74**(3): p. 348-62.

69. Hua, Y., et al., *Antisense masking of an hnRNP A1/A2 intronic splicing silencer corrects SMN2 splicing in transgenic mice.* American Journal of Human Genetics, 2008. **82**(4): p. 834-48.

70. Williams, J.H., et al., *Oligonucleotide-mediated survival of motor neuron protein expression in CNS improves phenotype in a mouse model of spinal muscular atrophy.* The Journal of Neuroscience : The Official Journal of the Society for Neuroscience, 2009. **29**(24): p. 7633-8.

71. Passini, M.A., et al., *Antisense oligonucleotides delivered to the mouse CNS ameliorate symptoms of severe spinal muscular atrophy.* Science Translational Medicine, 2011. **3**(72): p. 72ra18.

72. Porensky, P.N., et al., *A single administration of morpholino antisense oligomer rescues spinal muscular atrophy in mouse.* Human Molecular Genetics, 2012. **21**(7): p. 1625-38.

73. Mitrpant, C., et al., *Improved antisense oligonucleotide design to suppress aberrant SMN2 gene transcript processing: towards a treatment for spinal muscular atrophy.* PloS One, 2013. **8**(4): p. e62114.

74. Coady, T.H. and C.L. Lorson, *Trans-splicing-mediated improvement in a severe mouse model of spinal muscular atrophy.* The Journal of Neuroscience : The Official Journal of the Society for Neuroscience, 2010. **30**(1): p. 126-30.

75. Coady, T.H., et al., *Development of a single vector system that enhances trans-splicing of SMN2 transcripts.* PloS One, 2008. **3**(10): p. e3468.

76. Coady, T.H., et al., *Restoration of SMN function: delivery of a trans-splicing RNA re-directs SMN2 pre-mRNA splicing.* Molecular Therapy : The Journal of the American Society of Gene Therapy, 2007. **15**(8): p. 1471-8.

77. Hastings, M.L., et al., *Tetracyclines that promote SMN2 exon 7 splicing as therapeutics for spinal muscular atrophy.* Science Translational Medicine, 2009. **1**(5): p. 5ra12.

78. Passini, M.A., et al., *CNS-targeted gene therapy improves survival and motor function in a mouse model of spinal muscular atrophy.* The Journal of Clinical Investigation, 2010. **120**(4): p. 1253-64.

79. Ebert, A.D., et al., *Induced pluripotent stem cells from a spinal muscular atrophy patient.* Nature, 2009. **457**(7227): p. 277-80.

80. Rossi, S.L., et al., *Histological and functional benefit following transplantation of motor neuron progenitors to the injured rat spinal cord.* PloS One, 2010. **5**(7): p. e11852.

81. Wyatt, T.J., et al., *Human motor neuron progenitor transplantation leads to endogenous neuronal sparing in 3 models of motor neuron loss.* Stem Cells International, 2011. **2011**: p. 207230.

82. Keirstead, H.S., *Stem Cell Derived Therapeutic for Spinal Muscular Atrophy Type I*, in *15th Annual International Spinal Muscular Atrophy Research Group Meeting 2011*2011: Orlando, FL.

83. Park, I.H., et al., *Disease-specific induced pluripotent stem cells.* Cell, 2008. **134**(5): p. 877-86.

84. Corti, S., et al., *Genetic correction of human induced pluripotent stem cells from patients with spinal muscular atrophy.* Science Translational Medicine, 2012. **4**(165): p. 165ra162.

85. Singh, J., et al., *DcpS as a therapeutic target for spinal muscular atrophy.* ACS Chemical Biology, 2008. **3**(11): p. 711-22.

86. Van Meerbeke, J.P., et al., *The DcpS inhibitor RG3039 improves motor function in SMA mice.* Human Molecular Genetics, 2013. **22**(20): p. 4074-83.

87. Gogliotti, R.G., et al., *The DcpS inhibitor RG3039 improves survival, function and motor unit pathologies in two SMA mouse models.* Human Molecular Genetics, 2013. **22**(20): p. 4084-101.

88. Riessland, M., et al., *SAHA ameliorates the SMA phenotype in two mouse models for spinal muscular atrophy.* Human Molecular Genetics, 2010. **19**(8): p. 1492-506.

89. Liu, H.C., et al., *Sodium vanadate combined with L-ascorbic acid delays disease progression, enhances motor performance, and ameliorates muscle atrophy and weakness in mice with spinal muscular atrophy.* BMC Medicine, 2013. **11**: p. 38.

90. Rose, F.F., Jr., et al., *Delivery of recombinant follistatin lessens disease severity in a mouse model of spinal muscular atrophy.* Human Molecular Genetics, 2009. **18**(6): p. 997-1005.

91. Grondard, C., et al., *Regular exercise prolongs survival in a type 2 spinal muscular atrophy model mouse.* The Journal of Neuroscience : The Official Journal of the Society for Neuroscience, 2005. **25**(33): p. 7615-22.

92. Imlach W., L.F., Savner E., Choi B., Pellizzoni L., McCabe B. , *SMN regulates motor circuit function*, in *15th Annual International Spinal Muscular Atrophy Research Group Meeting*2011: Orlando, Fl.

93. Sen, A., et al., *Genetic circuitry of Survival motor neuron, the gene underlying spinal muscular atrophy.* Proceedings of the National Academy of Sciences of the United States of America, 2013. **110**(26): p. E2371-80.

94. Sen, A., et al., *Modeling spinal muscular atrophy in Drosophila links Smn to FGF signaling.* The Journal of cell biology, 2011. **192**(3): p. 481-95.

95. Chang, H.C., et al., *Modeling spinal muscular atrophy in Drosophila.* PloS One, 2008. **3**(9): p. e3209.

96. Sleigh, J.N., T.H. Gillingwater, and K. Talbot, *The contribution of mouse models to understanding the pathogenesis of spinal muscular atrophy.* Disease Models & Mechanisms, 2011. **4**(4): p. 457-67.

97. DiDonato, C.J., et al., *Regulation of murine survival motor neuron (Smn) protein levels by modifying Smn exon 7 splicing.* Human Molecular Genetics, 2001. **10**(23): p. 2727-36.

98. McGovern, V.L., et al., *Embryonic motor axon development in the severe SMA mouse.* Human Molecular Genetics, 2008. **17**(18): p. 2900-9.

99. Wishart, T.M., et al., *SMN deficiency disrupts brain development in a mouse model of severe spinal muscular atrophy.* Human Molecular Genetics, 2010. **19**(21): p. 4216-28.

100. Boyer, J.G., et al., *Early onset muscle weakness and disruption of muscle proteins in mouse models of spinal muscular atrophy.* Skeletal Muscle, 2013. **3**(1): p. 24.

101. Gogliotti, R.G., et al., *Molecular and phenotypic reassessment of an infrequently used mouse model for spinal muscular atrophy.* Biochemical and Biophysical Research Communications, 2010. **391**(1): p. 517-22.

102. Butchbach, M.E., J.D. Edwards, and A.H. Burghes, *Abnormal motor phenotype in the SMNDelta7 mouse model of spinal muscular atrophy.* Neurobiology of Disease, 2007. **27**(2): p. 207-19.

103. Park, G.H., S. Kariya, and U.R. Monani, *Spinal muscular atrophy: new and emerging insights from model mice.* Current Neurology and Neuroscience Reports, 2010. **10**(2): p. 108-17.

104. Ling, K.K., et al., *Severe neuromuscular denervation of clinically relevant muscles in a mouse model of spinal muscular atrophy.* Human Molecular Genetics, 2012. **21**(1): p. 185-95.

105. Bowerman, M., et al., *SMN, profilin IIa and plastin 3: a link between the deregulation of actin dynamics and SMA pathogenesis.* Molecular and Cellular Neurosciences, 2009. **42**(1): p. 66-74.

106. Bowerman, M., et al., *A critical smn threshold in mice dictates onset of an intermediate spinal muscular atrophy phenotype associated with a distinct neuromuscular junction pathology.* Neuromuscular Disorders : NMD, 2012. **22**(3): p. 263-76.

107. Gogliotti, R.G., et al., *Motor neuron rescue in spinal muscular atrophy mice demonstrates that sensory-motor defects are a consequence, not a cause, of motor neuron dysfunction.* The Journal of Neuroscience : The Official Journal of the Society for Neuroscience, 2012. **32**(11): p. 3818-29.

108. Hammond, S.M., et al., *Mouse survival motor neuron alleles that mimic SMN2 splicing and are inducible rescue embryonic lethality early in development but not late.* PloS One, 2010. **5**(12): p. e15887.

109. Frugier, T., et al., *Nuclear targeting defect of SMN lacking the C-terminus in a mouse model of spinal muscular atrophy.* Human Molecular Genetics, 2000. **9**(5): p. 849-58.

110. Gavrilina, T.O., et al., *Neuronal SMN expression corrects spinal muscular atrophy in severe SMA mice while muscle-specific SMN expression has no phenotypic effect.* Human Molecular Genetics, 2008. **17**(8): p. 1063-75.

111. Foust, K.D., et al., *Rescue of the spinal muscular atrophy phenotype in a mouse model by early postnatal delivery of SMN.* Nature Biotechnology, 2010. **28**(3): p. 271-4.

112. Nakano, T., et al., *Identification of a conserved 125 base-pair Hb9 enhancer that specifies gene expression to spinal motor neurons.* Developmental Biology, 2005. **283**(2): p. 474-85.

113. Placantonakis, D.G., et al., *Enriched motor neuron populations derived from bacterial artificial chromosome-transgenic human embryonic stem cells.* Clinical Neurosurgery, 2009. **56**: p. 125-32.

114. Thaler, J., et al., *Active suppression of interneuron programs within developing motor neurons revealed by analysis of homeodomain factor HB9.* Neuron, 1999. **23**(4): p. 675-87.

115. Odden, J.P., S. Holbrook, and C.Q. Doe, *Drosophila HB9 is expressed in a subset of motoneurons and interneurons, where it regulates gene expression and*

axon pathfinding. The Journal of Neuroscience : The Official Journal of the Society for Neuroscience, 2002. **22**(21): p. 9143-9.

116. Li, X., et al., *Generation of destabilized green fluorescent protein as a transcription reporter.* The Journal of Biological Chemistry, 1998. **273**(52): p. 34970-5.

117. Tiziano, F.D., et al., *SMN transcript levels in leukocytes of SMA patients determined by absolute real-time PCR.* European Journal of Human Genetics : EJHG, 2010. **18**(1): p. 52-8.

118. Marras, S.A., *Selection of fluorophore and quencher pairs for fluorescent nucleic acid hybridization probes.* Methods in Molecular Biology, 2006. **335**: p. 3-16.

119. Livak, K.J. and T.D. Schmittgen, *Analysis of relative gene expression data using real-time quantitative PCR and the 2(-Delta Delta C(T)) Method.* Methods, 2001. **25**(4): p. 402-8.

120. El-Khodor, B.F., et al., *Identification of a battery of tests for drug candidate evaluation in the SMNDelta7 neonate model of spinal muscular atrophy.* Experimental Neurology, 2008. **212**(1): p. 29-43.

121. Wilson, J.M., et al., *Conditional rhythmicity of ventral spinal interneurons defined by expression of the Hb9 homeodomain protein.* The Journal of Neuroscience : The Official Journal of the Society for Neuroscience, 2005. **25**(24): p. 5710-9.

122. Arber, S., et al., *Requirement for the homeobox gene Hb9 in the consolidation of motor neuron identity.* Neuron, 1999. **23**(4): p. 659-74.

123. Garbes, L., et al., *LBH589 induces up to 10-fold SMN protein levels by several independent mechanisms and is effective even in cells from SMA patients non-responsive to valproate.* Human Molecular Genetics, 2009. **18**(19): p. 3645-58.

124. Heier, C.R., R.G. Gogliotti, and C.J. DiDonato, *SMN transcript stability: could modulation of messenger RNA degradation provide a novel therapy for spinal muscular atrophy?* Journal of Child Neurology, 2007. **22**(8): p. 1013-8.

125. Wahlers, A., et al., *Influence of multiplicity of infection and protein stability on retroviral vector-mediated gene expression in hematopoietic cells.* Gene Therapy, 2001. **8**(6): p. 477-86.

126. Corish, P. and C. Tyler-Smith, *Attenuation of green fluorescent protein half-life in mammalian cells.* Protein Engineering, 1999. **12**(12): p. 1035-40.

127. Leveau, J.H. and S.E. Lindow, *Predictive and interpretive simulation of green fluorescent protein expression in reporter bacteria.* Journal of Bacteriology, 2001. **183**(23): p. 6752-62.

128. Kerr, D.A., et al., *Survival motor neuron protein modulates neuron-specific apoptosis.* Proceedings of the National Academy of Sciences of the United States of America, 2000. **97**(24): p. 13312-7.

129. Yanyan, C., et al., *Correlation of PLS3 expression with disease severity in children with spinal muscular atrophy.* Journal of Human Genetics, 2014. **59**(1): p. 24-7.

130. Stratigopoulos, G., et al., *Association of plastin 3 expression with disease severity in spinal muscular atrophy only in postpubertal females.* Archives of Neurology, 2010. **67**(10): p. 1252-6.

131. Oprea, G.E., et al., *Plastin 3 is a protective modifier of autosomal recessive spinal muscular atrophy.* Science, 2008. **320**(5875): p. 524-7.

132. Kong, L., et al., *Impaired synaptic vesicle release and immaturity of neuromuscular junctions in spinal muscular atrophy mice.* The Journal of Neuroscience : The Official Journal of the Society for Neuroscience, 2009. **29**(3): p. 842-51.

133. Avila, A.M., et al., *Trichostatin A increases SMN expression and survival in a mouse model of spinal muscular atrophy.* The Journal of Clinical Investigation, 2007. **117**(3): p. 659-71.

134. Schreml, J., et al., *Severe SMA mice show organ impairment that cannot be rescued by therapy with the HDACi JNJ-26481585.* European Journal of Human Genetics : EJHG, 2013. **21**(6): p. 643-52.

135. Yang, X., et al., *Patterning of muscle acetylcholine receptor gene expression in the absence of motor innervation.* Neuron, 2001. **30**(2): p. 399-410.

136. Li, X.M., et al., *Retrograde regulation of motoneuron differentiation by muscle beta-catenin.* Nature Neuroscience, 2008. **11**(3): p. 262-8.

137. Kummer, T.T., et al., *Nerve-independent formation of a topologically complex postsynaptic apparatus.* The Journal of Cell Biology, 2004. **164**(7): p. 1077-87.

138. Alaynick, W.A., T.M. Jessell, and S.L. Pfaff, *SnapShot: spinal cord development.* Cell, 2011. **146**(1): p. 178-178 e1.

139. Murray, L.M., et al., *Selective vulnerability of motor neurons and dissociation of pre- and post-synaptic pathology at the neuromuscular junction in mouse models of spinal muscular atrophy.* Human Molecular Genetics, 2008. **17**(7): p. 949-62.

140. Balice-Gordon, R.J., et al., *Neuromuscular junctions shrink and expand as muscle fiber size is manipulated: in vivo observations in the androgen-sensitive bulbocavernosus muscle of mice.* The Journal of Neuroscience : The Official Journal of the Society for Neuroscience, 1990. **10**(8): p. 2660-71.

141. Lee, A.J., et al., *Limited phenotypic effects of selectively augmenting the SMN protein in the neurons of a mouse model of severe spinal muscular atrophy.* PloS One, 2012. **7**(9): p. e46353.

142. Zagoraiou, L., et al., *A cluster of cholinergic premotor interneurons modulates mouse locomotor activity.* Neuron, 2009. **64**(5): p. 645-62.

143. Oberdoerffer, P., et al., *Unidirectional Cre-mediated genetic inversion in mice using the mutant loxP pair lox66/lox71.* Nucleic Acids Research, 2003. **31**(22): p. e140.

144. Hamilton, G. and T.H. Gillingwater, *Spinal muscular atrophy: going beyond the motor neuron.* Trends in Molecular Medicine, 2013. **19**(1): p. 40-50.

145. Zhang, Z., et al., *Dysregulation of synaptogenesis genes antecedes motor neuron pathology in spinal muscular atrophy.* Proceedings of the National Academy of Sciences of the United States of America, 2013. **110**(48): p. 19348-53.

146. Achsel, T., et al., *The intriguing case of motor neuron disease: ALS and SMA come closer.* Biochemical Society Transactions, 2013. **41**(6): p. 1593-7.

147. Cauchi, R.J., *Gem Depletion: Amyotrophic Lateral Sclerosis and Spinal Muscular Atrophy Crossover.* CNS Neuroscience & Therapeutics, 2014.

148. Papadimitriou, D., et al., *Inflammation in ALS and SMA: sorting out the good from the evil.* Neurobiology of Disease, 2010. **37**(3): p. 493-502.

149. Piao, Y., et al., *Survival motor neuron (SMN) protein in the spinal anterior horn cells of patients with sporadic amyotrophic lateral sclerosis.* Brain Research, 2011. **1372**: p. 152-9.

150. Jablonka, S., et al., *Reduced survival motor neuron (Smn) gene dose in mice leads to motor neuron degeneration: an animal model for spinal muscular atrophy type III.* Human Molecular Genetics, 2000. **9**(3): p. 341-6.

151. Chiaretti, A., et al., *Increased levels of glial cell-derived neurotrophic factor in CSF of infants with SMA.* Pediatric Neurology, 2009. **41**(3): p. 195-9.

152. McGivern, J.V., et al., *Spinal muscular atrophy astrocytes exhibit abnormal calcium regulation and reduced growth factor production.* Glia, 2013. **61**(9): p. 1418-28.

153. Lasiene, J. and K. Yamanaka, *Glial cells in amyotrophic lateral sclerosis.* Neurology Research International, 2011. **2011**: p. 718987.

154. Hunter, G., et al., *SMN-dependent intrinsic defects in Schwann cells in mouse models of spinal muscular atrophy.* Human Molecular Genetics, 2013.

155. Thomson, S.R., et al., *Morphological characteristics of motor neurons do not determine their relative susceptibility to degeneration in a mouse model of severe spinal muscular atrophy.* PloS One, 2012. **7**(12): p. e52605.

APPENDIX A

PROTOCOLS

Note: these detailed protocols complement the Materials and Methods section in Chapters II and III

DNA extraction from tissues (Sigma)*

1. Take tail-tip or ear-punch (≤5mm) from mouse and place in 0.5mL tube
2. Pipet 100µL of Extraction Solution into the tube and make sure the tissue is fully submerged
3. Add 25µL of Tissue Preparation Solution and mix thoroughly
4. Incubate at room temperature for 10 min
5. Incubate at 95°C for 3 min, vortex briefly (1-2 pulses), then transfer immediately to ice

Note – Make sure heat block has water in it to ensure proper heat conductivity

6. Add 100µL of Neutralization Solution B and mix well by vortexing for 30 sec
7. Pulse-centrifuge to pull down liquid from the cap
8. Transfer extract to a clean 0.5mL tube and store at -20°C

Note – Tail/tissue will appear undigested, but extract will contain sufficient DNA for genotyping. Leftover tissue can be stored at -20°C after extract has been removed

Genotyping Mice – Sigma PCR Protocol*

1. Thaw on ice: Red ReadyMix (Sigma) and respective forward and reverse primer mix.

Note – Primer aliquots are a mixture of both F and R primers at 20µM each. If a new aliquot is needed, make a 1:5 dilution with the original stocks (100µM)

2. DNA samples from 4°C refrigerator should remain on ice until needed; pull positive control sample along with samples to be screened
3. Label PCR tubes for each sample
4. Make a master mix: 5µL H_2O, 10µL Red ReadyMix and 1µL F+R primer mix

Note – This is the equivalent of what should be in each sample; to accommodate pipette error, make slightly more than needed to ensure adequate quantity

5. Aliquot 4µL of appropriate DNA to each of the PCR tubes; for the (-) control use 4µL H_2O
6. Distribute 16µL of master mix into the appropriate tubes and mix gently. Close caps securely
7. Place samples in PTC-100 PCR machine (or available lab thermo cycler), close lid, and tighten wheel securely

8. Run program depending on allele to be assayed. All cycles will start with a Taq polymerase activation phase of 95°C for 15 min. The other phases will depend on the nature of the primers and they all conclude with a 4°C hold final step that can go on indefinitely until the program is stopped.
9. Store samples in 4°C refrigerator until ready to run on an agarose (1.5 or 2%) gel

Whole mount muscle preparations

1. Euthanize animal with proper CO_2 protocol
2. Dissect muscles of interest
3. Fix muscles in 4% PFA for 1h at RT
4. Wash 3X with PBS for 15min
5. Carefully "cut" muscles using a forceps, separating fiber bundles to expose the insides of the muscle for better antibody penetration
6. Permeabilize with a bath of pre-chilled methanol for 5min at 4°C
7. Rinse with PBS
8. Block muscles with a 0.3% Triton X-100- 0.2% BSA solution for 30min at RT

Note: all of this is done on agar petri dish

9. Take muscles and place carefully in 1.5ml eppendorf tube and incubate with required antibody in the same blocking buffer and incubate ON at RT (For this study, 1:100 2H3 was used for NF accumulation assay)
10. The following day, wash muscles in PBS-T 3X for 15min each.
11. Incubate in required secondary antibodies for 2h (for NF staining used 1:200 rhodamine goat anti-mouse antibody (RGAM) and 1:1000 fluorescein bungarotoxin)
12. Wash 3X in PBS-T for 10min each
13. Mount on slides by carefully separating small bundles at a time and then adding one drop of vectashield (containing DAPI)
14. Place coverslip carefully avoiding bubbles and aggregation of the bundles
15. Straighten cover slip and seal edges with a light coating of clear nail polish
16. Move slides promptly into a darkened slide holder to protect the fluorescent tags and store at 4°C until ready to view

Tissue Sectioning*

1. The night before sectioning, transfer mold with Tissue Tek-embedded sample into the -20°C to allow ~12 hours to equilibrate to that temperature
2. Transfer mold with Tissue Tek-embedded sample to the cryostat and allow it to equilibrate there for ~1 hour
3. Lay out 10 slides and label each
4. Under Cryostat menu, turn on light and set Peltier station to 'cool'; place one mounting block in the Peltier station to cool as well

5. Remove Tissue Tek block out of the mold and carefully cut out a rectangle around the tissue (be sure to leave at least about a 1mm buffer of Tissue Tek on all sides of the tissue to help keep it protected and supported
6. Add Tissue Tek compound onto mounting block and immediately place tissue block in compound as it hardens quickly
7. Once the Tissue Tek has solidified, place the mounting block into slicing apparatus and tighten to hold in place. Adjust angle of the block towards the back of the machine at an approximate 45° angle so the slices taken will be flat cross sections through the muscle
8. Use the arrow buttons to move the apparatus holding the sample close to the knife; remove the protective covering over the knife to expose the blad
9. Return to menu and remove the brake on the rotating wheel that controls the slicer; set the cuts to 'trim' to take 50μm-thick pieces until the muscle has been cut down to a flat true cross section
10. Set the cuts to 'fine' and start with taking a 12μm slice; if a flat, clean slice does not come off, brush tissue away and make another cut until you get a good one
11. Carefully lift the cover (do not let tissue stick to cover) and gently touch face-down slide (slide number 1) to tissue section
12. Check tissue section using brightfield microscopy: turn on power to Nikon, switch knob from 'Off' to 'DIA', use motor or manually change objectives (start with 4x), and visualize cells (filter #8). If a lot of air holes are present, cut sections thicker
13. Brush away residue, lower cover, cut another slice, and put this section on slide number 2 in the same position as the piece from slide 1
14. Repeat this process for all 10 slides, resulting in a series of 10 tissue sections
15. Cut 5 extra sections and brush these away to get to a new part of the muscle
16. Begin a second series of sections as described above (place these sections just below the first one on each slide
17. Repeat this process of taking serial sections until the slides are full of serial sections or you run out of tissue
18. Allow slides to dry for a minimum of 1 hour (more if sections are >20μm thick), then place into a slide box and freeze at -80°C until needed

Free-floating sections

1. Remove slides from box in freezer
2. Carefully add PBS to slide to loosen tissue
3. Once tissue is loose (careful not to lose is), use a thin paintbrush and remove individual sections
4. Place in cell culture plate with small sized wells previously filled with PBS-T
5. Wash to once remove excess tissue tek surrounding sections
6. Wash 2-3X in PBS
7. To remove buffer at every wash use a 1ml pipette and carefully suction buffer, discard, and replace with fresh buffer.
8. Use enough for sections to "swim" freely in well

9. Remove PBS and add appropriate blocking buffer
10. Incubate for 30-60min
11. Use a paintbrush again to carefully pick up sections and place on a slide previously delineated with the Pap Pen.
12. Add appropriate antibody/blocking buffer mix
13. Proceed with standard immunostaining protocol. Instead of performing the washes on a slide, use cell culture dish wells. Overall protocol follows standard immunostaining steps below.

Immuno Staining for sectioned tissue on slides (or free-floating sections)*

1. Fix the slides in a Coplin Jar containing 1% paraformaldehyde (PFA) made in PBS for 5 min at room temperature, shaking gently

Note – PFA stock is 4% use 15mL of this mixed with 45mL PBS as 60mL fills the jar well

2. Pour solution in PFA waste container, then fill the jar with PBS-T (cover the slides) and shake gently for 5 min. Repeat this wash 2X
3. Remove jar from shaker but do not pour out PBS-T (slides must stay moist)
4. Remove a single slide from the jar with forceps, then carefully wipe the bottom and top with a kimwipe
5. Using a PAP Pen (RPIcorp catalog number 195505), draw a boarder around the tissue samples to make a hydrophobic 'well' to hold liquid
6. Gently add 200µL of blocking solution onto the samples, filling the 'well' completely, then place the slide into the humid chamber
7. Incubate at room temperature for 20-30 min
8. Add 200µL of primary antibody to the slides immediately after removing blocking solution (do not let slides dry out!) and put slides back into the humid chamber

Note – See individual experiment notes for what kind of antibody and dilution

9. Incubate either 2 hours at room temperature or overnight at 4°C (make sure chamber is closed tight to prevent slides from drying!)
10. Flick off the primary antibody solution and place slides back into Coplin Jar; fill with PBS-T until slides are covered and gently shake at room temperature for 15 minutes; repeat this wash 2 more times
11. Carefully flick the slides to remove excess PBS-T and wipe away excess fluid outside the hydrophobic well
12. Add 200µL of secondary antibody (with fluorescent tag) to the slides immediately after removing blocking solution (do not let slides dry out!) and put slides back into the humid chamber (make sure to cover chamber with foil to protect it from the light)

Note – See individual experiment notes for what kind of antibody and dilution

13. Flick off the secondary antibody solution and place slides back into Coplin Jar; fill with PBS-T until slides are covered and gently shake at room temperature for

15 minutes (cover jar with foil to protect from light); repeat this wash 2 more times

14. Wash slides one final time in PBS as above
15. Carefully flick the slides to remove excess PBS and wipe away excess fluid outside the hydrophobic well, then wick away excess PBS inside the well with a kimwipe
16. Carefully but firmly wipe the PAP residue flat with a kimwipe tissue paper (do not touch tissue!)
17. Place one drop of Vectashield Mounting medium (Vector Labs catalog number H-1000) in the center of the slide and use a set of forceps to carefully lower a coverslip onto the mounting medium
18. Straighten cover slip and seal edges with a light coating of clear nail polish
19. Move slides promptly into a darkened slide holder to protect the fluorescent tags and store at 4°C until ready to view

Fluorescent Microscopy*

1. Turn on microscope power and wait to hear 2 beeps
2. Turn on camera power and wait to hear 2 beeps
3. Open Metamorph software

Note – These machines must be turned on in this order; software will not recognize microscope otherwise

4. Turn off overhead light for better visualization and preservation of fluorescent tags
5. Use Brightfield microscopy to locate and focus image (filter #8)
6. Switch to filter #2 to visualize fluoroscein tags (light will be blue as the green tag excites on the blue wavelength) or #3 to visualize rhodamine tags (light will be green as the red tag excites on the green wavelength)
7. Find desired fields of view on 20x magnification, then add a drop of oil and switch to 40x oil lens for imaging
8. Pull out rod in microscope to switch image to camera; on computer, click "Show live" to open up a black and white live image; adjust focus and exposure (in ms) as needed
9. Once live display is satisfactory, capture image with "Acquire"
10. Without moving the field of view or changing focus, switch filters and adjust exposure to capture same image in different wavelength

Note – When not actively finding and taking an image, close the shutter to prevent rapid degradation of fluorescent tags from prolonged exposure to light

11. Stack rhodamine and fluoroscein images to visualize overlap using "Color Align" and assigning the image taken with filter #3 image to "Red" and the one taken with filter #2 to "Green" and pressing "Apply"
12. Save images in appropriate folder, and name according to fluorescent tag used (be sure to note the antibody concentration and magnification in "Annotate Image")

13. If a close-up is necessary, shift to the 100x oil lens and repeat steps 9-13
14. When finished, store slides at 4°C in dark slide holder
15. Close shutter (if not already shut), clean oil lenses with lens paper, and switch back to 10x objective for storage
16. Exit Metamorph software then turn off camera, microscope, and mercury lamp

Protein Extraction from Muscle – Liquid Nitrogen + Homogenizer*

1. 1 hour in advance, wrap ceramic mortar and pestle in aluminum foil and freeze in -80°C (use this approach for pulverizing samples if using adult muscles, skip for other tissues such as spinal cords, these can be added directly to the homogenizer + buffer)
2. Label 2 sets of 1.7mL eppendorf tubes for each sample being extracted
3. Aliquot extraction buffer sufficient for 0.5mL/sample

Note – See individual experiment for buffer used

4. Add necessary inhibitors to the aliquoted buffer

Note – See individual experiment for inhibitors used

5. Fill a thermos of liquid nitrogen
6. Remove mortar and pestle from -80°C, unwrap, and place in an ice bucket

Note – Bury mortar as much as possible without allowing ice to spill inside

7. Place homogenizer in ice
8. Transfer frozen tissue into cold mortar and promptly add liquid nitrogen
9. Use the pestle to carefully grind the tissue into powder, adding new liquid nitrogen as soon as it evaporates out of the mortar

Note – To avoid losing tissue pieces, start by pressing the pestle onto the tissue chunk and turning in place while applying pressure; once pieces are smaller, move on to a gentle stirring grind around the mortar interior

10. Add more liquid nitrogen and start to scrape any caked tissue-powder off the mortar and pestle; as soon as the last of the liquid nitrogen evaporates, pull mortar out of the ice and scrape powder into the cold homogenizer
11. Promptly add 0.5mL of buffer with inhibitors and use firm, careful strokes to completely grind the powdered tissue into solution with the glass pestle

Note – This should not take long if tissue was properly ground already

12. Allow to sit (on ice!) for 30-60 seconds to give bubbles a chance to dissipate, then pipet solution into one of the eppendorf tubes, close, and place on ice until all samples are finished
13. Clean the homogenizer between samples by adding 2mL of buffer (no inhibitors) and agitating with pestle, then dumping buffer and flicking excess liquid out
14. Repeat wash 2X
15. Clean ceramic mortar between samples by rinsing with liquid nitrogen to remove all of the residue
16. Retrieve the next sample in the same manner as the first, and continue process until all samples have been homogenized
17. Centrifuge samples at 14,000xg for 15 min at 4°C
18. Transfer supernatant to clean, labeled tubes and store at -80°C

Bradford Microassay (Protein Concentration)*

1. Dilute a small sample 1:10 in H_2O in an eppendorf tube (recommended – 2μL sample in 18μL H_2O)
2. Make a 1:100 dilution of the previous dilution in an eppendorf tube (recommended – 160μL is needed for assay, so use 1.6μL of sample dilution in 158.4μL H_2O)
3. Have a "blank" sample at hand – 160μL of H_2O
4. Add 40μL of Protein Assay Dye Reagent Concentrate (Bio-Rad catalog number 500-0006) to each tube and mix well by vortexing
   Note – Color should develop, anything between red and dark blue
5. Incubate 5 min at RT
6. Turn on Eppendorf BioPhotometer and attached printer; select assay #1 – Bradford and press that button until it loads the protocol with built-in calibration
7. Open an eppendorf UVette cuvette (Eppendorf catalog number 952010051) and pipette in 100μL of the H_2O "blank"
8. Insert cuvette into the reading compartment
   Note – Be sure the frosted sides are to the right and left, while the clear side faces the operator; in the right orientation the well inside the cuvette makes the clear side look like it has an arrow pointing downwards
9. Press the "Blank" button to obtain measurement (should be all 0's; if not, troubleshoot issue)
   Note – Printer will print automatically as long as it is on
10. Leave the cuvette in place and carefully pipette out *all* of the H_2O
11. Pipette in 100μL of the first sample and press the "Sample" button to obtain measurement
12. Leave the cuvette in place and carefully pipette out *all* of the sample
13. Repeat until all samples have been measured

Note – Results are given in μg/mL. However, because of the initial 1:10 and subsequent 1:100 dilution at the start of the assay, the sample being read is actually diluted a total of 1:1000, making the true concentration of the printed numbers μg/μL.

Western Blot Analysis SDS-PAGE*

14. Clean glass plates thoroughly and assemble them with 1.5mm spacers

Note – Optional step is to fill plates with water to see if they leak, then pour out water and blot dry with a Kimwipe tissue paper

15. Mix the separating gel (see recipe next page) in a 15mL falcon tube and pipette 7.5mL promptly into the space between the plates

Note – See individual experiments for what % separating gel to use

16. ***GENTLY*** layer ddH_2O on top of liquid gel to protect it during polymerization and allow it to sit at room temperature undisturbed for 20-30 min

Note – The remaining gel in the tube can be used to monitor polymerization progress of the gel

17. When the gel has polymerized, carefully pour off the water layer and blot dry with a Kimwipe
18. Mix the stacking gel (see recipe next page) in a 15mL falcon tube and pipette it on top of the separating gel until it nears the top of the plates (leave a little space)

Note – See individual experiments for what % stacking gel to use

19. Carefully add a comb with the desired number of wells and make sure no bubbles of air are trapped in the liquid gel
20. Allow the stack to polymerize undisturbed for 10-15 min

Note – The remaining gel in the tube can be used to monitor polymerization progress of the gel

21. Carefully remove the plates and gel (do not allow them to separate) and assemble the electrophoresis apparatus
22. Fill the apparatus with 1x Running Buffer (see recipe below) until the top of the gel is submerged
23. Carefully remove the comb, allowing the buffer to fill the wells and sluice out any un-polymerized gel mix
24. Load 8-10μL of a protein ladder (Bio-Rad catalog number 161-0324) into one well and put samples in all the others (see individual experiments for how much sample to load)

Note – If not all of the wells are needed for samples, load unused wells with plain sample buffer equal in volume to the loaded samples to prevent the protein from migrating horizontally through the gel

25. Run the gel at 100V until the samples have cleared the stack, then turn voltage up to 120V (should take 1.5-2 hours)
26. Gel is finished when sample buffer front reaches the bottom of the gel

Note – Watch the lower ladder marker to make sure you don't lose the small proteins

1L Running Buffer (10x)

144.1g Glycine
30g Tris
10g SDS
Fill to volume with ddH_2O
Dilute to 1x with ddH_2O for electrophoresis

Transfer – SemiDry

1. Cut 2 pieces of blotting paper and one piece of PVDF membrane to the size of a smaller glass plate with a razor

Note – Prepare membrane, paper, and buffers before the gel finishes running

2. Fill four clean containers, one with Methanol, one with ddH_2O, and two with Blotting Buffer

Note – If blotting something phosphorylated, be sure to include phosphotase inhibitors in the Blotting Buffer (NaF is a MUST, Na_3VO_4 recommended but not required)

3. Disassemble the electrophoresis apparatus and gently remove the small glass plate from the face of the gel

4. Carefully scrape away the stack and lift the gel from the lower plate, then place it into one of the Blotting Buffer containers
5. Activate PVDF membrane by soaking it 15 seconds in Methanol, then 2 minutes in ddH_2O, then move the membrane to the other Blotting buffer container
6. Soak blotting paper in ddH_2O until saturated
7. Set up the 'blotting sandwich' by laying one of the water-soaked blotting papers on the drying surface of a SemiDry Transfer Cell, then laying out the activated PVDF membrane on top of that, then place the gel on top of the membrane, then place the other water-soaked blot paper on top of the gel and firmly close the lid over it all

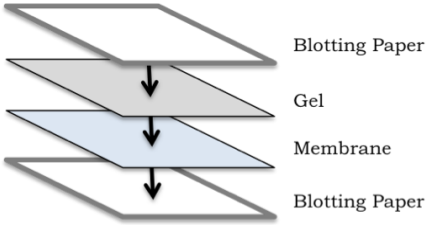

8. Connect the SemiDry Transfer Cell to a low-volt high-amp power supply and run for 1 hour at 18V

9. Remove the lid and discard the blotting paper, then carefully cut the membrane to the size of the gel, peel off and discard the gel, and quickly mark the protein ladder marks with a black ball-point pen

1L Blotting Buffer (1x)

5.8g Tris (final concentration 47.9mM)
2.92g Glycine (final concentration 38.9mM)
3.8mL 10% SDS (final concentration 0.038%)
200mL Methanol (final concentration 20%)
Fill to volume with ddH_2O

Probing

1. Transfer marked membrane to a 50ml Falcon tube and fill with with blocking solution

Note – See individual experiments for what kind of blocking solution was used

2. Gently shake/rotate at room temperature for 1 hour
3. Pour off blocking solution and add primary antibody solution

Note – See individual experiments for what kind of primary antibody solution was used

4. Gently shake/rotate at room temperature for 1 hour or overnight at 4°C
5. Pour off primary antibody (save and reuse unless solution is cloudy)
6. Wash the blot by adding 1x TBS-T (see recipe below) and shaking vigorously for 15 min
7. Pour off wash solution and repeat two more times
8. Pour off wash solution and add secondary antibody solution

Note – See individual experiments for what kind of secondary antibody solution was used

9. Gently shake/rotate at room temperature for 1 hour
10. Pour off and discard secondary antibody

11. Repeat the above 1x TBS-T washes three more times
12. After the last wash, dump the buffer and add just enough fresh buffer to cover the membrane to keep it wet until the last possible moment
13. Prepare the Western Lighting-ECL Enhanced Chemiluminescence Substrate by mixing 2mL each of the Oxidizing Reagent and the Enhanced Luminol Reagent in a falcon tube

Note – Work quickly as this chemical is light sensitive and will break down quickly

14. Lift the membrane from the wash buffer and remove excess liquid by tapping the edges on a Kimwipe to wick away fluid, then place face-up in a clean tip box lid
15. Pour the Substrate mix onto the membrane (the damp will create a surface-tension barrier that will hold the liquid on the membrane) and incubate for 1 minute at room temperature
16. Lift the membrane out of the Substrate mix and remove excess liquid by tapping the edges on a Kimwipe to wick away fluid, then place face-down on a clean piece of plastic wrap
17. Gently wrap the membrane (be sure the face surface only has the single layer of plastic over it)
18. Place into Alphaimager system and use the FluorChemQ software to expose membrane

Note – See individual experiments for exposure lengths

Quantification Analysis – Alpha Imager*

1. Open the gel image to be analyzed with the FluorChemQ program and zoom in 4x
2. Select the "Analysis Tools" tab and click "Band Analysis" to open a sub-menu
3. Under the "Region" tab, select the Single Region Tools square option, then use the cursor to draw a box around the first band of interest

   Note – A chart will appear at the bottom, labeling that box as "1n"
4. In the chart, select the "1n" frame, then go up the menu and click "Multi Region Copy" and duplicate the box over the band of interest in each of the lanes
5. Once all the desired bands have a box, deselect "Multi Region Copy"
6. Move and resize the individual boxes as necessary until they encompass the chosen bands and some of the background
7. Next, select the tab "Background" and click to select "Local Background" to subtract out the background from the quantities in the chart
8. Once this is done, select "Output" and choose to export to the clipboard
9. Open an excel file and paste in the analysis results, then label the bands as needed since they will be called "1n", "2n", etc
10. Repeat this process for as many sets of bands as necessary, then save the file

1L TBS-T (10x)

200mL 1M Tris-HCl pH 7.4 (final concentration 200mM)
87.66g NaCl (final concentration 1.5M)
10mL Tween (final concentration 1%)

Fill to volume with ddH_2O
Dilute to 1x with ddH_2O for washing

Membrane Stripping

1. Pre-heat stripping solution (see recipe below) to 50°C for 30 minutes

Note – Keep membrane wet while waiting by soaking in 1x TBS-T

2. Place membrane into a clean tip box lid and pour stripping solution over blot until it is completely submerged
3. Incubate at 50°C for 30 min
4. Pour off stripping solution (this can be saved and re-used as long as it smells strongly of β–mercaptoethanol, just store at 4°C)
5. Wash the blot by adding 1x TBS-T (see recipe below) and shaking vigorously for 15 min. Pour off wash solution and repeat wash once more
6. Store the blot for short term at 4°C in standing 1x TBS-T (wrap container in plastic to avoid evaporation and drying of blot) or long term at -20°C by sandwiching blot between two pieces of blotting paper soaked with 1x TBS-T and wrapping this in plastic wrap prior to freezing

50mL Stripping Solution

6.2mL 0.5M Tris-HCl pH 6.8 (final concentration 62mM)
10mL 10% SDS (final concentration 2%)
350µL 14.3M β–mercaptoethanol (final concentration 100mM)
Fill to volume with ddH_2O
Store at 4°C

RNA extraction from Tissues: Trizol method

1. Remove tissue of interest from freezer only if all of the materials and reagents required have been prepared and are available for immediate use. Weight the tissue in its same tube.
2. Add 1000ml of Trizol for every 50-100mg of wet tissue. Transfer to 50ml conical tube. Use polytron at level speed 5-6. Homogenize tissue for ~1min. Observe sample. If tissue particles are visible, keep homogenizing until the solution looks even. Certain tissues may require longer times.
3. Transfer liquid to a new eppendorf tube. Incubate samples at RT for 5 min.
4. In the mean time, clean Polytron extensively at least 3X with water and a final time with 100% ethanol. Allow drying. Use clean paper towel if needed.
5. Add 0.2ml chloroform/ 1 ml of Trizol used initially. Vortex samples vigorously until samples are opaque.
6. Incubate at RT for 2 minutes.
7. Centrifuge samples at <12000g for 10 mins at 4C
8. Transfer aqueous phase to new eppendorf tube. Aqueous phase volume will vary. Make sure to not transfer any of the whitish middle layer or the pink Trizol layer remaining below.
9. Add 0.5ml isopropyl alcohol (2-propanol) /1ml Trizol used initially.
10. Incubate at RT for 10 min.

11. Centrifuge at <12000g for 10 mins at 4C.

Note: RNA may form pellet at this time. If you do not see a pellet, it is ok. May form after next step.

12. Remove supernatant *(pour off carefully so the pellet is not disturbed)* and wash pellet with 1ml 70% ETOH/ 1ml of trizol used initially.
13. Vortex and centrifuge at <7500g for 5 mins at 4C.
14. Pour off supernatant and allow pellet to air dry (10-15mins).

Note: If you do not see a pellet it is ok. Small amounts of RNA will not have a visible pellet.

15. Resuspend pellet in 100µl DNAse free, RNAse free H2O.
16. Test concentration of RNA: Optimal 260:280 ratio is 2.0 for RNA.
17. For all of this procedure use only RNAse free water. This can be done in lab by incubating water with 0.01% of DEPC overnight and then autoclaving the next day.

High capacity cDNA reverse transcription

1. Remove the following reagents from the High Capacity cDNA Reverse Transcription Kit and thaw on ice: 10x RT buffer, dNTPs, and 10x random primers.

Note: leave the Multiscribe Reverse Transcriptase enzyme and the RNAse inhibitor in the freezer.

2. Calculate how much volume is needed from each RNA sample according to the results from the Nanodrop to use 1µg of RNA per reaction.

Note: this kit allows the reverse transcription of 0.2-2µg of RNA.

3. The total volume for the RNA sample needs to be 10µl. Depending on the volume needed per RNA sample, complete to 10µl with RNAse free water in single PCR tubes.
4. To prepare the Master Mix (total volume: 10µl) add the following per reaction: 3.2µl water, 2µl 10X RT Buffer, 2µl random primers and 0.8µl dNTP.
5. Once the Master Mix is made, add to each 10µl RNA sample for a total volume of 20µl/reaction.
6. Place all the PCR tubes in the thermocycler and run the program:
   - 10min-25°C
   - 120min-37°C
   - 5min-85°C
   - ∞-4°C

Set up qRT-PCR plate

Note: Load plates using metal cooling block stored at -20°C and in the order – A1; A2; B1; B2....etc. Tip: print out a map of the 384-well plate and write on each well (cell in the table) the sample name of what sample is going in each well and what primer/probe set will be added to each set

1. First dilute the cDNA. In a small rounded PCR tube add 1µl of cDNA per each well to be filled on plate and add 8 µl of nuclease-free water. Each sample is run

in triplicate for each primer/probe set to be assayed; therefore, make a diluted mix of cDNA/water with enough starting material for the number of wells needed plus 1 extra sample per every 10 wells. Place samples on ice.

2. Make the Master Mix by adding 1µl of primer/probe mix 20X gene expression assay (Life technologies) and 10µl of Taqman 2X reagent per well to be detected by that particular primer/probe set. Make extra reactions, 1 extra for every 10 wells.
3. Place on ice until distribution
4. Load 9µl of the cDNA/water dilution to each well
5. Distribute 11µl Master Mix accordingly to each well

Note: Each well will contain 20 µl of solution (9µl of cDNA diluted in nuclease-free water; 11µl Master Mix & Primer solution).

6. Cover the top of the plate using optical adhesive film (Life Technologies).
7. Spin plate in large centrifuge up to 1000 rpm
8. Place plate in PCR machine
9. Open the SDS 2.4 software, select standard curve, add detectors to list, select wells with samples, select cycle program and run.

Note: never leave plate in machine after run is over

Hindlimb Suspension (Tube) Test

1. Perform assessment every 3 days
2. Set up a 50ml conical tube on a stable surface
3. Place a cotton ball at the bottom of tube
4. Take pups one by one and suspend by their hindlimbs from the rim of the tube
5. Record the time of latency (time to fall inside tube)
6. Remove pup from tube carefully and place on a warm surface such as an electric blanket to rest between repeats
7. Repeat procedure and record time of latency again
8. If mouse is capable of changing position and hold itself from the opposite rim with front limbs or crawl on the surface of the tube, do not count as an appropriate run. Remove animal from study or try the 2 runs of the assay after a period of rest
9. Assay is stopped at 60s, remove pup from tube if it does not fall after this time

* Adapted from Rimer Lab protocol files, courtesy of Bonnie Seaberg